Characterisation of global regulators that control expression of a flagella system in *Rhodobacter sphaeroides*

Merton College

University of Oxford

Thesis submitted for the Degree of Master of Science by Research

Hillary Term 2015

Author:

Stuart Thomas

Supervisor:

Prof. Judith Armitage

Abstract

Stuart Thomas
Merton College
University of Oxford

Submitted for the Degree of Master of
Science by Research
Hillary Term 2015

The α-proteobacterium *Rhodobacter sphaeroides* expresses one flagellar system (Fla1) and two chemotaxis operons (*che*Op_2 and *che*Op_3) under laboratory conditions. It has another flagellar system (Fla2) with a proposed cognate chemotaxis operon (*che*Op_1) which until recently had not been seen to be expressed. Here we characterised Fla2 motility and show that *che*Op_1 can be expressed under Fla2-inducing conditions. Putative Fla2$^+$ strains AM1 and N29 were incubated on Sistrom's media and expression of the Fla2 system was confirmed with western blotting and mass-spectrometry. The Fla2 motility pattern was significantly different to Fla1 when measured on soft nutrient agar and by analysing free swimming cells. Fla2$^+$ strains swam in a corkscrew-like pattern which may favour movement through biofilms. Fla2$^+$ AM1 and N29 were significantly deficient in their capacity to form biofilms compared to Fla1$^+$ WS8N. AM1 and N29 were found to contain mutations in *cckA* and plasmids expressing these mutations were able to switch expression of Fla1 in WS8N to Fla2. Expression of mutant *cckA* also affected *che*Op_2 and *che*Op_3 expression and induced expression of *che*Op_1. Some members of the α-proteobacteria are known to engage in lifestyle switches from motile to sessile growth. It is suggested that a similar switch occurs in *R. sphaeroides* which uses the Fla1 system for motility in liquid environments and for the initial attachments to surfaces and the Fla2 system for movement through the highly-viscous biofilm. For the first time we have also shown expression of *che*Op_1 which may engage in cross-talk with the *che*Op_2- and *che*Op_3-expressed chemotaxis system. These results have implications for the regulation of dual flagellar systems in the α-proteobacteria.

Declaration

The work in this thesis was performed in the Department of Biochemistry (University of Oxford) from October 2011 until April 2015, under the supervision of Prof. J. P. Armitage. All work in this thesis is my own unless otherwise stated and has not been submitted for a degree at this or any other university.

Acknowledgements

Thanks to Judy and everyone in the Armitage lab for unbelievable support, friendship and guidance. Without the coffee times, pub visits and close friendships I've had with everyone in the group, I would not be submitting this work. Special thanks to the legendary and ever-patient Chris Jones and George Wadhams, who closely guided me in the lab and with the writing of this thesis and for teaching me that alcohol and coffee solve all of life's problems; and to Mark, Kathryn, Nic, Elaine and Jen who taught me how to science; and to Matt, Andrea, Jimmy and Gareth Blades for their ever-amusing distractions.

Thank you to my friends who accepted that "no I'm sorry I'm really busy today" meant "I'm tired as sin and need to go home" and therefore did not get upset when we couldn't see each other.

A special thank you to my family who got me to where I am today, by supporting me and letting me be my own man, and for patiently accepting that they wouldn't hear from or see me for periods of time in which ice ages seem short.

To my wife, I dedicate all the hard work and care that went into this thesis. I would have long since become a desperate hermit if it wasn't for your love, support and acceptance. Thank you *Cariad* for teaching me to be proud of my accomplishments and to take ownership of my failures. This is for you.

Contents

Chapter 1

Introduction

1.1 Bacterial motility

The ability to react to an environmental pressure is a favourable asset to species that otherwise could not respond; vulnerable to the indiscriminate changes of their habitat, they would become disadvantaged in the "hunger games" of natural selection. In order to properly adapt to the fluctuating conditions in which they find themselves, some bacteria have evolved motility systems to move in response to changes in their environment.

For motile bacteria, it is necessary for them to control movement into areas for optimal growth, for example toward or away from oxygen, light or metabolites. Some species have motility systems for swarming over a surface like *Myxococcus xanthus*, which can "glide" over a substrate or can move by social "twitching" that relies on the extension and retraction of pili (Shi and Zusman, 1993). In liquid environments, spirochetes can rotate their cell body in a helical fashion to actively create swimming motility (Li et al., 2000). To achieve this, spirochetes use the most common and well-characterised bacterial motility system, large organelle-like structures called flagella.

1.1.1 Flagellar-mediated taxis

More than half of the known bacterial species swim using the rotation of flagella (Fig. 1.1) (Armitage and Schmitt, 1997; Blair, 1995). Flagellar function is implicated in many diverse cellular functions including pathogenicity, biofilm formation and symbiosis (Wadhams and Armitage, 2004). For example, mutations that impair flagella-driven motility in *Helicobacter pylori* reduce pathogenicity which would otherwise result in peptic ulcers. Similarly mutated *Vibrio cholerae* is unable to correctly infect the small intestine and cause cholera (Soutourina and Bertin, 2003).

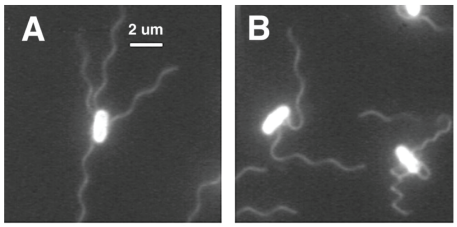

Figure 1.1: Flagella in *E. coli* labelled with a fluorescein dye and displaying normal (**A**) and semicoiled and curvy (**B**) flagella. Adapted from Turner et al. (2000)

There is great diversity in the number and position of flagella around the cell body. Some bacteria exhibit a single structure (like in the monotrichous *Caulobacter crescentus*) or have multiple flagella surrounding the cell as seen in the peritrichous *Escherichia coli*. The lophotrichous *Vibrio fischeri* has multiple flagella found at a single locus at the cell pole (McCarter, 2004).

Flagellar motility is mediated by rotation of the flagellum structure. For example, in the well-characterised system of *E. coli* counter-clockwise (CCW) rotation of the flagellum results in swimming motility or a "run". Clockwise (CW) rotation results in reorientation of the cell, or a "tumble," which ensures that the next run is in a different direction to the last. This "random walk" made up of runs and tumbles does not allow a cell to move in a net direction. However, the activity of chemoeffectors on cellular receptors allows a cell to control how often runs are interspersed with tumbles. This "chemotaxis" grants cells the ability to move in

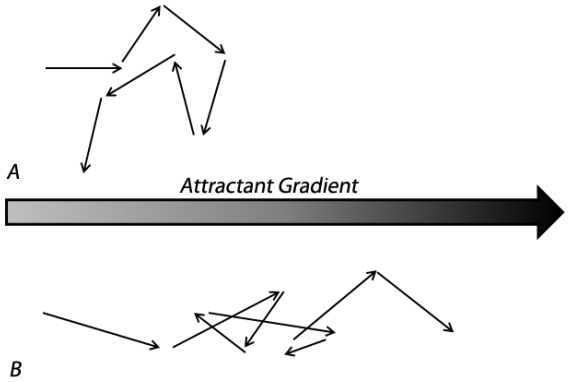

Figure 1.2: Diagram of a random walk (**A**) and a biased random walk (**B**). Mediation of the frequency of tumbles allows cells to travel in a favourable direction. If a cell moves down a desired gradient it will initiate a tumble to reorient. If a cell is travelling up a gradient in the desirable direction it will delay reorientation so as to travel further in the favourable direction.

response to and along a chemical gradient in a method known as a "biased random walk" (Fig. 1.2). If a cell travels in an unfavourable direction then it will initiate a tumble more frequently than if it was travelling in a favourable direction. Net movement is therefore in a favourable direction (Wadhams and Armitage, 2004).

In *E. coli*, a run is characterised by CCW rotation of the flagella which form a co-operative bundle that rotates together to drive swimming motility. A tumble occurs when the multiple flagella disentangle and rotate CW (Fig. 1.3 **A**). However, in the monotrichous *R. sphaeroides* runs are mediated by CCW rotation of the flagella and tumbles occur when the flagellum halts rotation, the cell reorienting from Brownian motion (Fig. 1.3 **B**). In this way, both species direct movement in their favour to travel along a gradient (Armitage and Schmitt, 1997).

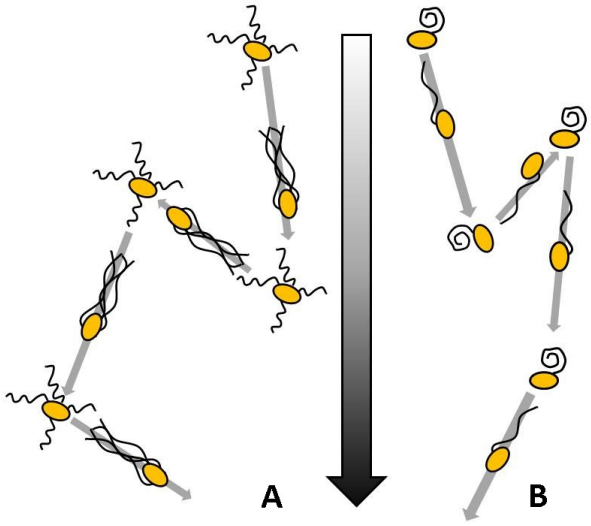

Figure 1.3: Chemotaxis. Block arrow represents chemical gradient from low to high attractant concentration. Biased movement is achieved by increased tumbling frequency when moving down a chemoeffector gradient and decreased frequency of tumbling when moving up a gradient. A run is defined as a period of uninterrupted movement; a tumble is defined as a change in direction. **A**: In *E. coli* a run is caused by counter clockwise rotation of the flagella which bundle together, a tumble is initiated by clockwise rotation and separation of the flagella bundle (Larsen et al., 1974). **B**: In *R. sphaeroides* a run occurs during flagellar rotation, a tumble during a cessation of flagella rotation, cells re-orient by brownian motion (Armitage and Macnab, 1987).

1.2 Free swimming studies on bacteria

Tracking bacterial cells using microscopy has been useful for investigating the motility patterns of *E. coli*, *Pseudomonas putida* and *Vibrio alginolyticus*, among others (Berg and Brown, 1972; Duffy and Ford, 1997; Atsumi et al., 1996; Rosser et al., 2013). A motility pattern is based on such things as swim speed, run to stop ratio and angle of direction change. For example, *E. coli* has a mean swimming speed of 33 μm /s and *R. sphaeroides* swims at 40 μm /s, whereas *V. alginolyticus* can reach speeds of 70 μm /s.

1.3 Flagellar structure

The flagellum is one of the most complex molecular structures. Its construction requires a minimum of 50 genes resulting in multiple copies of about 25 proteins

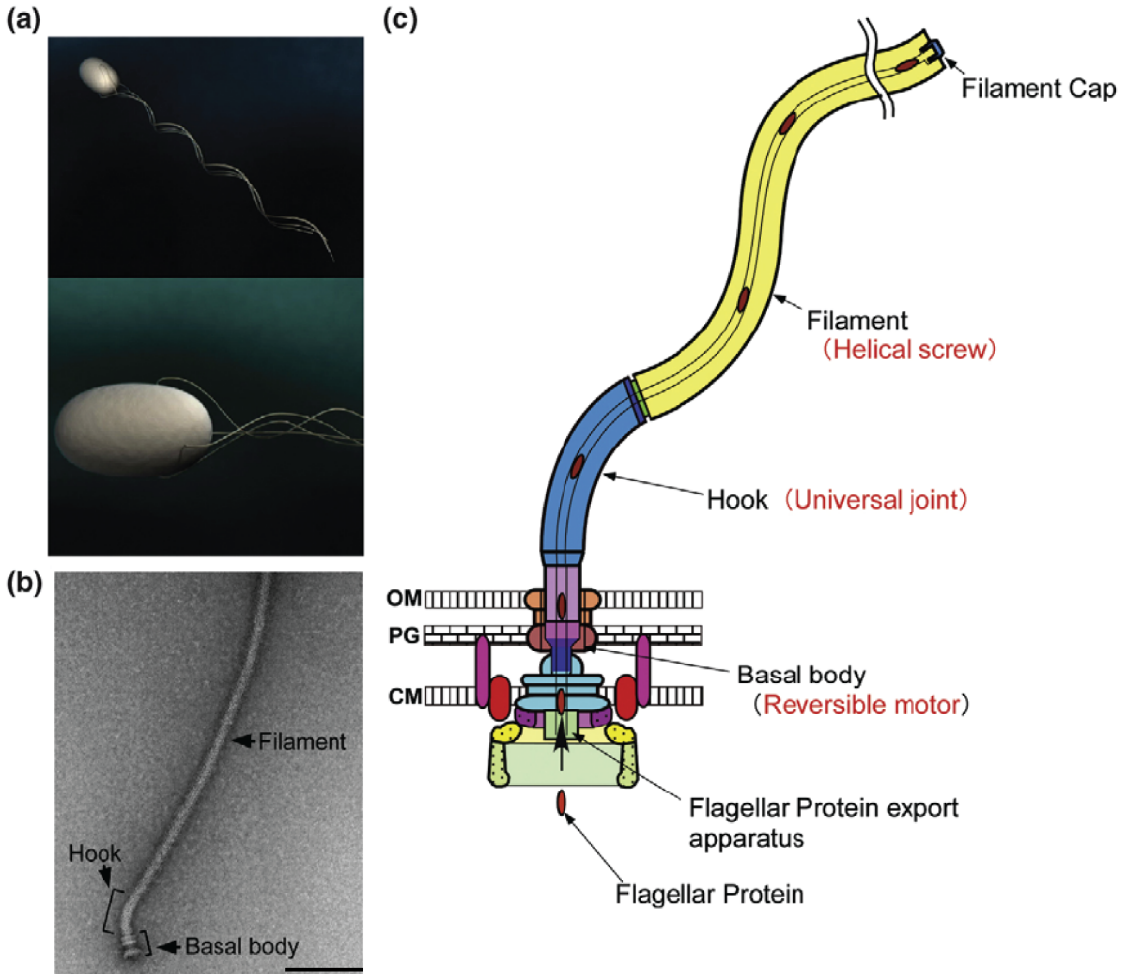

Figure 1.4: **(a)** Schematic drawing of a bundle of flagella. **(b)** Electron micrograph of the *Salmonella* flagellum isolated from WT cells. Scale bar = 100 nm. **(c)** Diagram of the flagellum with the main structures highlighted. The extracellular apparatus is made up of the filament (yellow) and hook (blue). The basal body is made up of a conglomerate of proteins within the membrane and cell wall. The export apparatus (pale green) is found within the basal body and is responsible for transporting components of the flagellum out of the cell. **a**, **b**, and **c** adapted from Minamino et al. (2008)

(Chilcott and Hughes, 2000; Macnab, 2003).

Fig. 1.4 shows the flagellar structure of Gram negative *Salmonella* species detailling the major components of the structure.

1.3.1 Filament and hook

The extracellular portion of the flagellum is referred to as the hook and filament. The filament, comprised of many thousands of copies of FliC is the structure which

drives motility. It attaches to the cell body at the hook. The hook, comprised of multiple FlgE copies, is a universal joint which links the filament to the rotation of the rotor body. It angles the position of the filament up to 90° perpendicular to the rest of the structure, which allows flagellar to bundle during CCW rotation (Fig. 1.5) (Ikeda et al., 1987).

1.3.2 Basal body

The hook attaches to the "basal body" which is the part of the structure embedded in the membranes. This structure provides the torque for rotation and is composed of the rotor and the stator. The basal body is composed of a central rod and a series of rings which act as a bushing between the spinning rod and the membranes. The C-, MS-, P- and L-rings interact with the cytoplasm, inner membrane, peptidoglycan layer and the outer membrane, respectively. The rings surround the rod which is hollow to allow for the export of the flagellar machinery out of the cytoplasm. The extracellular components travel through the flagellar body to assemble on the other side of the membrane. The C-ring is the rotor responsible, with a stator, for driving rotation and is comprised of FliG, FliM and FliN. The rod complex attaches directly to the hook and spins along with the MS- and C-rings, collectively all known as the rotor. The L-and P-rings do not spin but remain static (Fig. 1.5).

The last component of the basal body is the stator complex. The stator is made up of multiple copies of MotA and MotB in proton-driven flagella (if the flagella is powered by the sodium motive force, *smf*, then the stator is comprised of the proteins PomA and PomB) (Imae and Atsumi, 1989).

Torque is generated from the interaction between the stator and the C-ring and derives energy from the proton motive force (*pmf*) or the *smf*. H^+ or Na^+ interactions with the stator provide the energy to rotate the rotor and therefore the filament.

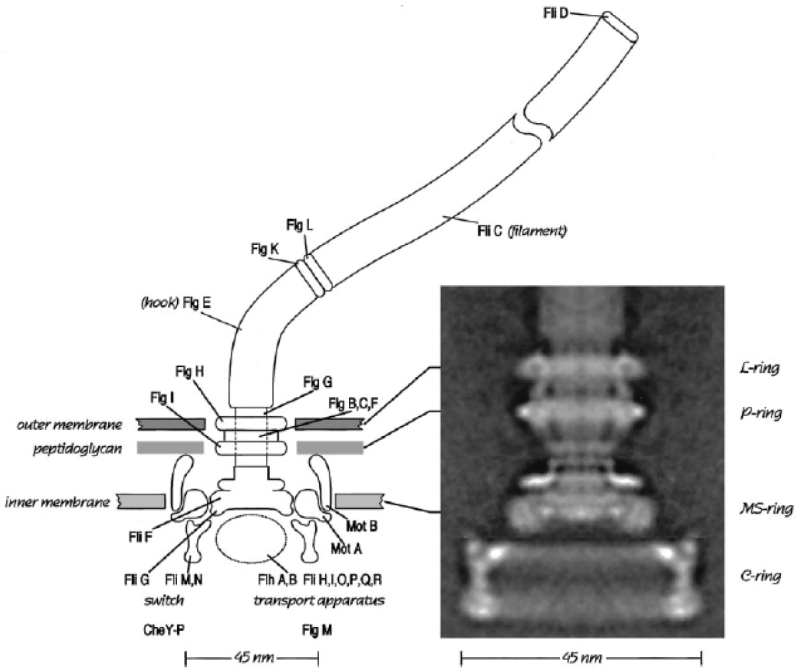

Figure 1.5: Flagellar structure of *E. coli* and *Salmonella* flagellum. Diagram drawn to scale compared to structure seen using electron microscopy (EM). Inset: EM image through the cross-section of the flagellum from *Salmonella* strain SJW880. Adapted from Berg (2003)

1.4 Flagellar assembly

1.4.1 Export aparatus

The export apparatus is found within the C- and MS-rings (Minamino et al., 2008) and shares a high similarity to the type III secretion system (Cornelis, 2006). The function of the export apparatus is to transport flagellar proteins through the rod. FliJ, FliL and FliH act as a targeting complex (Fig. 1.5).

The flagellum assembles in a controlled and sequential manner. Firstly the MS ring is inserted into the membrane to act as a frame for the export apparatus (Fig. 1.6 (Macnab, 2003).

The export apparatus, the C-ring and the stator are then assembled on and around the MS-ring.

With the export apparatus complete, the remaining structure is assembled using

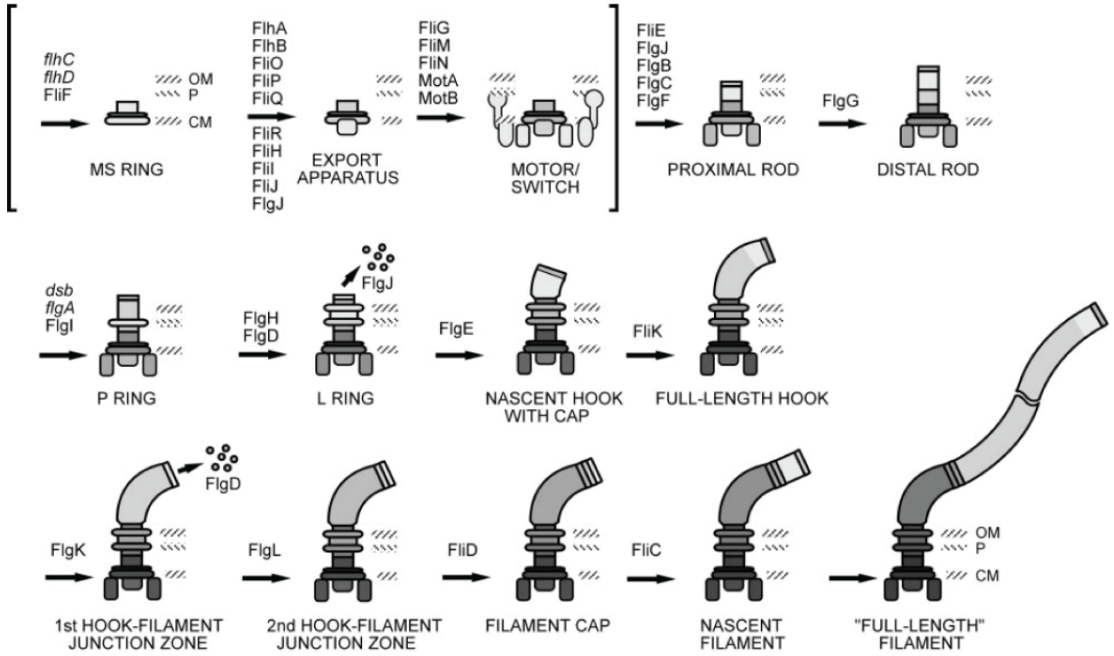

Figure 1.6: Diagram of the assembly of the *Salmonella* flagellum showing proteins involved and structures formed in order of assembly. Structures within brackets are assembled before the completion of the type III secretion system. Adapted fromMacnab (2003)

the type III secretion pathway which is categorised by distal addition of subunits which travel down a channel. The rods and P- and L- rings form next. The unfolded proteins involved are targeted to the export system and fold after passage through the central channel. The hook and filament are the final proteins that travel through the channel.

The flagellum is sequentially self-assembled as can be seen above. Without strict regulation, the extracellular apparatus may get expressed before it is able to be exported and the export apparatus would try to export proteins regardless of whether they can form at the distal end of the half-formed machinery. Thousands of copies of FliC would also accumulate within the cytoplasm, leading to disruption of cellular function. It is necessary, therefore, for temporal regulation of expression of the flagellar components.

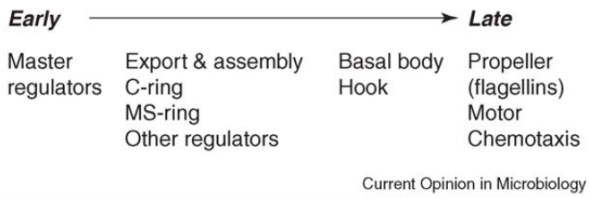

Figure 1.7: Diagram of the general hierarchy of flagellar genes and their expression from early in the process to late. Adapted from McCarter (2006)

1.5 Flagellar regulation

Flagellar genes are organised into a discrete hierarchy that is related to when the proteins are neccessary during the assembly process (Chilcott and Hughes, 2000). Each tier within this hieracrchy is dependent on the last tier and relies on different promoters and sigma factors to ensure genes are expressed in the correct order. Therefore, genes at the beginning of the hierarchy can be called early genes due to their expression early in the process of flagellar assembly. Late genes are expressed toward the end (Fig. 1.7).

1.5.1 Regulation of flagellar synthesis in *E. coli*

The most well-characterised flagellar system is found in *E. coli* and *Salmonella typhimurium*. This system has 3 tiers of transcriptional control (McCarter, 2006).

The first tier, Class I, contains the master regulator genes *flhD* and *flhC*. The FlhDC complex acts as a transcriptional regulator of Class II genes which encode the proteins involved in the secretion system and basal body.

Class III genes which encode the extracellular apparatus are transcriptionally regulated by *fliA* which encodes the sigma factor σ^{28}, and *flgM* which encodes an antisigma factor. FlgM prevents the expression of Class III genes while the basal body is being assembled. When the rod and secretion system are complete, FlgM is exported out of the cell via the semi-constructed flagellum. This removes the

repression enacted on FliA which can then promote expression of the last tier of flagellar genes (McCarter, 2006; Soutourina and Bertin, 2003).

1.6 Dual flagellar systems

Some species of bacteria produce two kinds of flagella, which produce locomotion in different growth conditions. Swimming motility is seen in low-viscosity environments as described above. Swarming motility is also seen on higher viscosity environments (0.4-0.8% agar) (Moens et al., 1995).

These dual systems can occur in some α-proteobacteria species, commonly for example in species of *Azospirillum*. The purple photosynthetic *Rhodospirillum centenum* (also from the α-proteobacteria) possesses a single polar flagellum. When grown on solid media flagella develop laterally along the cell length which facilitate swarming in this case in response to light (Mcclain et al., 2002). Switching from lateral flagella for swarming motility to the single polar flagellum for swimming is also seen in for example *Vibrio parahaemolyticus* (McCarter, 2006).

It has been questioned as to why dual systems are favourable despite the large metabolic cost of flagellar biosynthesis. It has been noted that lateral flagella are preferable for swarming, as co-ordinated flagellar bundles are able to overcome surface tension. Some peritrichous bacteria that use multiple flagella to swim upregulate their number of flagella when grown on solid media (Harshey, 1994). As multiple flagella are not necessary in liquid media, the reduced metabolic cost of a single flagellum could drive cells to reduce flagella number. Additionally, a single flagellum may be desirable for swimming motility. In *Vibrio alginolyticus*, a polar flagellum results in a faster swimming speed than lateral flagella in low viscosity media. In higher viscosities, cells with lateral flagella are faster (Atsumi et al., 1996).

1.7 *Rhodobacter sphaeroides*

R. sphaeroides is a motile, photosynthetic member of the α-proteobacteria. It is one of the most metabolically diverse groups of bacteria, able to grow on a range of organic compounds in the presence or absence of light and of oxygen (Table 1.1).

	Light	Dark
Aerobic	Respiration	Respiration
Anaerobic	Photosynthesis	Fermentation

Table 1.1: Growth capabilites of *R. sphaeroides* in relation to aerobicity and light

As stated above, *R. sphaeroides* has a single flagellum and swims in a run/stop pattern. It is a model organism for studying bacterial chemotaxis and motility (Armitage and Schmitt, 1997).

1.7.1 Regulation of Fla1 flagellar synthesis in *R. sphaeroides*

As stated above, *R. sphaeroides* has a single flagellum under almost all observable conditions which rotates CCW to drive swimming motility and halts rotation to allow the cell to re-orient. This flagellum is expressed from multiple operons grouped together as the Fla1 system.

The flagellar hierarchy of the Fla1 flagellum is separated into 4 tiers or classes (Poggio et al., 2005).

Class I

The master regulator which drives expression of all other flagellar genes is FleQ, without a functional master regulator, cells remain non-flagellate (Poggio et al., 2005). Further biosynthesis of flagella is likely caused only by expression levels of the constitutively active FleQ and by possible post-transcriptional modification of the mRNA.

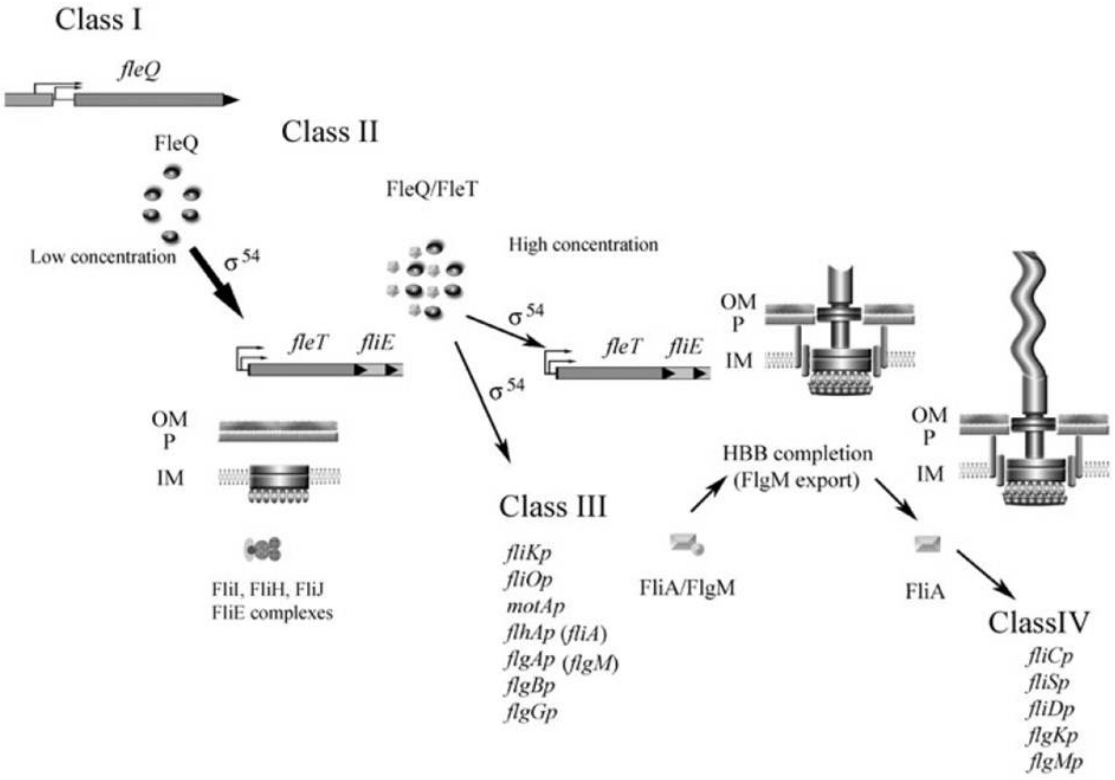

Figure 1.8: Regulation of flagellar expression in *Rhodobacter sphaeroides*. FleQ is the Fla1 master regulator which initiates transcription of Class II genes which include regulatory genes like *fleT* and also components of the hook basal body. Class III genes are expressed under the control of the FleQ/FleT complex and in turn complete the export apparatus and co-ordinate the expression of the Class IV genes which complete the flagellar apparatus (Wilkinson et al., 2011). This hierarchy ensures the correct expression of flagellar proteins. Adapted from Poggio et al. (2005).

FleQ is capable only of activating the FleT promoter to which it has a high affinity, resulting in expression of the *fleT* operon, including the Class II genes *fliL*, *fliH* ,*fliJ*, *fliE*, *fliF*, *fliI* and *fleT*.

Class II

The majority of Class II proteins are responsible for the biosynthesis of the export apparatus and the beginning of the C-ring.

FleT is a Class II regulatory protein which functions only through an interaction with FleQ allowing expression at promoters which would otherwise have too low an affinity for FleQ alone. The FleQ/FleT complex activates expression of Class III genes.

Class III

Class III genes are mostly concerned with the establishment of the basal body and completion of the secretion system. As in *E. coli* expression of the Class IV genes is inhibited by the antisigma factor FlgM. When the basal body is complete, FlgM is secreted and the sigma factor FliA is able to activate the last tier of flagellar gene expression.

Class IV

The Class IV genes are under the control of FliA, a σ^{28} factor. As in enteric bacteria, the last tier contains genes concerned with the extracellular filament - *fliC*, *fliD*, *flgK* and *flgM*.

1.7.2 The Fla2 flagellar system in *R. sphaeroides*

R. sphaeroides has an additional set of flagellar genes which encode the Fla2 system which is unexpressed under laboratory conditions in WS8N (Poggio et al., 2007). The Dreyfus laboratory identified a *R. sphaeroides* mutant that under photoheterotrophic conditions expresses the Fla2 system in a non-motile, non-flagellate Δ*fleQ* background (Fig. 1.9). This mutant is motile. Fla2 flagellar filaments are physiologically distinct from the Fla1 flagellum (Fig. 1.9). Fla2 flagella are half the width of the Fla1 filament and multiple filaments form a tuft located distinctly at the pole, as opposed to the Fla1 filament which is randomly located along the cell body.

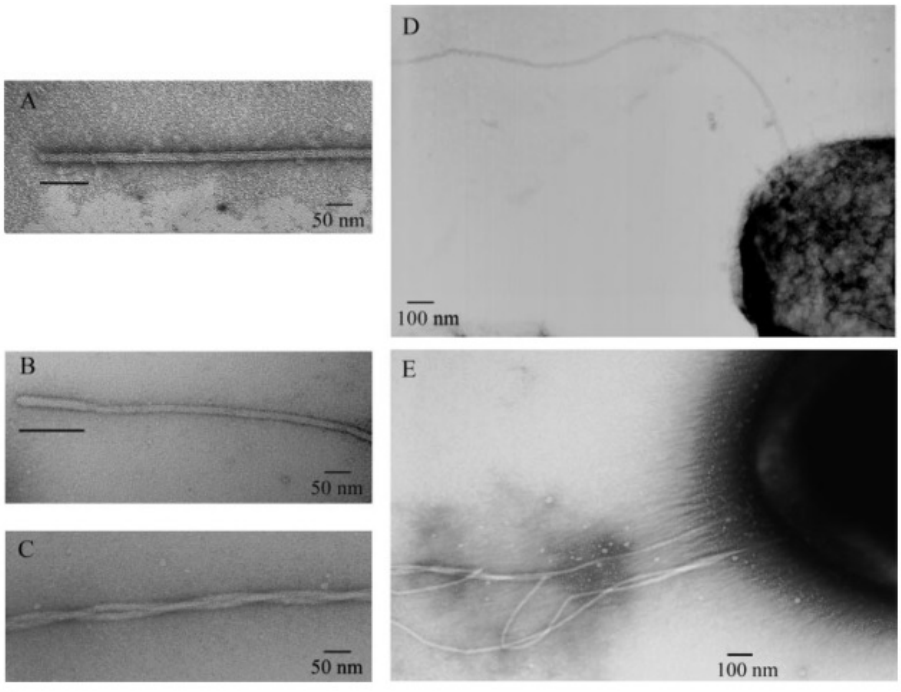

Figure 1.9: Electron microscopy images of representative *R. sphaeroides* flagella. **A** and **D**: WS8N flagella encoded by *fla*1. **B**, **C** and **E**: Flagella separately and in polar tufts from the AM1 strain which expresses only the Fla2 operon. Adapted from Poggio et al. (2007).

1.8 Vega-Baray et al., 2014

A number of months prior to the completion of this project, an article was published by Vega-Baray et al. (2015) which examined the same subject matter as this work. This article was generally supportive of our research and examined other research questions on the Fla2 flagellar system. Nevertheless, there is some overlap with Vega-Baray et al. (2015) and this project. This is acknowledged where applicable.

1.9 Two component systems

Two-component systems are a class of regulatory proteins that are made up of a histidine kinase (HK) protein and a response regulator (RR) (Fig. 1.10). HKs autophosphorylate in response to specific signals. HKs are dimeric and each monomer is responsible, through the action of a HATPase domain) of transferring a phosphoryl group from an ATP donor to a conserved histidine on the neighbouring monomer. The phosphoryl group is transfered to a conserved asparate residue on the response regulator which usually becomes active in its phosphorylated state. Two-component systems are subject to more complex regulation due to their bipartite nature (Perraud et al., 1999).

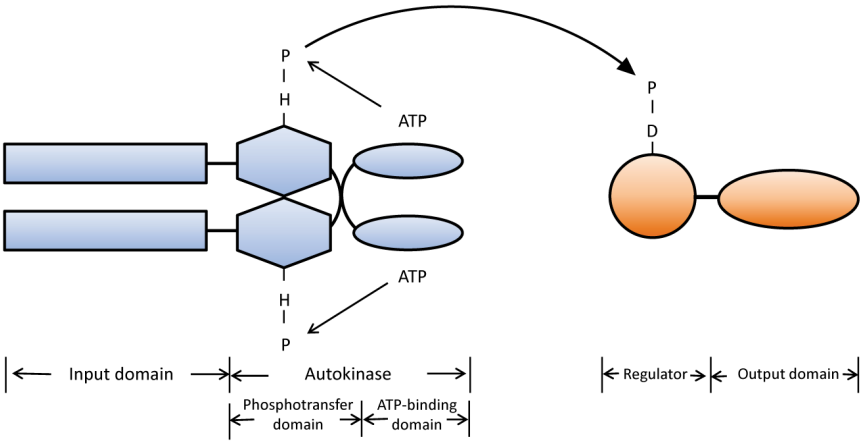

Figure 1.10: Two component system featuring a histidine kinase and a response regulator. The histidine kinase (HK, blue) is composed of an input domain and an autokinase region, made up of a phosphotransfer domain and an ATP-binding domain. HKs dimerise and the ATP-binding domain from one monomer catalyses the transfer of a phosphoryl group from an ATP molecule to a conserved histidine residue on the neighbouring monomer. The phosphotransfer domain is involved with the transfer of the phosphoryl group to a Response Regulator (RR, orange) which contains a regulator and an output domain. A conserved asparate residue accepts the phorphoryl group which instigates a response from the output domain. Figure adapted from a similar diagram in Hoch (2000).

1.10 Chemotaxis

It has already been stated that motile bacteria can direct movement through a biased random walk whereby the random changes in direction can be temporally controlled by selectively choosing when to reorient. When this is a response to metabolites or chemicals in the environments this method of motility is referred to as chemotaxis.

1.10.1 Chemotaxis in *E. coli*

E. coli is a model system for studying chemotaxis as it is the simplest system known and allows for the simplest interpretation of how the different components interact (Fig. 1.11).

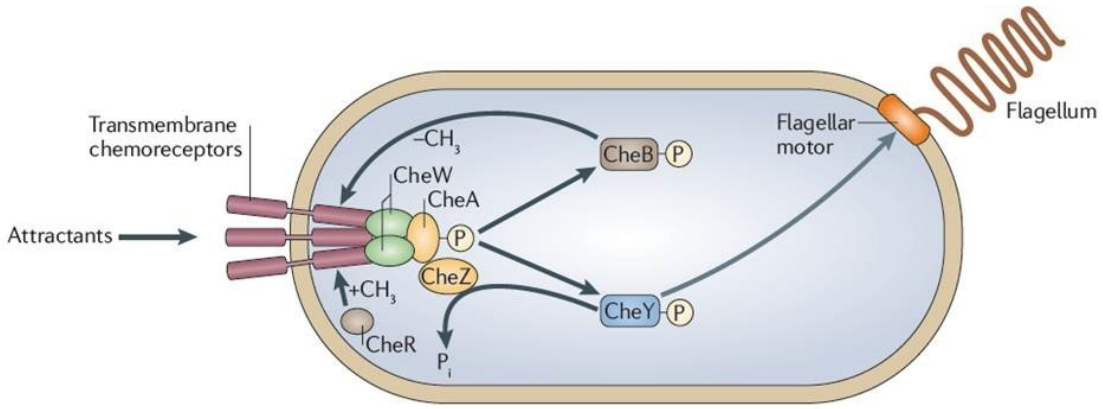

Figure 1.11: Chemotaxis in *E. coli*. Chemoreceptors (MCPs) relay extracellular signals to CheA which autophosphorylates. CheA phosphorylates CheY, a response regulator, which causes a tumble by binding to the flagella rotor. CheY-P is dephosphorylated by CheZ to terminate the signal. CheA also phosphorylates CheB which demethylates MCPs. CheR methylates receptors to alter their sensitivity and, together with CheB, forms an adaptation mechanism. Adapted from Porter et al. (2011).

Chemosensing

Methyl-accepting chemotaxis proteins (MCPs) are transmembrane sensory proteins which are responsible for binding chemoeffectors (metabolic componds that effect a response) and are therefore responsible for initiating a tumble or continuing a run. Ultimately, if there is a decrease in attractant or an increase in repellant then a cell will tumble. This is caused by a change in the conformation of the MCP.

Chemotactic signalling

The change in MCP conformation is detected by CheA, a histidine kinase (Section 1.9). CheW proteins act as an essential linker between CheA and its RR proteins. CheA has two cognate response regulators: CheB and CheY. CheB is a methylesterase which demethylates MCPs which desensitises them. This is part of the adaptation pathway which results in continued runs if the attractant concentration increases but a tumble if the concentration of attractant drops or remains steady (Kehry et al., 1985). CheR returns the MCPs to a sensitive state by methylating them.

The other response regulator that recieves a phosphoryl group from CheA is CheY, which effects a change in flagellar activity. Phosphorylated CheY (CheY-P) binds to FliM at the flagellar switch complex at the C-ring and causes a change in flagellar rotation to CW, causing a tumbling event (Dyer et al., 2009). CheZ dephosphorylates excess CheY-P to prevent continuous interaction with FliM and therefore continuous tumbling.

1.10.2 Complexity in chemotactic systems

The *E. coli* system is the paradigm for bacterial chemotaxis due to its simplicity. However, complex chemotaxis systems are found that rely on the interaction of multiple homologues of the proteins described above. For example, hundreds of known bacterial species have 2 or more CheA homologues, which is indicative of separate chemotaxis systems within a single cell (Porter et al., 2008). In other bacteria, for example the Spirochetes, there are two flagellar bundles at each pole of the cell which rotate independently of each other. The spirochetal chemotaxis system must signal to both bundlesin a way as to co-ordinate a response. If both flagella rotate CW or CCW at the same time, the cell's movement stalls (Charon and Goldstein, 2002). It is therefore important to recognise that the *E. coli* chemotaxis system is overly-simplistic in terms of signal differentiation and integration.

1.10.3 Chemotaxis in *R. sphaeroides*

R. sphaeroides serves as a suitable organism to study chemotactic complexity as the mechanism is more complex than *E. coli* while remaining somewhat simple. *R. sphaeroides* has multiple homologues of the chemotaxis genes on 3 major operons. Of these operons, one (*che*Op_1) is unexpressed under laboratory conditions. The products of the remaining two, *che*Op_2 and *che*Op_3, form two spatially separate

chemotaxis clusters, one that localises at the pole of the cell in the membrane and one that localises in the cytoplasm (Fig. 1.12). Both clusters are required for wild-type chemotaxis (Porter et al., 2002).

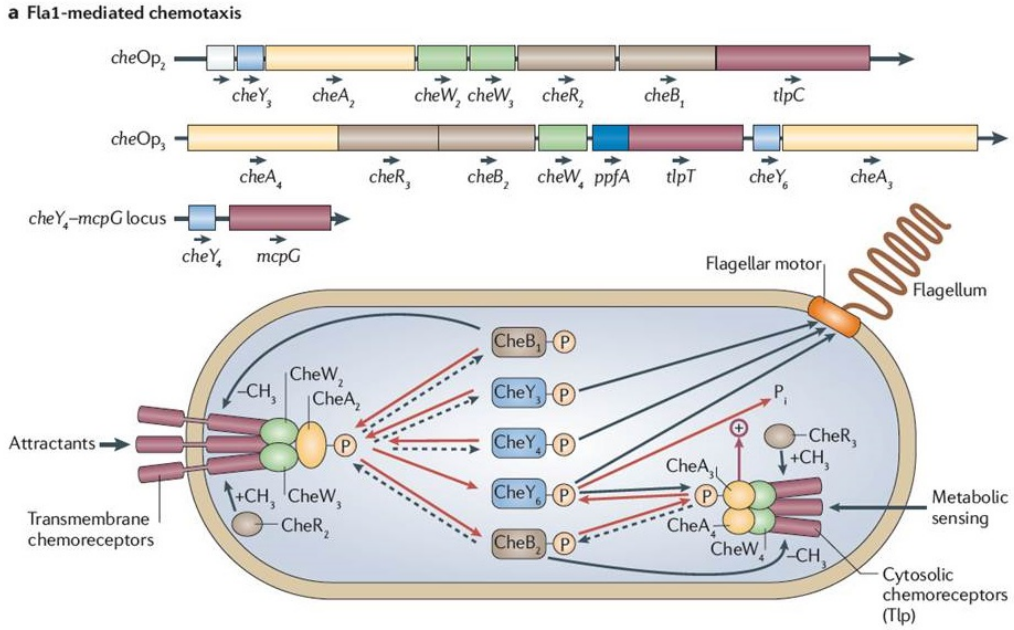

Figure 1.12: Chemotaxis in *R. sphaeroides*. Two major and one minor chemotaxis operon are known to express in *R. sphaeroides*: *che*Op$_2$ and *che*Op$_3$ and the *cheY4-mcpG* locus. The polar cluster is homologous to the system in *E. coli* and is primarily coded for by *che*Op$_2$. The cytoplasmic cluster is somewhat homologous to the *E. coli* system but contains two CheA proteins and cytosolic chemoreceptors Tlps. The two clusters are thought to integrate signals via the action of CheY$_6$, CheB$_2$and CheR$_2$. The cytoplasmic cluster is primarily coded for by *che*Op$_3$. There are multiple homologues of several proteins in both clusters. Both clusters signal to the Fla1 flagellum. Adapted from Porter et al. (2011).

Polar cluster

MCPs cluster together as a chemosensory array in *R. sphaeroides*. Signals pass from MCPs (via an interaction with the binding proteins CheW2 and CheW3) to the dimeric CheA2. CheA2 phosphorylates the response regulators CheY3, CheY4 and CheY6. It can also phophorylate CheB1 and CheB2.

Cytoplasmic cluster

At the cytoplasmic cluster, chemotaxis proteins cluster around an array of Tlp's which are chemosensory proteins that do not contain a transmembrane domain. Deletion of either TlpT or TlpC stops the clusters from forming and abolishes chemotaxis in the cell (Porter et al., 2002). Through the linker protein CheW4, Tlps signal to CheA3 and CheA4 which are non-classical CheA proteins. Neither has the full number of domains required and owned by a classical CheA but together they have the combined domains necessary to function (Porter et al., 2008). The CheAs at the cytoplasmic cluster only only phosphorylate CheY6 and CheB2. However, Tlps are methylated by CheR2 which also methylates membrane bound MCPs.

Concerted action of the clusters

It is known that CheY6 and either (but not both) CheY3 or CheY4 are needed to effect chemotaxis (Porter et al., 2006).

The cytoplasmic cluster is hypothesised to sense internal nutrient levels in the cell, whereas the polar cluster senses and responds to external stimuli.

As there is no CheZ in *R. sphaeroides* to terminate the signal, CheY6 is dephophorylated by CheA3 (Porter et al., 2008) and CheY6-P also has a half-life far shorter than *E. coli* CheY.

che$\mathbf{Op_1}$

Fig. 1.13 shows the layout of *che*$\mathrm{Op_1}$ in *R. sphaeroides* and how it is proposed to act in the cell. *che*$\mathrm{Op_1}$ has so far been unexpressed under laboratory conditions, despite containing all the genes necessary to express a full chemotaxis system. It has been suggested that components of the *che*$\mathrm{Op_1}$ operon interact with the Fla2 flagellar

system and it is therefore inferred that the products of *che*Op$_1$, if expressed, form the cognate chemotactic system for Fla2 (Martínez-del Campo et al., 2011).

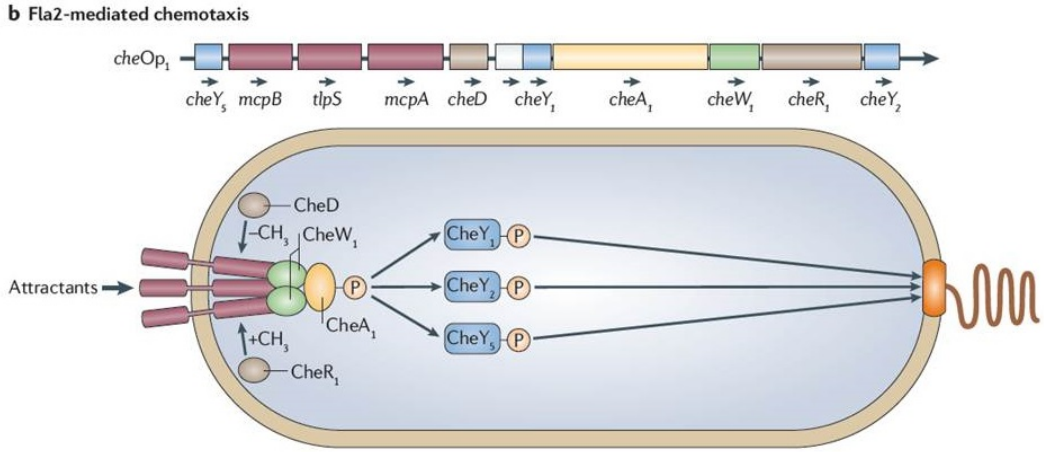

Figure 1.13: Proposed chemotaxis in *R. sphaeroides* from *che*Op$_1$. Layout of *che*Op$_1$ is shown as well as the proposed location of the chemotaxis system it putatively encodes. Adapted from Porter et al. (2011).

1.11 Biofilms

A biofilm is a community of sessile cells encased in a hydrated polymeric medium of exopolysaccharides created by the microbes. Biofilms allow cells to more completely withstand environmental changes and alterations to pH, oxygen levels, antimicrobials and nutrient deprivation.

1.12 Motile to sessile lifestyle switch

Cells attach to a surface via a cellular switch from motile to sessile growth, characterised by a change in gene expression. In a range of bacteria, for example in *Pseudomonas aeruginosa*, *Shewanella oneidensis* and *Acetobacter xylinum*, this is positively affected by cyclic diguanylate (c-di-GMP) a second messenger which is also an important signal for cell cycle progression and differentiation. It is known

to be important for so-called life transitions from motile, planktonic cells to sessile, biofilm-forming cells by an interaction with c-di-GMP receptors. A c-di-GMP receptor in *P. aeruginosa*, for example, is FleQ which represses motility and promotes biofilm formation.

1.12.1 Biofilm formation in *R. sphaeroides*

Motility has been found to be instrumental to the formation of biofilms in *E. coli* and *P. aeruginosa* (Pratt and Kolter, 1998; Shrout et al., 2006).

R. sphaeroides is a known primary coloniser of surfaces, leading to the formation of bacterial biofilms (Dang and Lovell, 2002). This essential stage of biofilm formation is dependent on flagellar assembly. Although we know little about *R. sphaeroides* biofilms, studies on the FliA/FlgM regulation system shows that both regulators are necessary for wild-type biofilm formation. FliA also regulates chemotaxis operon expression and therefore chemotaxis, in addition to motility, may be required for surface colonisation (Wilkinson et al., 2011).

1.13 CckA and CtrA

CckA is a part of a two-component system (Section 1.9). It is a membrane bound histidine kinase which signals to the response regulator CtrA via a phosphorelay protein ChpT (Jacobs et al., 1999; Mercer et al., 2012). CtrA is an essential protein in *Caulobacter cresecentus* (Laub et al., 2000). CtrA regulates the cell cycle and is a global regulator for multiple functions including DNA replication and methylation, chemotaxis, and flagella synthesis (Quon et al., 1998; Mercer et al., 2010). CtrA is a contributing factor to motility in members of the α-proteobacteria, a family in which it is conserved but not always essential for growth (Fig. 1.14) (Barnett and Hung, 2001; Bellefontaine et al., 2002; Miller and Belas, 2006).

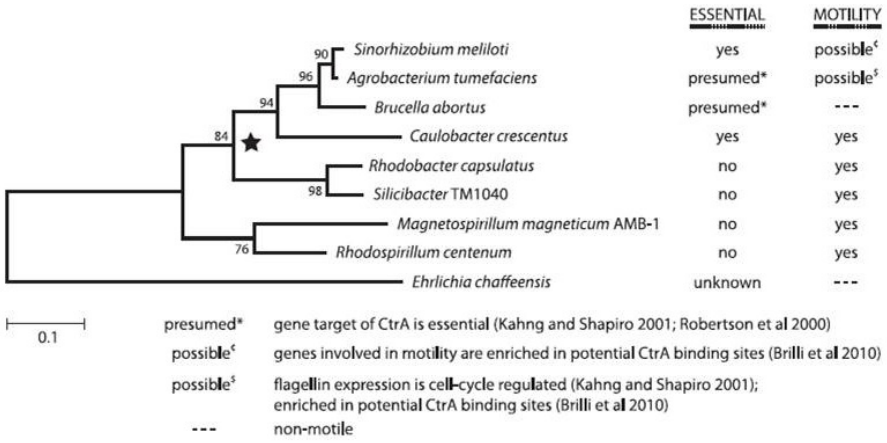

Figure 1.14: Phylogenetic tree showing the known actions of CtrA in the α-proteobacteria . The sequences of 8 highly conserved proteins were used to construct the phylogenetic tree to illustrate the evolutionary relationships between members of the α-proteobacteria . After the tree was constructed, the authors attached the CtrA activity to each species to visually represent the attributes of CtrA within clades. *R. sphaeroides* occurs in the same clade as *Rhodobacter capsulatus* and *Silicibacter* TM1040 (Gupta and Mok, 2007). The star indicates a proposed diversion event between essential and non-essential *ctrA* . CtrA is non-essental but linked to motility in *Rhodobacter capsulatus* and proposed to be non-essential and linked to motility in its relative *R. sphaeroides* . Adapted from Greene et al. (2012)

CtrA is known to regulate motility by promoting expression of flagellar genes. It also regulates biofilm formation in some species, evidenced by control of exopolysacharides (Francez-Charlot et al., 2015). It's not known what signals to CckA, except that it is mediated through DivL and DivK. The transcriptional regulator SciP acts a repressor of CtrA as part of a feedback loop (Lang and Beatty, 2002), as does CpdR in *Sphingomonas meloni* (Francez-Charlot et al., 2015). Fig. 1.15 shows the known CckA-CtrA interaction from *S. meloni*.

1.14 Support for CckA involvement with motility in *R. sphaeroides*

Recently, Vega-Baray et al. (2015) identified the CckA L391F mutation in *R. sphaeroides* strain AM1, a derivative strain of *R. sphaeroides* WS8N. This single mutation was capable of initiating expression of the Fla2 system under conditions which have only

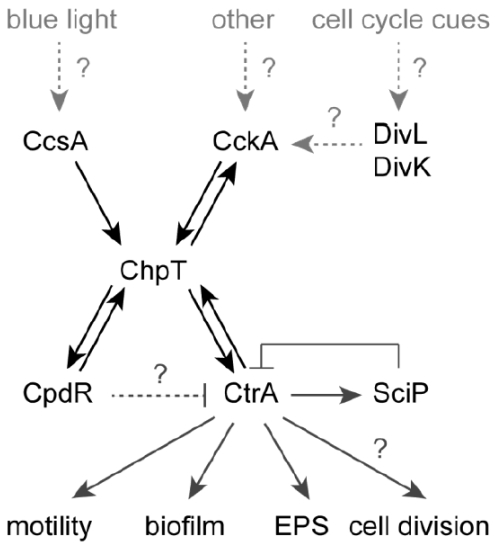

Figure 1.15: CckA/ChpT/CtrA phosphorylation relay in *S. meloni*. Multiple signals are assumed to funnel through CckA and ChpT to CtrA which has a negative feedback loop with SciP and CpdR. CtrA regulates motility and biofilm formation. Adapted from Francez-Charlot et al. (2015)

ever produced Fla1 expression. Fla2 expression was dependent on the presence of ChpT and CtrA, indicating that CckA specificity was not altered, and that CtrA is the protein responsible for Fla2 expression. Fla2 expression was shown to be related to concentration of phosphorylated CtrA, and that CckA L391F autophosphorylates faster than wild-type CckA, causing an increase in CtrA-P. Jones et al. (2001) also showed that expression of a chemotaxis operon in *C. crescentus* is dependent on CtrA activity. It may also be the case that this dependency is found in other organisms.

1.15 Project aims

This project will address the following research topics:

1. Express the Fla2 system under laboratory conditions
2. Characterise the Fla2 system including the motility pattern
3. In conjunction with expression of the Fla2 system, attempt to express the *che*Op_1 chemotaxis system

Chapter 2

Expressing Fla2

As previously stated, the Dreyfus laboratory has been able to express the Fla2 flagella system in *R. sphaeroides* AM1, a motile supressor of the Fla1 knockout Δ*fleQ* strain (Poggio et al., 2007). Additionally, a motile supressor has been found of a His-tagged *fliC* (Fla1 flagellin) strain (N29) from the Sockett laboratory (Liz Sockett, personal communication). This motility underwent initial characterisation to determine the flagellar system governing the motility which was found to be Fla2-mediated (Woods, 2007). Initially, to achieve the aims of this project, conditions needed to be found that promoted motility in the Dreyfus Fla2$^+$ strain (AM1) and the Sockett Fla2$^+$ strain (N29) to confirm that Fla2 can be expressed and measured in our laboratory.

2.1 Confirming AM1 and N29 motility

A low concentration (0.25%) of agar results in a semi-solid medium (soft agar) through which cells can swim. Non-motile cells inoculated onto a plate of soft nutrient agar form colonies with a defined ring of growth. Motile cells are able to swim outward from the point of inoculation, resulting in a larger diameter ring.

Chemotactic cells respond to the chemical gradient that results when nutrients are depleted at the site of inoculation. They are able to swim further outward than non-chemotactic, motile cells. Therefore, soft nutrient agar swim plates are a measure of growth, motility and chemotaxis (Section 6.8). It was hypothesised that Fla1$^+$ WS8N, Fla2$^+$ AM1 and Fla2$^+$ N29 may produce different swim diameters based on the influence of the Fla1 and Fla2 systems on motility and chemotaxis. Work from the Dreyfus laboratory found that the growth curves of WS8N and AM1 did not differ from each other (Vega-Baray et al., 2015). This eliminates the possibility that different growth rates will affect a strain's diameter on a swim plate.

2.1.1 Swim plates

As mentioned above, swim plates are a measure of chemotaxis and motility. This is demonstrated in Fig. 2.1 as the swim diameter of non-motile JPA467 (Δ*fliA*) is due only to growth of cells in the medium, and is smaller than the swim diameter of Fla1$^+$ motile, non-chemotactic strain JPA1301 ($\Delta cheY_6$). As cells grow on swim plates nutrients are depleted. This leads to a chemical gradient developing from the point of inoculation. JPA1301 does not respond to chemical gradients whereas WS8N actively swims up the gradient outward from the point of inoculation. Therefore WS8N which is both Fla1 motile and chemotactic has a larger swim diameter than JPA1301.

Fig. 2.1 also shows the swim diameters of the Dreyfus Fla1$^-$/Fla2$^+$ strain AM1 and the Sockett presumed Fla1$^-$/Fla2$^+$ strain N29 with either the 100 μm of the common attractant propionate or 100 μm combined of aspartate and glutamate. Both amino acids can act as a carbon source or as a source of nitrogen, and both are found in Sistrom's medium in which the Fla2 system was identified. AM1 and N29, which are putatively expressing Fla2 have swim diameters that are statistically no different to WS8N with sodium propionate as an attractant under photoheterotrophic conditions

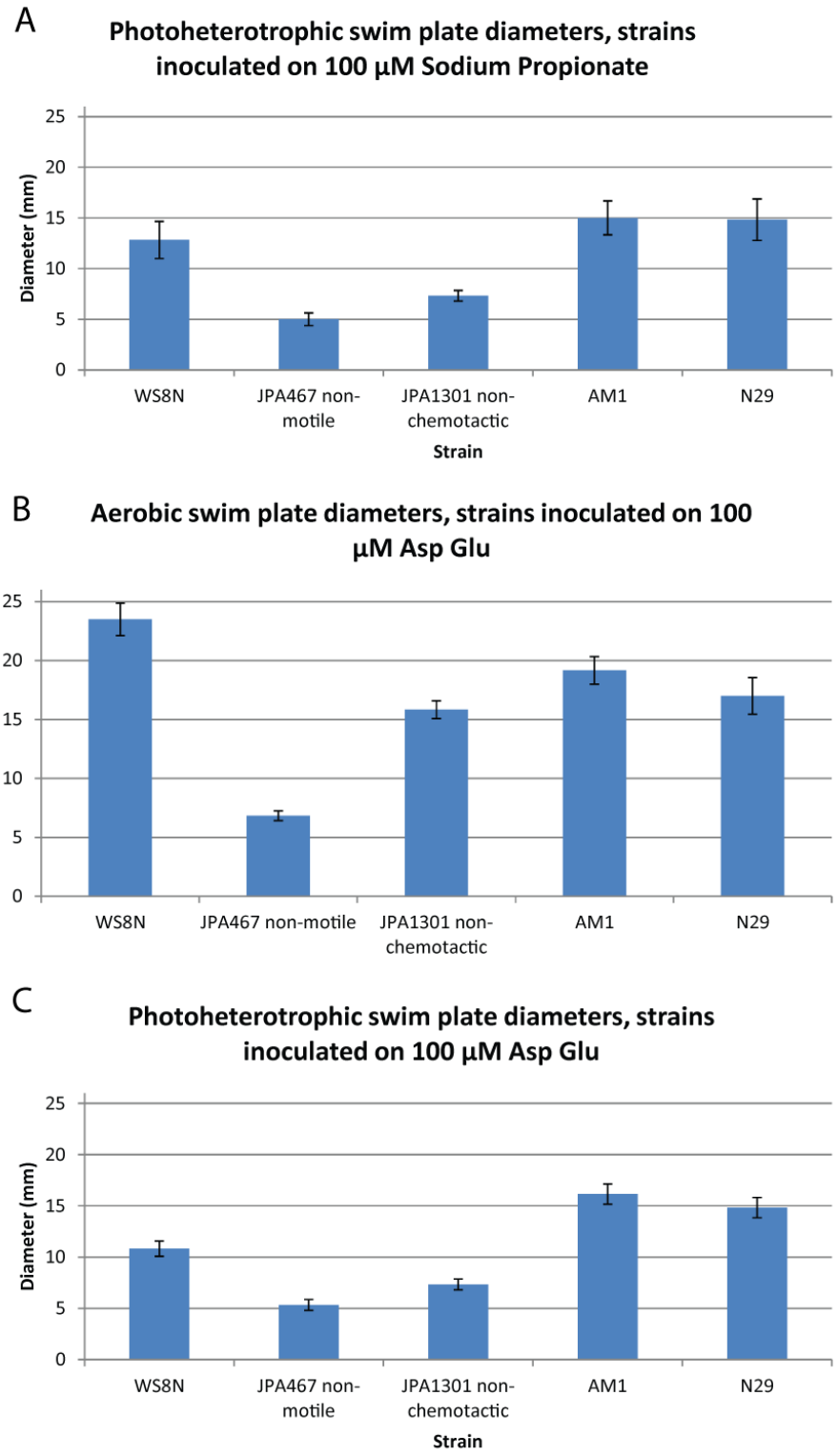

Figure 2.1: Swim diameters of strains grown initially in Sistrom's media and inoculated onto 100 μM sodium propionate (**A**) or 100 μM Asp Glu (64 μM glutamate and 36 μM aspartate) under aerobic (**B**) or photoheterotrophic (**C**) conditions. Mean values obtained from 3 technical repeats of 2 biological replicates. Error bars represent 1 standard deviation. WS8N: wild-type *R. sphaeroides*. JPA467: non-motile Δ*fliA*. JPA1301: non-chemotactic $\Delta cheY_6$. AM1: the Fla1$^-$/Fla2$^+$ strain from the Dreyfus lab. N29: the Fla1$^-$/Fla2$^+$ strain from the Sockett lab.

(p-value >0.05 using a Mann-Whitney U-test), indicating that AM1 and N29 are both motile and chemotactic (Fig. 2.1 **A**).

(Vega-Baray et al., 2015) found that Fla2 expression is dependent on growth media. Fla2 expression was initially seen in cells growing in Sistrom's media which contains 1 g/L glutamate and 0.4 g/L aspartate. Glutamate and aspartate were used as attractant in swim plates at a ratio of 1:0.4 (at a total concentration of 100 μM). With these attractants and under aerobic conditions (Fig. 2.1 **B**) AM1 and N29 produce significantly smaller swim diameters than WS8N (p-value <0.05, Mann-Whitney). This implies a difference in motility and/or chemotaxis compared to WS8N. Poggio et al. (2007) concluded that the Fla2 expression is higher under photoheterotrophic not aerobic conditions. Under photoheterotrophic conditions with aspartate and glutamate as attractant (Fig. 2.1 **C**) both AM1 and N29 have significantly larger swim diameters than WS8N (p-value <0.05, Mann-Whitney). AM1 and N29 are also not significantly dissimilar to each other.

This suggests that AM1 and N29 are expressing the Fla2 system and that swim diameter in Asp/Glu gradients is enhanced over the normal Fla1 system exhibited by WS8N, for example the Fla2 system may be faster than Fla1. Alternatively, the putative Fla2 chemotaxis system encoded on *che*Op$_1$ may be being expressed and this chemotaxis system may produce a stronger chemotactic response under photoheterotrophic conditions to aspartate or glutamate than the *che*Op$_2$ /*che*Op$_3$ encoded systems that control Fla1 swimming.

2.2 Flagellar proteins reveal Fla2 expression

Section 2.1 concluded that AM1 and N29 had a different response on swim plates compared to WS8N under different growth conditions and that this is likely the result of Fla2 expression. It was therefore necessary to confirm the flagella systems

by identifying the flagellar proteins. The Fla1 system includes a single, randomly-positioned flagellar filament composed of the protein FliC which is 50 kDa in size. The Fla2 system forms a polar flagellar bundle of several filaments. The Fla2 filaments are composed of the 28 kDa protein FlaA which has 47% sequence similarity to FliC along 91% of the length of FlaA. As FliC and FlaA differ in size, it is possible to distinguish them using SDS-PAGE (Section 6.4) as demonstrated in Woods (2007) which identified FlaA in a Fla1$^-$ strain using SDS-PAGE and Western blotting.

2.2.1 SDS-PAGE analysis

Passing a flagellate bacterial culture repeatedly through a 0.2 mm capillary results in flagellar filaments becoming detached or "sheared" from bacterial cells. Centrifuging this solution at 2060 x g separated the intact cells and sheared flagellar into pellet and supernatant, respectively. The filament proteins in the supernatant can be separated using SDS-PAGE.

WS8N, JPA467, AM1 and N29 were sheared to isolate their extra-cellular flagellar proteins as described fully in Section 6.3. The resulting solution containing sheared flagella was separated by SDS-PAGE on a 4-20% poly-acrylamide gel (Section 6.4) and stained with coomassie blue for visualisation (Fig. 2.2 **A**).

There is a protein in the WS8N sample which corresponds to the Fla1 filament protein FliC (50 kDa). This protein is absent in non-flagellate JPA467 confirming it to be a flagellar protein. Western blotting (Section 6.5) with an anti-FliC antibody (Fig 2.2 **B**) confirms the identity of this band. This band is absent for AM1 and N29 suggesting that their motility is not Fla1-mediated. Western-blotting the same samples with an anti-FlaA antibody shows a band of the approximate size of the Fla2 filament protein FlaA (28kDa) for both AM1 and N29 (which is absent in both WS8N and JPA467) which successfully binds the FlaA antibody (Fig. 2.2 **C**). This shows that shearing and subsequent Western blotting with flagellin-specific

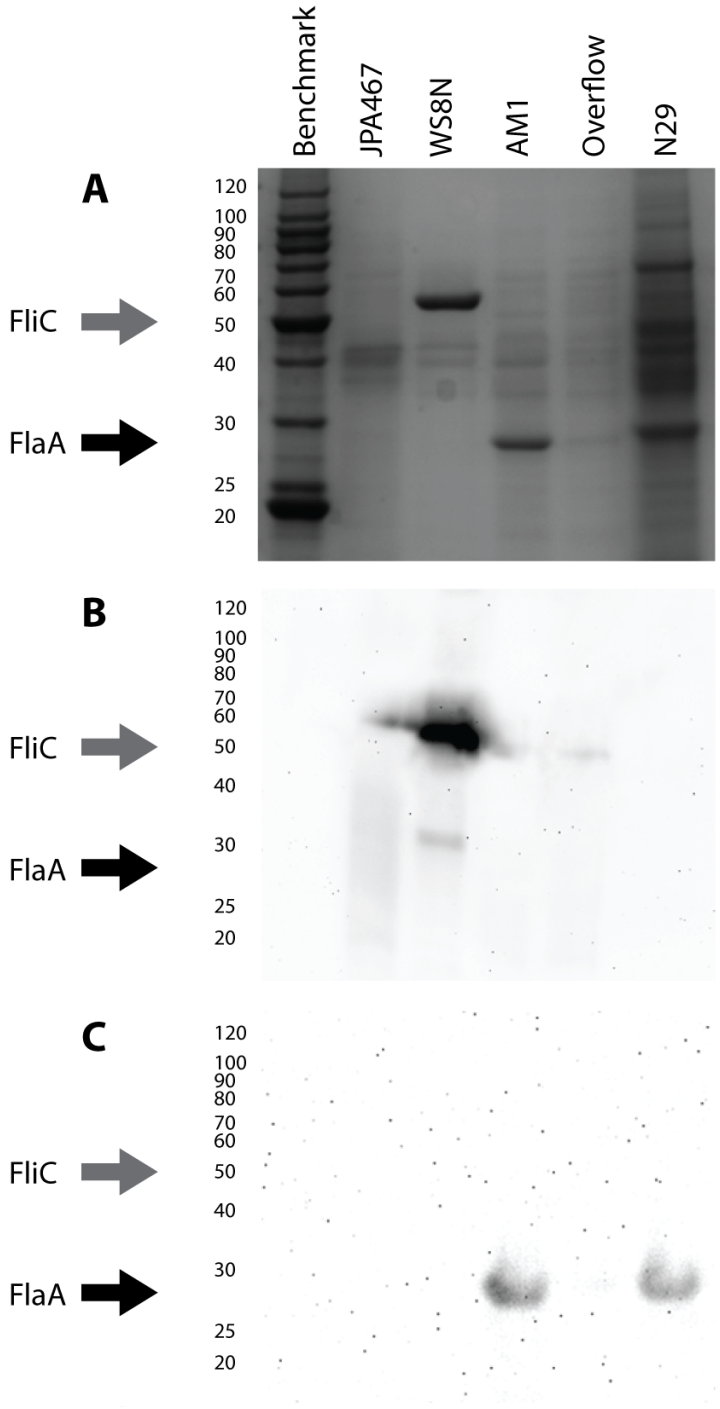

Figure 2.2: **A**: Coomassie-stained SDS-PAGE gel showing sheared flagellar proteins. Numbers represent molecular weights in kDa that were positioned using benchmark protein ladder. Grey arrow represents position of Fla1 flagellin protein FliC. Black arrow represents position of Fla2 flagellin FlaA. Overflow lane contains excess protein sample from AM1 lane. **B**: Western blot of SDS-PAGE gel with anti-FliC antibody. **C**: Western blot using anti-FlaA antibody.

antibodies is a conclusive assay for determining whether strains are expressing Fla1 or Fla2.

2.2.2 Mass Spectrometry confirms flagellar identity

For further confirmation, the flagellin-positive bands from WS8N and AM1 underwent Mass-Spectrometry to unequivocally determine the flagellin identity at the Central Proteomics Facility, University of Oxford.

Mass-Spec procedure

WS8N and N29 were sheared of flagella as described previously (Section 2.2.1) and the flagellar proteins separated by SDS-PAGE. The bands corresponding to the putative filament proteins FlaA and FliC were excised from an SDS gel with a clean scalpel and sent to the Central Proteomics Facility (CPF), University of Oxford for mass-spec. Samples were washed in 25 mM ammonium bicarbonate with 50% acetonitrile and reduced with 10 mM DTT and 55 mM iodoacetamide. Samples were then digested with 0.5 mg trypsin overnight at 37 °C and extracted with 0.1% formic acid in 50% acetonitrile. Analysis of the peptide fragments was performed using a Q Exactive mass spectrometer (Thermo Scientific) coupled to an Ultimate 3000RSLCnano system (Dionex). The CPF uses the programs IProphet, the ModLS algorithm (Beausoleil et al., 2006) and ProteinCenter (Proxeon) to analyse and interpret the peptide sequences, matching them against a custom UniProt-derived WS8N protein sequence database.

2.2.3 Mass-Spec results

Fig. 2.3 shows the sequence coverage of the peptides identified as above. Protein identity was confirmed at a significance of over 99.9%. Fig. 2.3 **A** is the band taken

Figure 2.3: Sequence coverage of proteins identified by Mass Spectrometry. **A**: Identified as Fla1 protein FliC with 89% sequence coverage. **B**: Identified as Fla2 protein FlaA with 100% sequence coverage. Where the protein sequence from the database had peptides match to it, those residues are coloured red. If a region of the known sequence had no peptides match to it, that region remains black.

from WS8N which was identified as FliC. Fig. 2.3 **B** is the band from N29 and was identified as FlaA, in support of Woods (2007) which similarly identified the presence of FlaA using Mass Spec.

2.3 Summary

The aim of the work presented in this chapter was to confirm expression of the Fla2 system in the motile Δ*fleQ* supressor strain AM1 and the motile His-tagged *fliC* supressor strain N29. If the Fla2 system could be expressed then there exists the possibility of studying the chemotaxis system encoded within *che*Op$_1$. This system has never been found to be expressed, and the ability to study how it interacts with its cognate flagellar system and whether it can interact with the well-characterised system encoded by *che*Op$_2$ and *che*Op$_3$ would be both novel and may help to explain further the role of two chemotaxis systems. Initially, AM1 and N29 were inoculated

on swim plates, which can be used to identify how a culture responds to a chemical gradient. Both a strain's ability to sense and initiate a response to a chemical gradient (chemotaxis) and their motility phenotype swimming up these gradients can be measured.

Swim plates identified that AM1 had significantly different swim diameters to WS8N under a range of growth conditions and with different attractants. The swim diameter of N29 was similarly distinct from WS8N and proved statistically no different from those of AM1. To confirm the conclusion that AM1 and N29 were expressing the Fla2 system, the flagellar filaments were sheared and visualised using SDS-PAGE. Western blotting with specific anti-FlaA or anti-FliC antibodies correctly identified the expressed flagellins. Further confirmation using mass-spectrometry supported the existing work from citePoggio2007 and Woods (2007) that the flagellar proteins from AM1 and N29 were FlaA, and therefore that these strains were expressing the Fla2 system.

Returning to the swim plate data with the certainty that AM1 and N29 are Fla2$^+$ raises the question of why Fla2$^+$ strains produce different-size swim diameters to Fla1$^+$ strain WS8N. According to Poggio et al. (2007) photoheterotrophic conditions with Sistrom's media is most conducive to Fla2 expression. Under these conditions, Fla2$^+$ strains AM1 and N29 produce larger swim diameters than WS8N. This could be a result of a different motility phenotype of AM1 and N29 compared to WS8N under photoheterotrophic conditions. Alternatively, the chemotaxis system that governs Fla2 rotation may respond more favourably to aspartate and glutamate than does the system that governs Fla1. The Fla2 chemotaxis system, encoded within *che*Op$_1$, has hitherto not been expressed under laboratory conditions. Further experiments were designed to study the motility of Fla2$^+$ strains and to test the expression of the different chemotaxis systems in Fla2$^+$ strains.

Chapter 3

Novel characterisation of Fla2

The previous chapter confirmed the presence of Fla2 expression by identifying the filament protein using Western blotting and mass-spec. The aim of this chapter is to find alternate methods of identifying the Fla2 system that are less expensive than Mass-Spec. These assays would also allow further characterisation of the Fla2 system by describing how it functions. This might in turn explain why *R. sphaeroides* has two flagellar systems, one of which has not been observed to be expressed in wt WS8N under any lab conditions.

The previous chapter concluded that the Fla2 motility exhibited by AM1 and N29 may have two facets that distinguish it from Fla1$^+$ WS8N. It's possible that the *che*Op$_1$ system is expressed in conjunction with Fla2 which opens up the avenue of exploring how *che*Op$_1$ functions and signals to the Fla2 system. Because of the difference in swim diameters under a range of conditions, it is also possible that Fla2 motility has an alternate phenotype to Fla1 driven motility.

3.1 Microscopy provides several possible assays to distinguish Fla1 from Fla2

3.1.1 Fla1 and Fla2 flagella are visually similar when stained

The Fla1 system in *R. sphaeroides* features a single, randomly positined flagellum as opposed to the Fla2 system which is defined by a polar bundle of flagellar filaments. It was hoped that this bundle of Fla2 flagella filaments would be visible and easily distinguished from the single Fla1 flagellum using light microscopy as they appeared notably different in TEM images from the Dreyfus laboratory (Fig. 1.9). Fig. 3.1 shows cells visualised at x100 magnification after treatment with the Ryu stain (Section 6.2) which uses a mordant to thicken the filament before adding a dye (Ryu, 1937; Heimbrook et al., 1989).

WS8N, AM1 and N29 all have visible filaments which the non-flagellate strain JPA467 is lacking (Fig. 3.1). The Ryu stain is therefore capable of staining both Fla1 and Fla2 *R. sphaeroides* filaments. However, the single filaments of WS8N are identical by eye to the AM1 and N29 flagellar bundle using this stain. It is concluded that the filaments in the Fla2 bundle may have become attached by the stain, giving the appearance of a single filament. However, the fact that these flagella can be stained and visualised using light microscopy allows further inspection and possible characterisation.

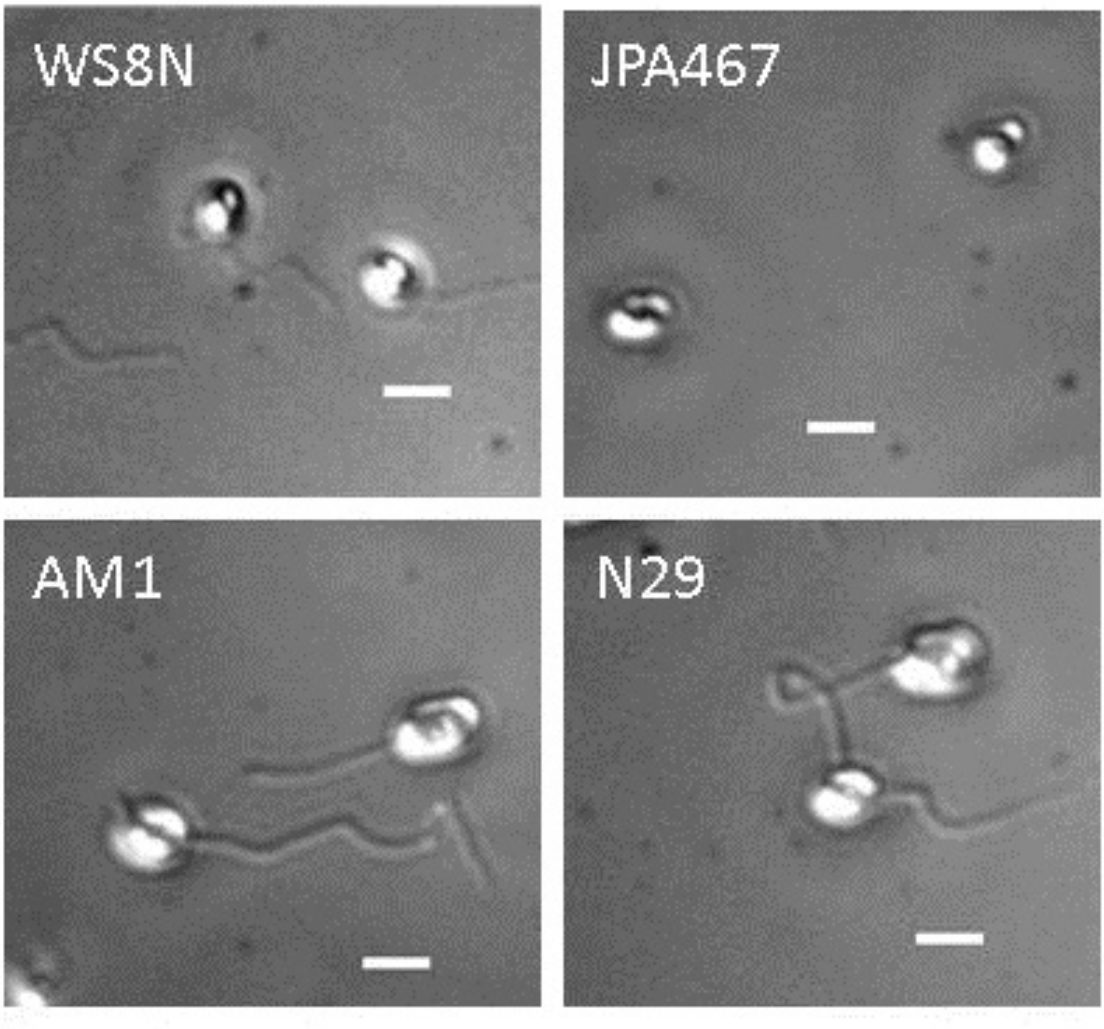

Figure 3.1: Representative flagella visualised using Ryu stain. The Ryu stain thickly coats cellular material including flagellar filaments (Heimbrook et al., 1989). WS8N, AM1 and N29 have apparently similar flagella. Non-motile JPA467 negative control has no visible flagella. Scale bar = 1 μm . Images are typical examples of flagella seen for each strain.

3.1.2 Using microscopy to measure filament thickness

To determine whether Fla1 and Fla2 flagella could be distinguished using microscopy with the Ryu stain, the stained flagellar thickness was examined. Fla1 filaments have been measured by the Dreyfus laboratory to be 40 nm in diameter, approximately double the thickness of Fla2 filaments at 20 nm (Poggio et al., 2007). The number of Fla2 filaments in a bundle remains unmeasured. However, Poggio et al. (2007) stated that 1, 2 or 3 were common, and Fig. 1.9 (reproduced from that article) shows 5 filaments. Fig. 3.2 shows the possible orientations of 1, 3 and 5 filaments.

The thickness of the bundle therefore ranges from 20 nm to 60 nm depending on how many and how tightly packed the filaments are.

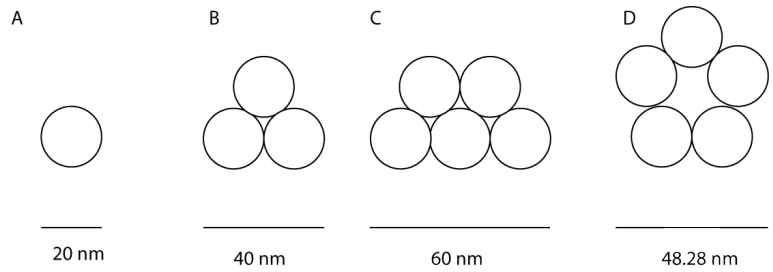

Figure 3.2: Different orientations of the Fla2 bundle if 1-5 filaments were glued together by the Ryu stain

WS8N, AM1 and N29 were treated with the Ryu stain described previously (Section 3.1.1) and images captured using light microscopy as described in Section 6.2. An example of a stained cell is shown in Fig. 3.3. The cross-section of the Fla2$^+$ cell's filament has been highlighted by a thin white line, 38 pixels or 2 μm in length.

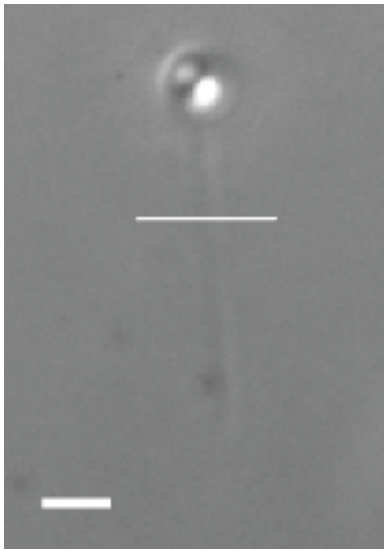

Figure 3.3: Flagellar filament visualised with Ryu stain using the assay from Section 6.2. Thin white line across the filament cross-section used to determine grey value of pixels along its length. Scale bar (thick white line) equals 1 micron, or 19 pixels.

It is clear from Fig 3.3 that the Ryu stain thickens the filament. Each pixel in this figure is equal to 53 nm and so a difference between 20 nm and 40 nm is unlikely to be measurable at this resolution. However, it was hoped that there might be a proportional difference in the thicknesses of stained Fla1 filaments and Fla2 flagellar

bundles.

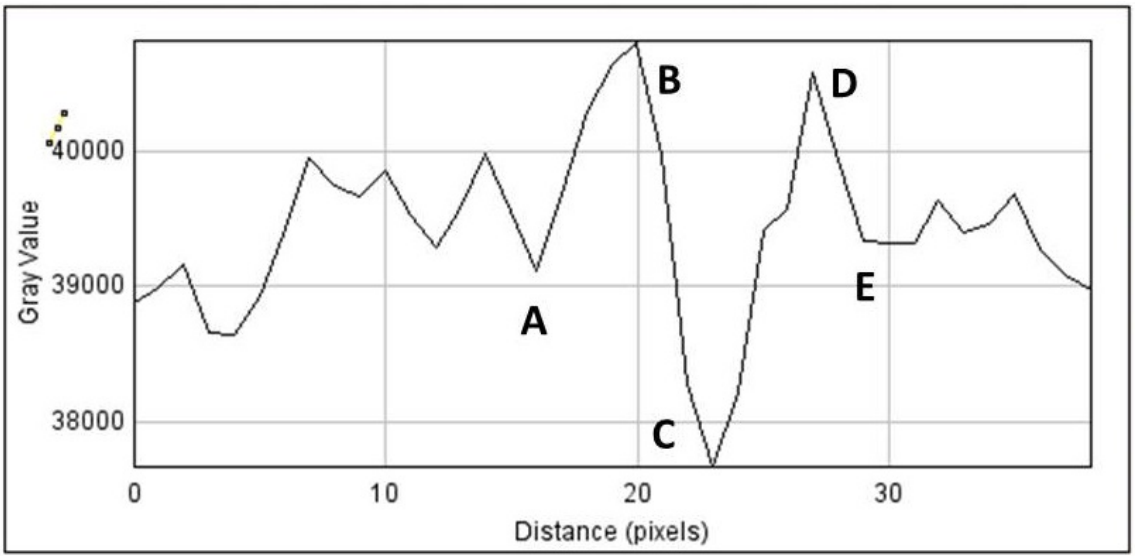

Figure 3.4: Graph of pixel grey value along the length of a 38 pixel line from Fig. 3.3 across the cross section of a filament. The peak **B**, trough **C** and the peak D are a result of the DIC effect on a filament.

The flagellate cells were imaged using DIC microscopy for its ability to created a contrasted, high-resolution image with a pseudo-3D effect. Objects imaged in this way have distinct shadows and highlights as a result of DIC. In consequence, filaments appear to have a light side and a dark shadow causing the grey value across the cross-section of filaments to follow a pattern of light and dark. The image processing program ImageJ (Abràmoff et al., 2004) was used to plot the grey value of the pixels along the filament's cross section. To illustrate this, the grey value of the pixels along the 2 μm line across the filament in Fig. 3.3 have been plotted in Fig. 3.4.

The plot above shows the pattern of pixel grey value that develops across the filament. The pattern can be interpreted as points **A** through **E**.

- a peak (**B**) between point **A** and point **C**
- a trough (**C**) between the two peaks **B** and **D**
- a peak (**D**) between point **C** and point **E**

Measuring the distances between these points gives a measure of the stained filament diameter and may show a difference between the single 40 nm diameter Fla1 filament and the bundle of 20 nm diameter Fla2 filaments.

Fig. 3.5 shows the distances between points **A** through **D** for WS8N Fla1 filaments and Fla2 filaments from AM1 and N29. Distances including point **E** were highly variable regardless of strain and so are not included in this figure.

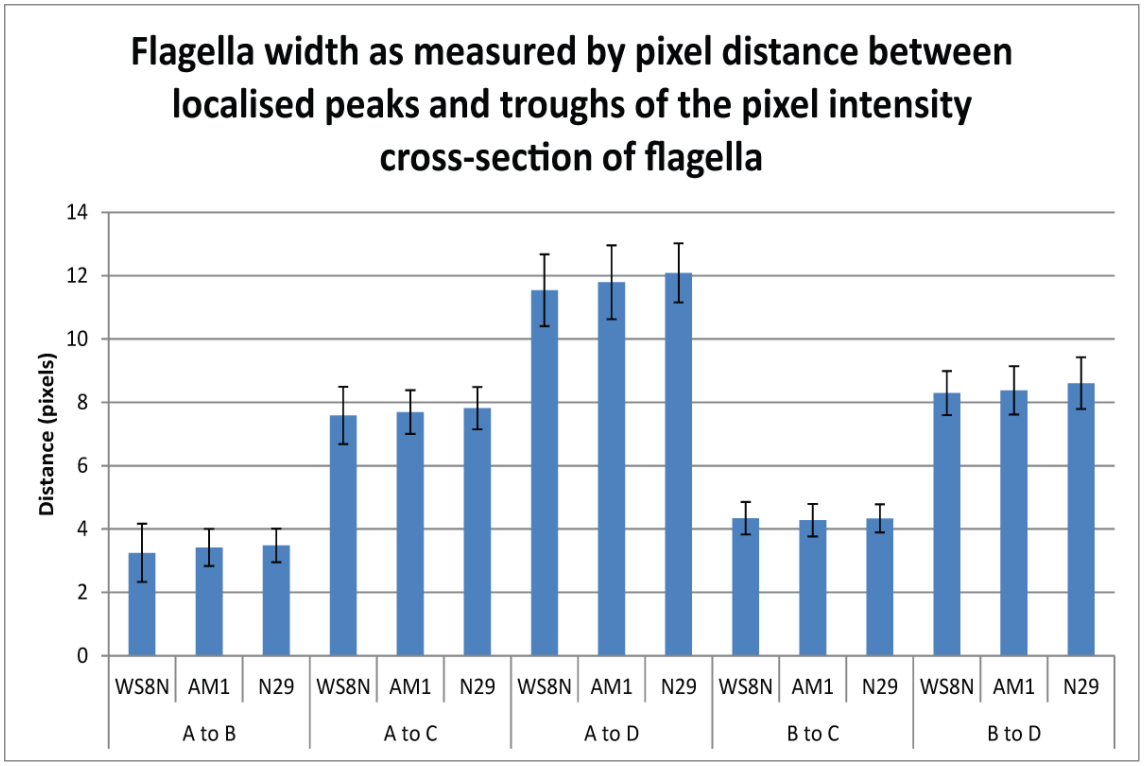

Figure 3.5: Graph of flagella thicknesses measured using pixel grey values along the cross-section of a filament. 31 WS8N, 40 AM1 and 27 N29 filaments were measured and the mean distances graphed between set peaks and troughs shown in Fig 3.4. Error bars represent 1 standard deviation from the mean.

Between 27 and 40 filaments were measured per strain and the various distances between points plotted in pixels. The distances were reliably similar between strains, which implies that the Fla2 bundle does not vary in thickness when stained in this manner, despite having a range of diameters dependent on the number of filaments within the bundle. Additionally, none of the distances provided a distinction between Fla1 and Fla2 as was hoped. It is therefore concluded that the Ryu stain coats flagella so thickly that the difference between a Fla1 filament and either a Fla2

filament or a Fla2 bundle is not distinguishable when measured with this assay.

3.1.3 Flagella can be distinguished using positioning

Poggio et al. (2007) found that the Fla2 flagella system was positioned at the cell pole, whereas the Fla1 system is randomly positioned around the cell body. Using the microscopy images of Ryu stained cells, it was hypothesised that Fla1$^+$ and Fla2$^+$ strains could be distinguished using flagella positioning.

A preliminary assay was performed using a total of 56 WS8N, 81 AM1 and 40 N29 flagellate cells grown under photoheterotrophic conditions. Images were numbered and randomised to hide their strain classification and flagella scored as polar or non-polar by eye. If the position of the filament was unclear the flagella remained "uncategorised". This was common, particularly in spherical or near-spherical cellls. *R. sphaeroides* grown photoheterotrophically alters cell shape from rodlike to almost coccoid (Slovak et al., 2005), resulting in an abundance of spherical, flagellate cells that could not be categorised. The results of this assay are shown in Fig. 3.6.

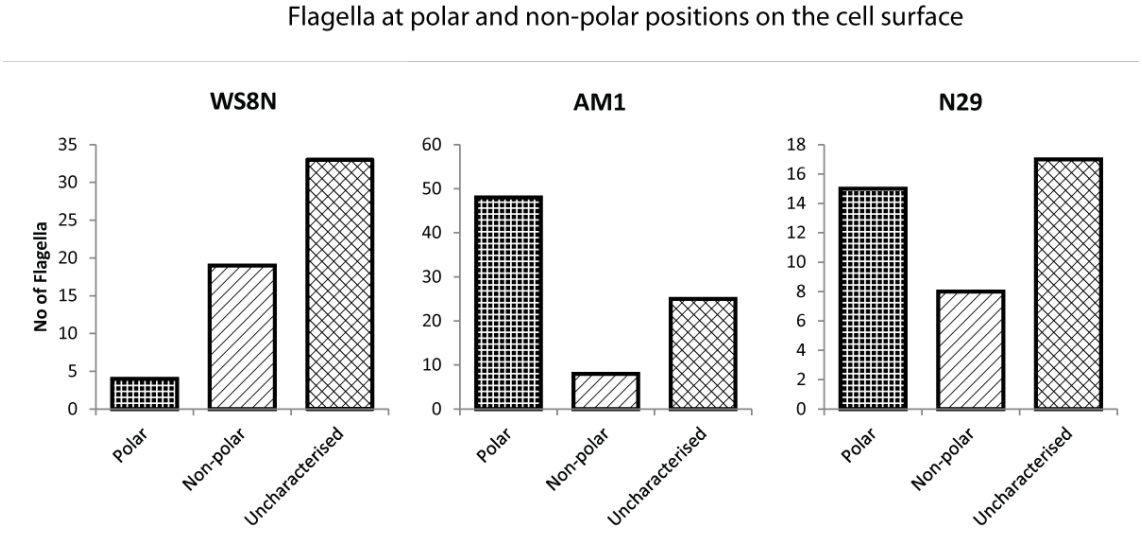

Figure 3.6: Polar, non-polar and uncategorised flagella measured by eye using the Ryu stain.

Firstly, it should be noted that in all 3 cases there are a high proportion of uncategorised cells. The percentages of only categorised cells (polar or non-polar) are

presented in Table 3.1. As the flagellum in WS8N is randomly positioned, it was expected that there would be a larger number of non-polar flagella in the sample. Also present would be flagella that had been randomly positioned at the cell pole. It was also expected that the majority of AM1 and N29 flagella would be found at the poles.

Strain	Categorised total	Polar (%)	Non-Polar (%)	Categorised	Matches Prediction
WS8N	23	17.4	82.6	Non-polar	Yes
AM1	56	85.7	14.3	Polar	Yes
N29	23	65.2	34.8	Polar	Yes

Table 3.1: Comparing the observed flagella position against the predicted position based on percentage of polar and non-polar categorised flagella. Preliminary data from 23 WS8N, 56 AM1 and 23 N29 cells that could be categorised as either polar or non-polar.

Despite a low number of categorised flagella for each strain, this assay is still capable of categorising the position of Fla1 and Fla2 flagella correctly. Fla1 flagella are randomly positioned and hence not found in abundance at the cell pole. Fla2 flagella are found primarily at the cell pole. The significance of this result will be discussed further in Section 3.3.

3.2 Free Swimming

Swimming behaviour is a valuable method of defining and comparing flagellate bacteria, as well as being an important phenotypic measure of how changes to the motility or chemotactic pathway affect changes in the cell (Berg and Brown, 1972; Poole et al., 1993). Elements of motility that are of particular value are the distribution of swimming speeds and the frequency of tumbling events (Rosser et al., 2013). Due to the relatively recent discovery of Fla2 expression, the current scientific literature does not contain characterisation of Fla2 motility properties. Therefore, it was decided to study the free swimming capabilities of $Fla2^{+}$ strains.

3.2.1 Data Gathering

Mid-log *R. sphaeroides* cultures were diluted 5x in 10 mM PIPES (pH 7.2) and samples placed in 0.2 x 2.0 mm glass capillary tubes. 2 minute videos at 50 Hz, 20x magnification were captured for each capillary tube. Using phase contrast microscopy, 3 videos were taken for a minimum of 3 biological repeats per strain.

3.2.2 Choosing parameters for processing

During processing it is necessary to set parameters for the programs used. $Fla1^+$ has previously been subjected to the tracking software and parameters have been chosen that allow for proper analysis. The Fla2 system has not previously been analysed in such a way and therefore parameter values for $Fla2^+$ strains are unknown. However, as can be seen in Section 3.2.5, the motility patterns of AM1 and N29 appear by eye to be not overly dissimilar from WS8N. Therefore, it was decided that for consistency it would be appropriate to use the Fla1 set parameters for both $Fla1^+$ and $Fla2^+$ strains.

3.2.3 Tracking Software

Tracks were generated using software developed by Dr. C. Yates and Dr. T. Wood (Wood et al., 2012). The software identifies objects that move frame to frame by noting differences in pixel intensity against the background and tracks these objects through the video using probability densities until they move out of focus or out of frame. The Niblack algorithm was used with the following parameters:

- Disk radius = 15
- Upper weight = 3
- Lower weight = 3

- Min cluster size = 5

A representative set of tracks is shown in Fig. 3.7.

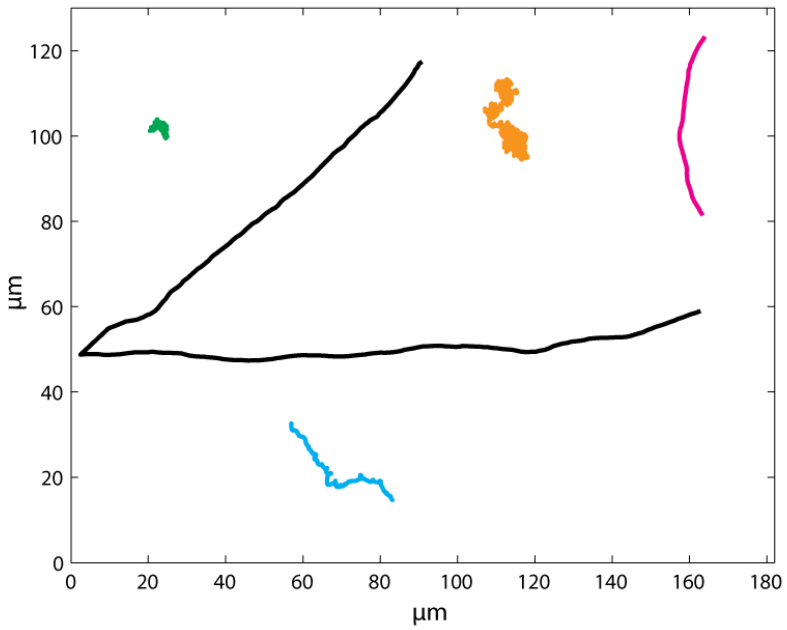

Figure 3.7: Representative tracks from the Tracker software. Each coloured line is an object identified by the Tracker program that moves within the field of view. Example tracks include non-motile (green), drifter (orange), smooth (pink), corkscrew (cyan) and WT run-stop-run (black).

The figure contains a field of view from the videos captured for the tracking software. Tracks are visualised as a coloured line that shows the objects movement from frame to frame. Fig. 3.7 contains examples of various types of tracks that can occur. A non-motile track is shown in green, and a typical run-stop-run track is in black. Also shown are types of tracks that need to be removed using a censor program. These include a "corkscrew" cell (cyan) which occurs when the center of the cell is off-balance as it moves, a common occurance if a cell is dividing. Also shown is a "smooth swimmer" (pink) which is a track of a swimming cell with no changes in direction resulting from a stop. Non-motile cells (green) are a consequence of dead cells or cells that have become sheared during handling. These also create a track, as they move due to Brownian motion. They may also be buffeted by passing motile cells, resulting in "drifters"(orange). The censoring software is designed to remove

these undesirable tracks.

3.2.4 Censoring

Unusable tracks are removed from the dataset to avoid skewing the true motility pattern. There are 4 categories of unusable tracks:

- "Jumps" occur as an artifact of the tracking software. Cells swimming past or close to each other can be erroneously stitched together. The frame-to-frame transition of this jump is faster than would be expected if the track was correctly following the movement of a single cell. Therefore, any transition that is greater than twice the average transition speed (40 μm/s) discounts that track.

- "Truncated" tracks refers to short tracks that occur when a cell swims out of focus. These tracks are discounted because they skew the data to show a higher number of runs. A set minimum track distance discounts these (measured in frames).

- Non-motile cells are removed because their tracks will skew the data to show a misleadingly high number of stops. "Drifters" occur when non-motile cells are buffeted within their environment and show some movement which can be atributed to motility by the program. These are removed by calculating the minimum bounding radius to a track which is the radius of the circle needed to encapsulate the entire track. This threshold discounts anything which therefore does not move an appreciable distance to be deemed motile. It is calculated by trial and error on a non-motile strain until 99% of those non-motile tracks have been removed. This parameter is then applied to experimental strains.

- "Corkscrew" tracks occur when the cell's center point is off-balance or moves.

This occurs, for example, when a cell is dividing. These tracks can interfere with the data because they are interpreted as a series of stops and short runs. These can be eliminated by sorting all tracks according to their "tortuosity" or how high their median curvature is. Tracks with extremely high median curvatures are more likely to be corkscrewing cells, therefore the top 10% tortuous tracks in a data set are removed. However, it was found that the data for AM1 and N29 contained an abnormally high number of corkscrew tracks. To remove the corkscrew cells, the top 80% of tracks with the highest tortuosity had to be removed by the censoring program for AM1 and N29 and, for consistency, WS8N. We attribute this disparity to the growth conditions that cells were under (Sistrom's media at an OD_{600} of between 0.2 and 0.4, as specified by Poggio et al. (2007)) which encouraged cell growth and division. However it is equally possible that the Fla2 swimming pattern of AM1 and N29 is such that the censoring program recognises it as corkscrewing. Analysis was continued on the low number of remaining cells that the program recognised, however it is with the caveat that the true motility pattern of the Fla2 system may require analysis of the corkscrewing behaviour.

The following parameters were therefore used for censoring in this study:

Type of unusable track	Parameter	Value
Jumps	Top Speed cutoff	90 μm/s
Truncated	Minimum track length	50 frames
Non-motile	Minimum bounding radius	9 μm
Corkscrews	Percentage most tortuous	80%

Table 3.2: Unusable track types and the set parameters for this study.

3.2.5 Representative censored tracks

A representative set of tracks for a non-motile strain (JPA467), a motile Fla1$^+$ "smooth swimmer" (JPA1353) and Fla1$^+$ WS8N are shown in Fig. 3.8. JPA467 is non-motile and the software has detected several objects (cells) which move relative to the background. However, this movement is due only to Brownian motion and the tracks are later picked up in the software as non-motile. JPA1353 is a smooth swimmer that does not produce stops, only runs. These tracks are therefore long and do not contain acute changes in direction typical of Fla1-mediated *R. sphaeroides* motility seen in WS8N. Fig. 3.9 shows representative tracks for AM1 and N29. By eye, as stated in Section. 3.2.2, these tracks look similar to those obtained for Fla1$^+$ WS8N.

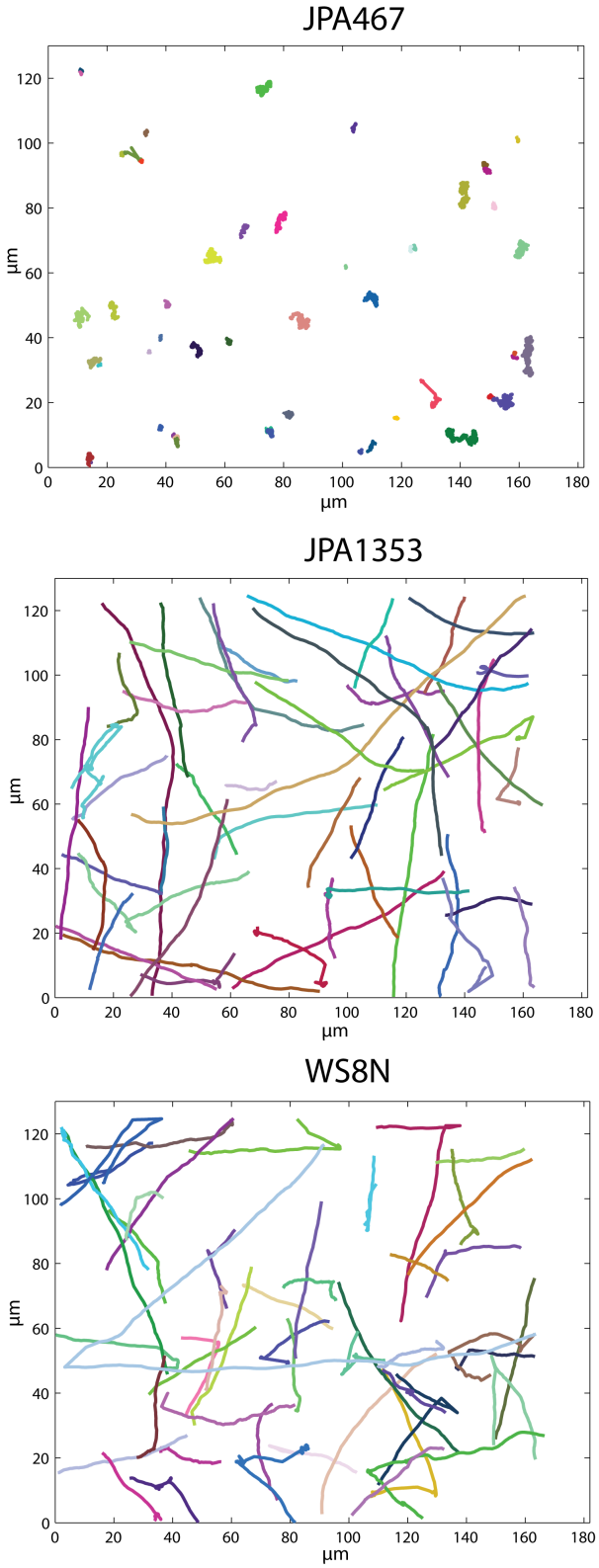

Figure 3.8: Representative tracks for non-motile JPA467, smooth swimming JPA1353 and WS8N. Each coloured line is an object identified by the Tracker program that moves within the field of view.

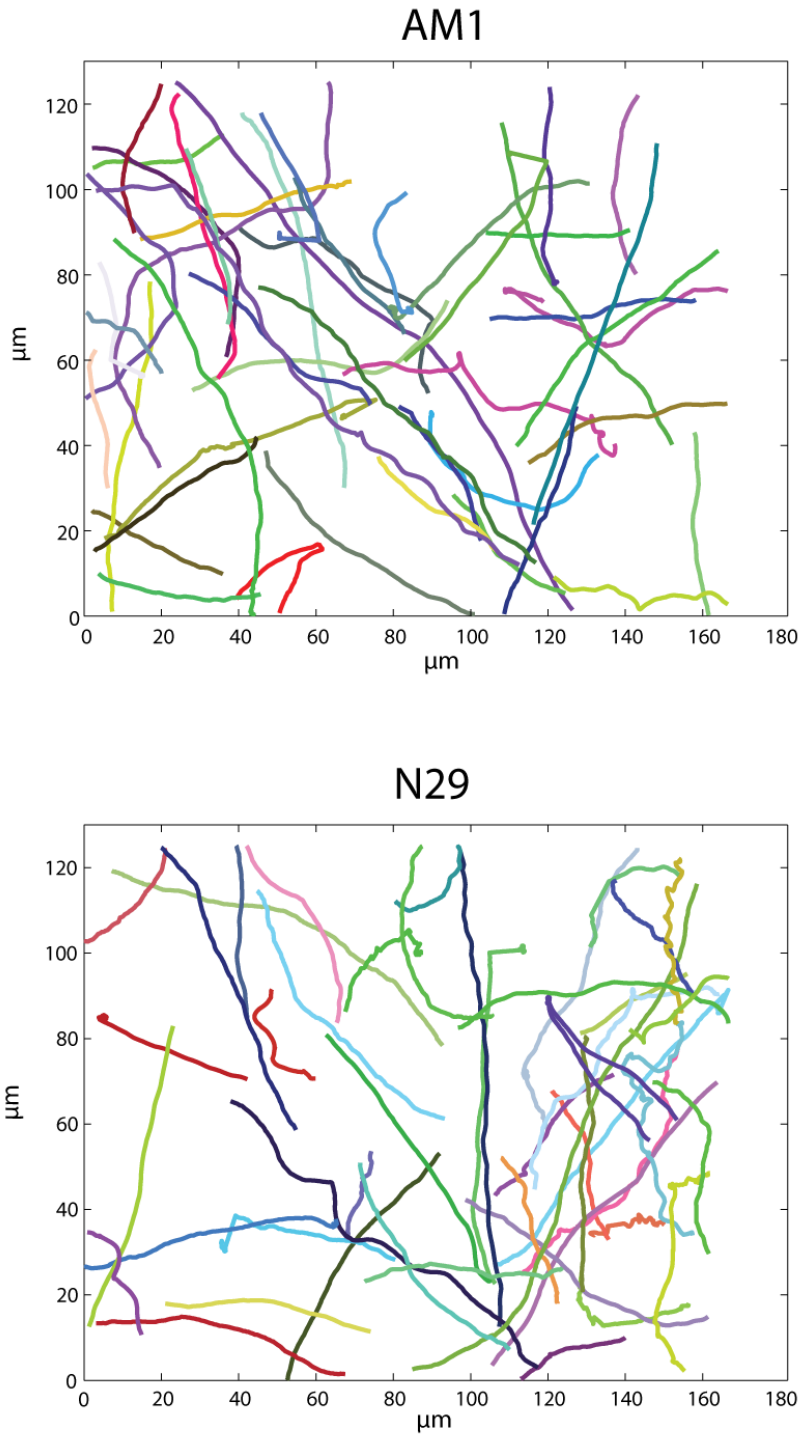

Figure 3.9: Representative tracks of AM1 and N29 identified using the Tracker software.

Tracks are censored as described in Rosser et al. (2013). Finally, using JPA467 as a control for a stopping event and JPA1353 as a control for a run event, the data on strain's runs and stops can be processed in SPSS statistical analysis software (ref).

3.2.6 Fla1 and Fla2 have different free swimming patterns

Median run speed

Fig. 3.10 shows the median run speeds for Fla1$^+$ WS8N and Fla2$^+$ AM1 and N29. The data is presented in the form of boxplots to accurately illustrate the spread of the data. Table 3.3 details the median running speed for the experimental strains and how they compare to the published speed for Fla1$^+$ WS8N.

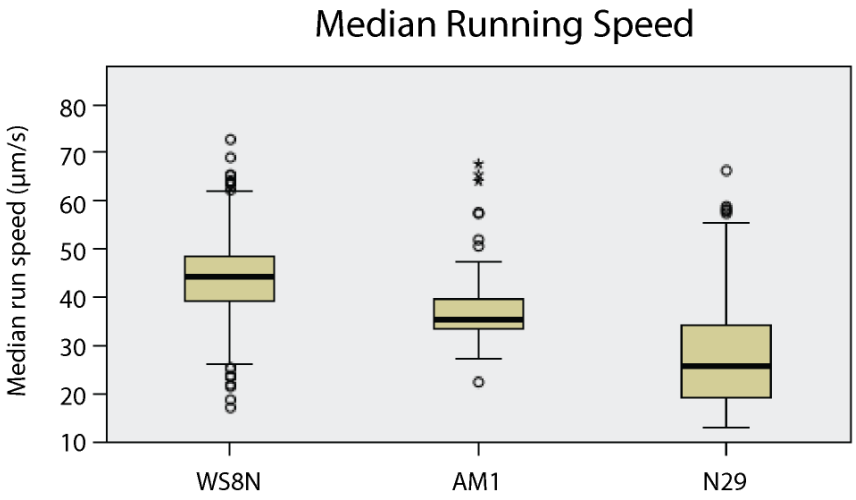

Figure 3.10: Boxplots of the median run speed for WS8N, AM1 and N29. The range of data in this figure is defined by the upper and lower brackets, with outlying data represented by circles or stars depending on the level of deviation from the range. This is a standard production of the SPSS software. The interquartile range is denoted by a yellow rectangle and the mean is at the level of the thick black line.

	Run Speed	Number of cells tested
Published data	40	-
WS8N	44	850
AM1	38	63
N29	28	132

Table 3.3: Summary of data presented in Fig. 3.10. Median run speeds are presented, also the number of tracks these data are derived from. Value of run speed previously known published in Brown (2009)

The median run speed of WS8N for our data was 44 μm/s. This is slightly higher than the published average of 40 μm/s. However, the values were collected in different growth conditions and it is possible for the speed to vary as the boxplot in Fig. 3.10 shows.

Both AM1 and N29 have a median run speed significantly slower than Fla1$^+$ WS8N. This was judged significant to a p-value <0.05 using a Mann-Whitney U-test. This indicates that the Fla2 system has a mean running speed lower than that of Fla1. In Section 2.1 (p 26) it was concluded that AM1 and N29 may be faster than WS8N on a swim plate inoculated under photoheterotrophic conditions with aspartate and glutamate as attractant (Fig 2.1 p 28). This shows that this is not the case, and that WS8N cells may swim faster than AM1 and N29 under photoheterotrophic conditions in Sistrom's media. It should be noted that with a low sample size for AM1 and N29, due to the increased censoring, the statistical significance may not be a true representation of the data.

Additionally, it was expected that as AM1 and N29 are both Fla2$^+$, they would share the same motility pattern and that their mean run speed would be significantly similar. However, N29 has a mean run speed of 28 μm/s, 10 μm/s less than AM1 which is significantly lower. This implies that AM1 and N29 have physiologically different swimming patterns, despite both expressing Fla2. This difference in motility pattern may reflect the difference seen in the swim plate data (Section

2.1.1) and explain why Fla2$^+$ strains have larger diameters under certain conditions than Fla1$^+$ WS8N.

Fraction of time stopped

Fig. 3.11 shows the fraction of time stopped for WS8N, AM1 and N29. This statistic is used to distinguish different types of swimming *R. sphaeroides* cells in De Beyer (2013), which studied smooth and 'stoppy' swimmers. A non-motile cell would have a value of 1 and a swimming track that does not contain a stop would have a value of 0. The number of tracks examined for this parameter was reduced from the above section as only tracks that contained a stop were counted. If all tracks had been used, the tracks without stops would have skewed the data, as this parameter is concerned with the time that a track spends running and stopping. Boxplots have been used to illustrate the spread of the data (Fig. 3.11). A summary of the median values, as well as the published value of this parameter are shown in Table 3.4.

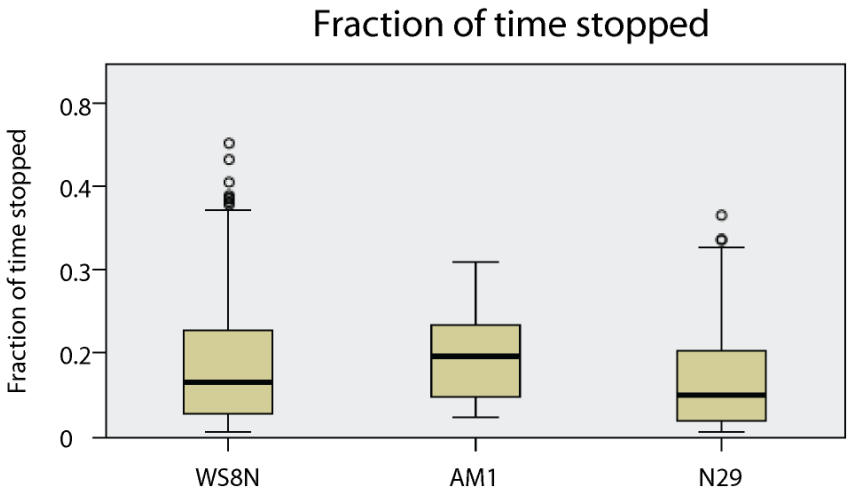

Figure 3.11: Boxplots of the fraction of time stopped for WS8N, AM1 and N29. The range of data in this figure is defined by the upper and lower brackets, with outlying data represented by circles or stars depending on the level of deviation from the range. This is a standard production of the SPSS software. The interquartile range is denoted by a yellow rectangle and the median is at the level of the thick black line.

	Fraction of time stopped	Number of cells
Published data	0.2	-
WS8N	0.17	320
AM1	0.21	17
N29	0.14	79

Table 3.4: Summary of data presented in Fig. 3.11. Median fraction of time stopped is presented, also the number of tracks these data are derived from. Value of time stopped previously known published in Brown (2009)

The published value for the fraction of time stopped of *R. sphaeroides* WS8N is 0.2 (Brown, 2009) which is similar to the value for WS8N presented in Fig. 3.11 and Table. 3.4 which is 0.17. Due to the low number of tracks that could be analysed due to the large number of corkscrewing cells and the removal in the data set of any tracks not containing a stop, it is likely that any statistical significance will be highly prone to error. Therefore, it is argued that the fraction of time stopped for all strains was not dissimilar enough to confirm that this contributes to a different motility pattern to Fla2.

This deviation between the motiliy phenotypes of AM1 and N29 could be due to the separate mutations that have caused Fla2 to express in these strains. Alternatively, it may be due, in part, to the mutations that cause these strains to be Fla1$^-$. AM1 is a Δ*fleQ* strain, lacking the master regulator that controls all Fla1 expression causing a loss of expression of the hierarchy of genes as shown in Section1.7.1. N29, however, is a Δ*fliC* strain. *fliC* is one of the last flagellar genes to be expressed, as it forms the filament. It is only required after the components of the basal body are expressed and the export apparatus formed. Therefore, although it has been proven that FlaA is expressed (Section 2.2) it has not been proven that the only flagella system expressed is Fla2. N29 may be expressing components of both flagella systems, and the difference in motility seen above is due to the combination of both Fla1 and Fla2.

Fla1 and Fla2 were proven to have mutually exclusive expression in Vega-Baray et al. (2015). The Dreyfus laboratory expressed a fluorescent marker tagged to either FliL1 or FliL2, from the Fla1 and Fla2 systems respectively. FliL is proposed to modulate the flagellar motor via the protein MotB (Suaste-Olmos et al., 2010) and was chosen by the Dreyfus laboratory as it is the first gene in the putative flagellar operon and therefore the most likely gene to be expressed downstream of the promoter region. Fluorescence of the two markers and therefore expression of FliL1 or FliL2 was never seen in the same cell (Vega-Baray et al., 2015). Therefore, either the measurement of FliL1 or FliL2 is not indicative of the expression of the whole flagella system or another factor is responsible in N29. FliL1 and FliL2 were chosen as they are found at the putative beginning of the flagellar operons and therefore assured to be expressed when the operon is. Therefore, it is believed that the later option is most likely, that the difference in motility between AM1 and N29 is due to an as yet unknown cause.

3.3 Biofilm Formation

Bacterial species can engage in life transitions from planktonic or motile behaviour to sessile or biofilm-forming (Hengge, 2009). In *E. coli* and *P. aeruginosa* the flagellum is the target for this change. Motility is repressed, driving the cell toward sessile, biofilm-forming behaviour (Kuchma et al., 2014).

To discover whether either the Fla1 or Fla2 systems of *R. sphaeroides* can allow biofilm formation, the ability of Fla1$^+$ WS8N and Fla2$^+$ AM1 and N29 to form biofilms on a solid surface was examined using a biofilm formation assay (Section 6.11).

Briefly, a culture of mid-log cells grown in either SUX or Sistrom's media were inoculated in the wells of a 96-well plate. After 1 hour incubation in photoheterotrophic

conditions the wells were washed, leaving only adhered cells. These were then stained with 0.1 M crystal violet (which has an affinity for the high level of exopolysacharide present in biofilms) washed and the remaining stain extracted and its optical density measured. The OD_{595} is therefore proportional to the concentration of adhered cells after 1 hour of initial biofilm formation.

Fig. 3.12 shows the ODs of strains assayed in this manner, incubated with either SUX or Sistrom's medium.

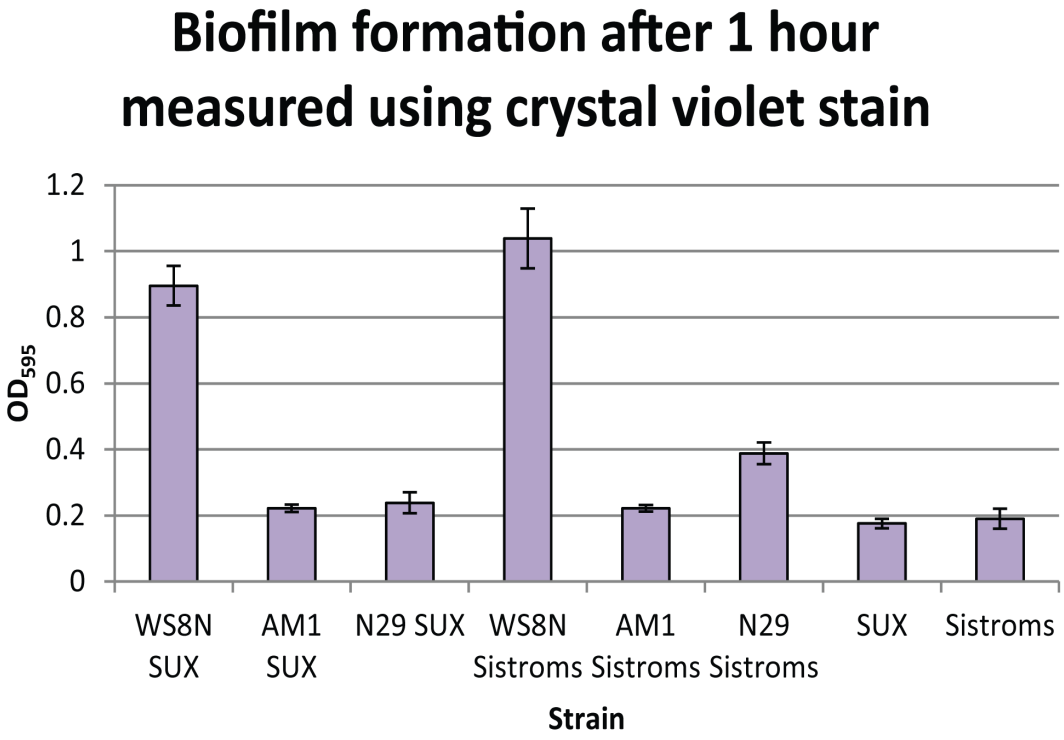

Figure 3.12: Biofilm formation as measured by mean OD_{595} of adhered cells stained with 0.1 M crystal violet. Cells incubated for 1 hour to form biofilms. Data based on 1 biological repeat with the mean OD calculated from 4 technical replicates. Error bars represent 1 standard deviation from the mean.

SUX and Sistrom's media were used to allow for biofilm formation from the promotion of either flagella system. SUX and Sistrom's without inoculation provided a negative control for the OD expected with crystal violet and no cells.

With both media, the OD_{595} for WS8N is significantly higher than uninoculated SUX or Sistrom's. This indicates that WS8N was able to adhere to the well of

the plate and form a biofilm. However, the biofilms of AM1 and N29 have an optical density near that of SUX or Sistrom's, implying that they are unable to form biofilms.

Using the OD_{595}, the ability of AM1 and N29 to form biofilms was calculated relative to WS8N in both SUX and Sistrom's media by subtracting the optical density of SUX or Sistrom's media and dividing by the OD_{595} of WS8N so that the optical density of each strain is a decimal relative to WS8N which has the value 1 (Fig. 3.13).

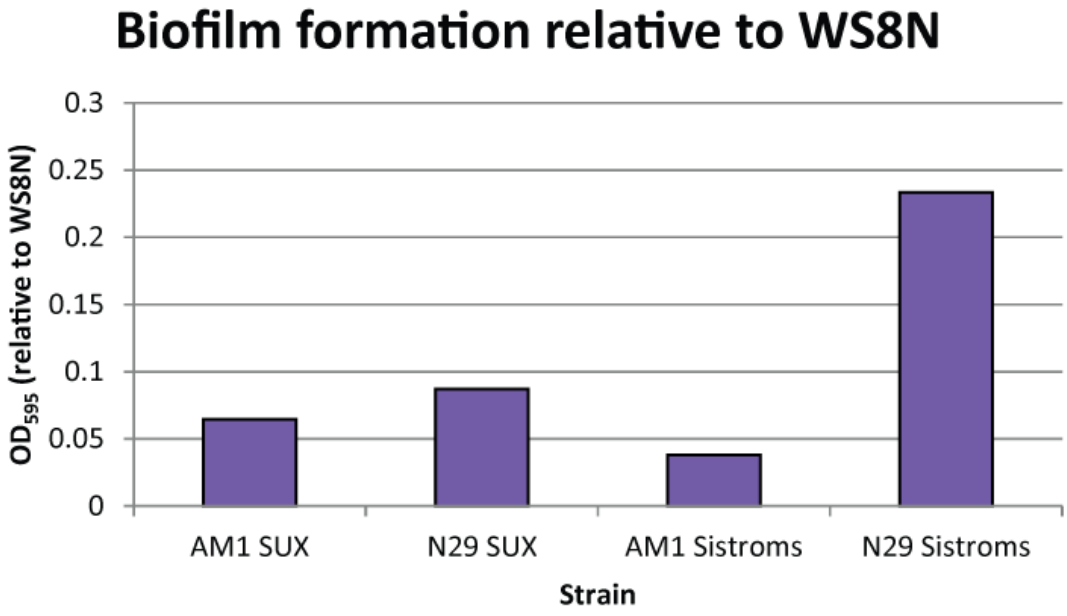

Figure 3.13: Relative biofilm formation as measured against WS8N (value of 1). Cells incubated in SUX or Sistrom's media to form biofilms and OD_{595} measured after 1 hour. OD_{595} of uninoculated SUX subtracted from strains incubated in SUX calculated to reflect the ability to form biofilms relative to WS8N in SUX. The same calculation was made for AM1 and N29 inoculated in Sistrom's media. Data based on 1 biological repeat with the mean OD calculated from 4 technical replicates.

The stained biofilms of AM1 have an optical density of 0.06 that of WS8N in SUX medium. Fla2 is, however, more favourably expressed in Sistrom's than in SUX (Vega-Baray et al., 2015) but under these conditions the optical density is 0.04 that of WS8N. N29 has an OD of 0.09 that of WS8N in SUX and 0.23 in Sistrom's, indicative of heightened biofilm formation in the later condition. However, Fla2

does not appear to be capable of inducing the early stages of biofilm formation.

3.4 Chapter Summary

In this chapter, characterisation of the Fla2 system was performed to compare its phenotype against the well-studied Fla1 system.

Firstly, the appearance of the two flagellar systems was examined using microscopy. Although no difference was found between the flagella in terms of width due to the activity of the Ryu stain, the systems could be distinguished by evaluating their location by eye along the cell length. The majority of flagella for WS8N were correctly identified as randomly positioned and the majority of Fla2 filaments were found at the cell pole as hypothesised.

It was also found that Fla2$^+$ cells were vastly deficient in their ability to colonise a surface in the first hour of biofilm formation compared to Fla1. The optical density of stained biofilm-forming Fla2$^+$ cells was not found to be above 25% that of Fla1$^+$ cells. This separates the flagella into biofilm-forming and non-biofilm forming systems. This is echoed in *E. coli* and in *P. aeruginosa* which are known to switch between a biofilm-forming sessile state and a non-biofilm-forming motile state regulated by c-di-GMP. In *P. aeruginosa* this life transition is dependent on stator interaction with the flagellum. The MotA/B system represses motility and the MotC/D system supports it, although the flagellum structure remains under both conditions. With *R. sphaeroides* , we might be seeing a similar switching pattern where the Fla2 system was the original motile or planktonic system whereas Fla1 was the sessile, biofilm-forming system although evolution has now placed it as the dominant flagellum.

At the end of Chapter 2, it was summarised that Fla2 motility is phenotypically different to Fla1 and that under the correct growth conditions Fla2$^+$ cells might be

faster than Fla1$^+$ cells. Using free swimming software it was determined that the swimming patterns of Fla1 and Fla2 are indeed different and that the Fla2 system is not faster than Fla1 but slower. It was also determined that AM1 and N29 are phenotypically dissimilar, their swimming speeds differing from each other. This implies there is more to Fla2 motility than simply turning on Fla2 expression and turning off Fla1.

Therefore it is necessary to examine the specific effects of the mutations that make AM1 and N29 Fla2$^+$.

Chapter 4

CckA influence on flagellar systems

As previously stated, Poggio et al. (2007) first expressed the Fla2 system in a motile suppressor of a Δ*fleQ* strain. This strain, AM1, was recently sequenced in case Fla2 expression was linked to a mutation in a regulatory gene (Vega-Baray et al., 2015). A mutation was isolated in *cckA* which codes for the histidine kinase CckA (Section 1.13). Deleting *cckA* and reintroducing the mutant allele (L391F) in a Δ*fleQ* strain was sufficient to restore Fla2 motility, indicating that CckA is a major factor in the initiation of Fla2 expression, and that the L391F substitution is critical for this function. Wild-type CckA did not rescue motility when reintroduced (Vega-Baray et al., 2015).

CckA is a key protein in the cell cycle control of α-proteobacteria and of lifestyle switches. In *C. crescentus*, for example, the CckA-CtrA pathway mediates the switch from a flagellated swarmer cell to a non-motile, stalked cell. In the last chapter it was shown that the Fla1 and Fla2 systems have different roles during a lifestyle switch and therefore CckA is a promising target for inspection in *R. sphaeroides*.

It was decided to confirm this mutation in AM1 and discover whether N29 had a

similarly mutated copy of *cckA*. It was also decided to use these mutations to try to induce expression of the Fla2 system in WS8N without inhibiting the Fla1 system. If this is possible then it might also be possible to express the Fla2 cognate chemotaxis system from *che*Op_1.

4.1 Genome Sequencing

To confirm that AM1 contained a mutation in *cckA*and to discover whether N29 has a mutation which initiated Fla2 expression, AM1, N29 and the Armitage laboratory strain of WS8N underwent full genomic sequencing at the University of Exeter sequencing service (Steve Porter, personal communication) (Section 6.9.10).

Fig. 4.1 shows the bases found in AM1 or N29 that differ from the standard WS8N sequenced genome (GenBank identifier: GCA_000212605.1). Only 2 genes were found to have a mutation occuring in both N29 and AM1.

Both AM1 and N29 have the same mutation (position 2714509) in the gene RSWS8N_13040. This gene (alternatively called *regB* and *prrB*) is part of a regulatory system responding to a cell's redox state (Eraso et al., 2008). The mutation was studied by Vega-Baray et al. (2015) and was found to affect but not solely control motility.

The second mutated gene in both AM1 and N29 was *cckA* (RSWS8N_07570), which manifests as CckA L391F in AM1 and as CckaA G588C in N29. The AM1 mutation was investigated in Vega-Baray et al. (2015) but the identity of a putative Fla2-inducing mutation in N29 was hitherto unknown.

Chromosome	Position	AM1	WS8N	N29	Gene and Description
AFER01000001	47878	G	G	T	RSWS8N_00245 anthranilate synthase component II
AFER01000001	353681	A	C	C	RSWS8N_01715 hypothetical protein
AFER01000001	1195392	A	G	A	RSWS8N_05655 hypothetical protein
AFER01000001	1591529	C	C	A	RSWS8N_07570 multisensor hybrid histidine kinase
AFER01000001	1592120	A	G	G	RSWS8N_07570 multisensor hybrid histidine kinase
AFER01000001	2014263	C	C	A	RSWS8N_09645 Sulfotransferase
AFER01000001	2155941	G	G	T	RSWS8N_10340 succinate dehydrogenase flavoprotein subunit
AFER01000001	2714509	T	C	T	RSWS8N_13040 integral membrane sensor signal transduction h
AFER01000001	2862167	A	G	G	RSWS8N_13755 50S ribosomal protein L10
AFER01000002	311247	A	G	G	RSWS8N_16629 ABC Fe+3 siderophore transporter%2C periplasr
AFER01000002	436332	A	C	C	RSWS8N_17214 ApbE family protein
AFER01000002	620635	G	G	A	RSWS8N_18064 chromosomal replication initiator DnaA domain

Figure 4.1: The position, identity and gene description of substitutions found in the AM1 and N29 sequenced genomes that differ from WS8N. *cckA* is identified here by its gene identifier RSWS8N_07570.

4.2 Mutations in CckA may alter structure or function

The domain architecture of CckA is shown in Fig. 4.2. The position of the G588C mutation from N29, as well as the position of L391F from AM1 are shown.

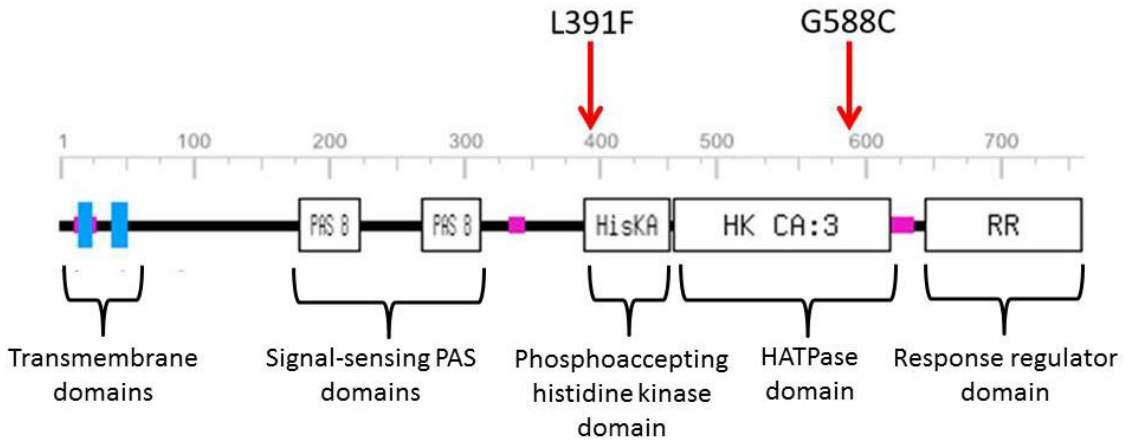

Figure 4.2: Domain architecture of CckA showing the position of the L391F and G588C mutations

CckA is a homodimeric protein with several key functional domains. There are two transmembrane domains at the N-terminal end of the protein, which anchor it to the membrane. A PAS domain senses an as-yet-unknown stimulus and causes autophosphorylation of the HisKA domain which is usually also responsible for dimerisation.

The HATPase domain assists with autophosphorylation by binding the ATP necessary as a phosphoryl donor (Stock et al., 2000). Phosphorylation occurs *in trans* with the HATPase domain of one monomer phosphorylating the HisKA domain of the other monomer. The function of the response regulator (RR) domain of CckA is not completely understood. The RR domain is a member of a domain family found chiefly as phosphoryl receiver domains in response regulator proteins. Whereas CckA is primarily a kinase, it also demonstrates phosphatase activity, removing the phosphoryl group from, and therefore deactivating, CtrA-P (Chen et al., 2009). The method of CckA phosphatase activity isn't fully known. The activity of the HisKA and HATPase domains has been implicated in other kinase/phosphatase proteins (Gao and Stock, 2009) but RR domains have also been theorised to act as competition to the cognate receptors to stabilise the rate of phosphotransfer (Laub and Goulian, 2007). It is possible that the CckA RR domain functions in this way to aid phosphatase activity.

The mutated L391 residue in AM1 is found in the HisKA domain of CckA. Vega-Baray et al. (2015) examined the phosphotransfer ability of WT CckA and CckA L391F. The conclusion was that there is increased phosphotransfer from CckA to CtrA in AM1. This increase may lead to the expression of the Fla2 system. In N29, the mutated G588 residue is present in the HATPase domain. It is unknown whether this mutation might have a similar effect to CckA function to affect kinase activity, but it might equally affect CckA phosphatase activity resulting in a similar or dissimilar phenotype.

There is no published structure for CckA in the current literature. Instead, the sequence for CckA was aligned against the sequence for CovS, a sensor histidine kinase with a published structure (4I5S, PDB), complete with sensory and signalling domains (Wang et al., 2013). This structure represents that of a typical dimeric histidine kinase to allow putative placement of key residues in relation to each other.

The structure with the conserved histidine residue and the mutated residues previously discussed is shown in Fig. 4.3.

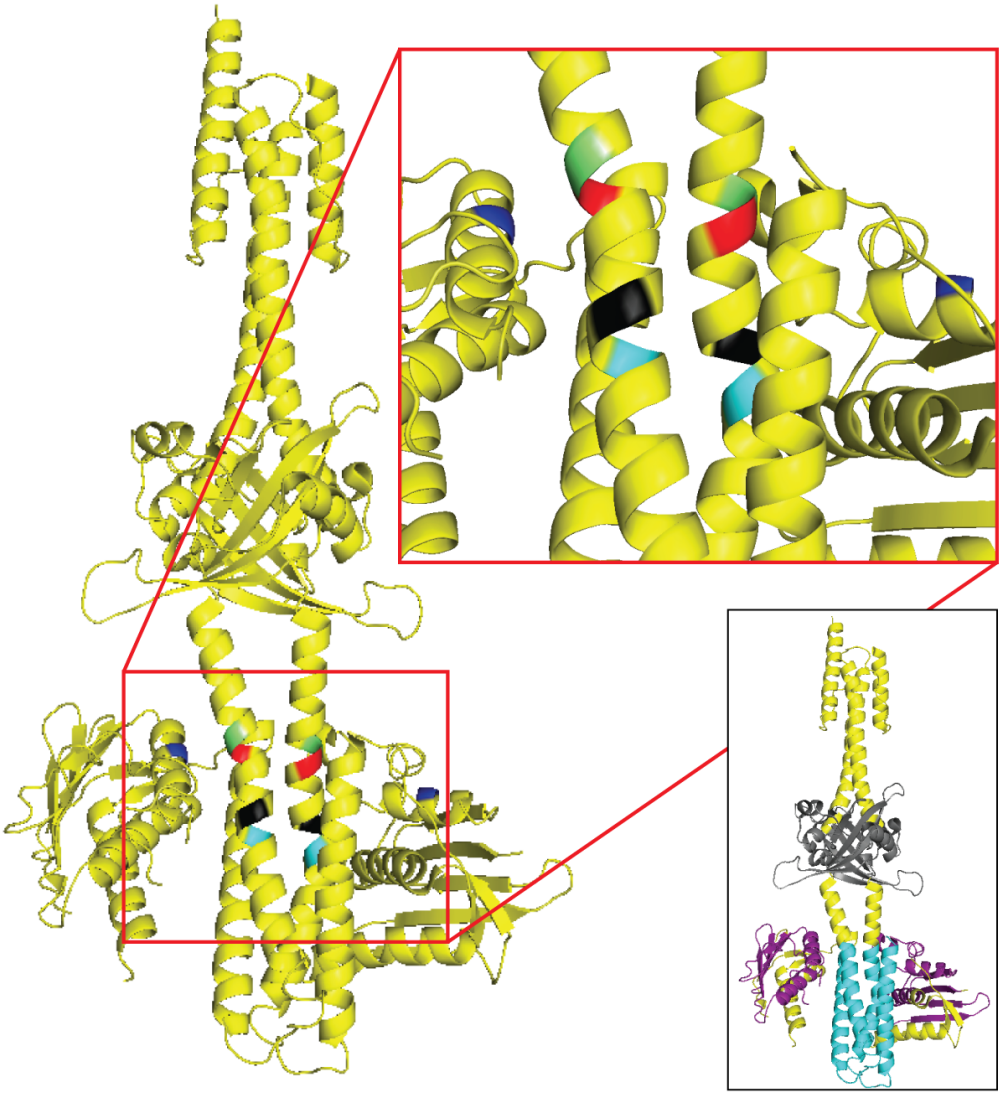

Figure 4.3: Structure of typical histidine kinase CovS (4I5S) from the PDB database with residues highlighted to reflect the approximate position of their counterparts in CckA: conserved phosphorylated histidine (black), L391F mutation from AM1 (red), G588C mutation from N29 (Blue), A387P and F399C mutations identified in Vega-Baray et al. (2015) that cause heightened activity of CckA (pale green and pale blue, respectively). Inset: Domain architecture of 4IS5, PAS (grey), HisKA (cyan) and HATPase (purple)

Fig. 4.3 shows the domain architecture of CckA in grey (PAS), cyan (HisKA) and purple (HATPase). The conserved residue which is phosphorylated by a donor ATP molecule is shown in black. The positions of the mutations L391F and G588C are highlighted red and blue, respectively. Vega-Baray et al. (2015) found two additional

mutations (A387P and F399C) in *cckA* that caused faster autophosphorylation, and therefore heightened activity of CckA but did not change the specificity of the kinase. The positions of the mutated residues are shown in pale green and pale blue, respectively.

There exists the posibility that the G588C has dramatically altered the structure of the protein. Replacing a glycine residue with a cysteine in this dimeric protein increases the possibility that a disulfide bridge can form between the monomers, or if not, that a structural abnormality can occur. L391F may also induce a change in conformation. It is evident that the proximity of these mutations to the conserved histidine, or in the case of G588C between the HisKA and HATPase domains, may alter the function of CckA either directly or indirectly via alteration of CckA structure.

4.3 Replacing *cckA* in WS8N with inducible mutant *cckA*

To see if WS8N could be made to express Fla2 and/or *che*Op_1 by expressing mutant *cckA* it was necessary to delete *cckA* from the WS8N genome so that mutant *cckA* could be expressed free of constitutive *cckA* expression.

4.3.1 Deleting *cckA*

cckA locus

The position of *cckA* on the WS8N genome is shown in Fig. 4.4. CckA is found at the RSWS8N_07570 locus of chromosome 1 according to the published genome sequence (GenBank reference GCA_000212605.1). The 5' end of *cckA* is separated

by 124 from the 3' end of the next upstream gene locus RSWS8N_07575. The 3' end of *cckA* is separated from the 3' end of the next downstream gene RSWS8N_07565 by only 4bp. Using the BPROM promoter identification software (Solovyev and Salamov, 2011), the sequence of *cckA* did not contain any promoters for surrounding genes. Therefore deletion of *cckA* would not affect expression of the genes upstream and downstream. This is supported by work from the Dreyfus laboratory which concluded that a *cckA* deletion produced a viable strain (Vega-Baray et al., 2015).

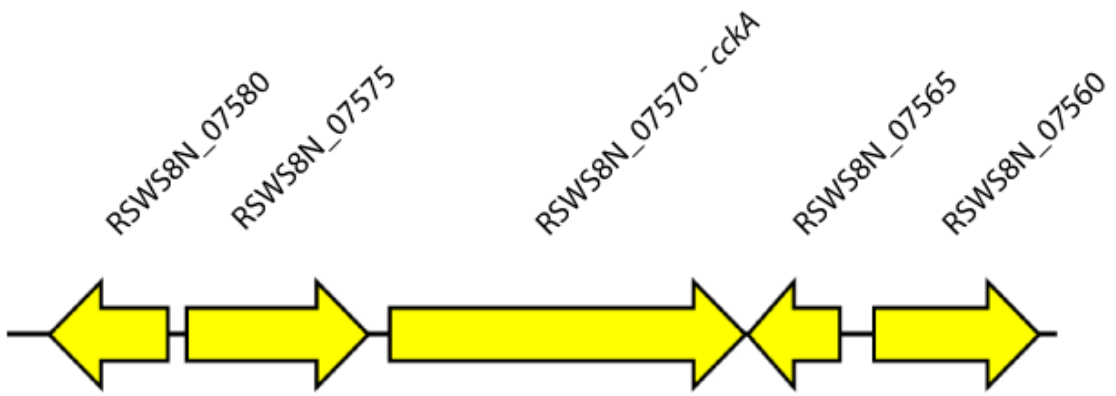

Figure 4.4: Locus of *cckA* and surrounding genes. The genes, in order, are: RSWS8N_07580 DeoR family transcriptional regulator, RSWS8N_07575 RNA cytosine methylase, RSWS8N_07570 *cckA*, RSWS8N_07565 hypothetical protein, RSWS8N_07560 Recombinase A. Diagram represents a spread of genomic DNA 6295 bp in length. Position, length and and orientation of genes taken from the MIST2 database (Ulrich and Zhulin, 2009).

Plasmid Design

The full method of engineering a *cckA* deletion mutant is shown in Fig. 4.5. The 506 bp upstream of *cckA* and 463 bp downstream of *cckA* were amplified using PCR with the ST_cckA_upstream and ST_cckA_downstream primers respectively. The PCR products were separated on an agarose gel and the bands corresponding to the correct size were excised and purified (Section 6.9).

The above primers were designed to include an *Xba*I restriction site and a *Sph*I restriction site on the upstream PCR product and a *Sph*I and a *Hind*III restriction site on the downstream PCR product. The two purified PCR products were di-

gested with their respective restriction endonucleases and ligated together and into pK18*mobsac*B which had been digested with *Hind*III and *Xba*I only. pK18*mobsac*B is kanamycin-resistant and includes a gene that inhibits growth on sucrose, allowing for a selection assay. The ligation resulted in pK18_Δ*cckA* which contained within its multiple coloning site (MCS), in order, the upstream region of *cckA* , a six bp stretch of DNA matching the *Sph*I recognition site and the downstream region of *cckA* .

pK18_Δ*cckA* was transformed into *E. coli* S17-1 λ*pir* and conjugated into *R. sphaeroides* WS8N. A recombination procedure was carried out as detailed in Section 6.9.8 leaving WS8N cells that had replaced *cckA* on their genome with the *Sph*I recognition site. PCR was conducted on these strains using the primers ST_cckA_upstream_F and ST_cckA_downstream _R and the product separated using gel electrophoresis to screen for correct genomic insertion. Strains that produced a 975 bp band rather than a 3328 were successful recombinants.

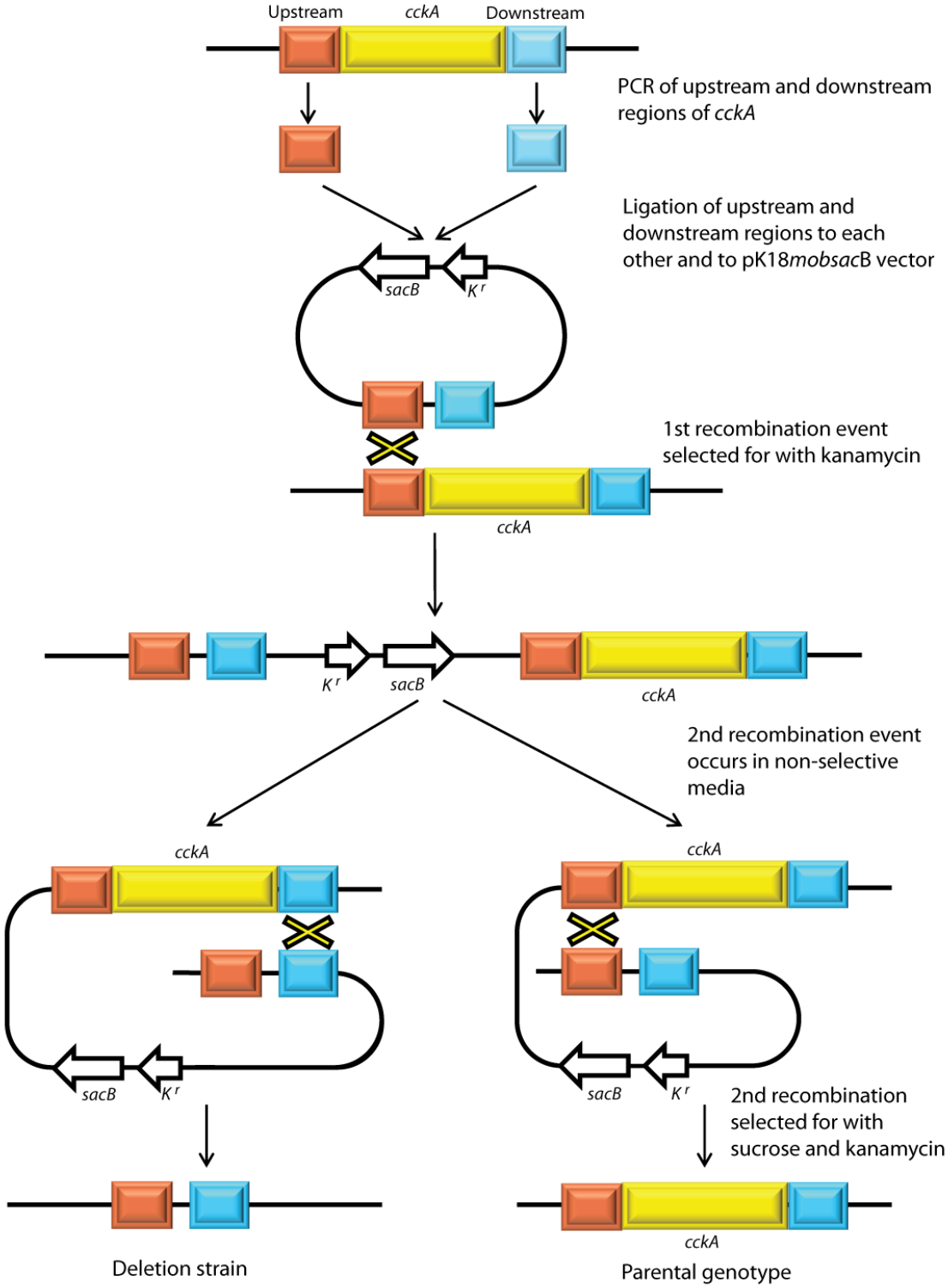

Figure 4.5: Method of deleting *cckA* from the WS8N genome. Upstream (red) and downstream (blue) regions of *cckA* (yellow) amplified from the WS8N genome with primers which engineer a restriction site onto the PCR product. Products digested and ligated into pK18*mobsac*B recombination plasmid which is conjugated into *R. sphaeroides* WS8N. The recombination protocol selects for successful recombinants that have placed the PCR products on the genome in the place of the *cckA* region. The plasmid integrates on the genome during the first recombination event and a second recombination event loses the plasmid by either returning the parental genotype or by deleting *cckA*. A yellow cross symbolises a recombination event.

Confirming CckA deletion phenotype

Vega-Baray et al. (2015) found that their WS8N Δ*cckA* strain would express the Fla1 operon. Casamino acids were found by them to be the biochemicals most strongly associated with Fla2 expression in Vega-Baray et al. (2015). Swim diameters of $Fla2^+$ strains were larger on 0.2% casamino acids than on 15 mM or 100 μM succinate or 0.6% glycerol. Therefore, if a strain is expressing the Fla2 system on these swim plates then we would expect to see a noticable difference in swim diameter. Inoculating our WS8N Δ*cckA* strain (classified JPA2744) on a swim plate with casamino acids under either aerobic or photoheterotrophic conditions revealed that JPA2744 has motility equal to $Fla1^+$ WS8N, as expected (Fig. 4.6, Fig. 4.7).

A

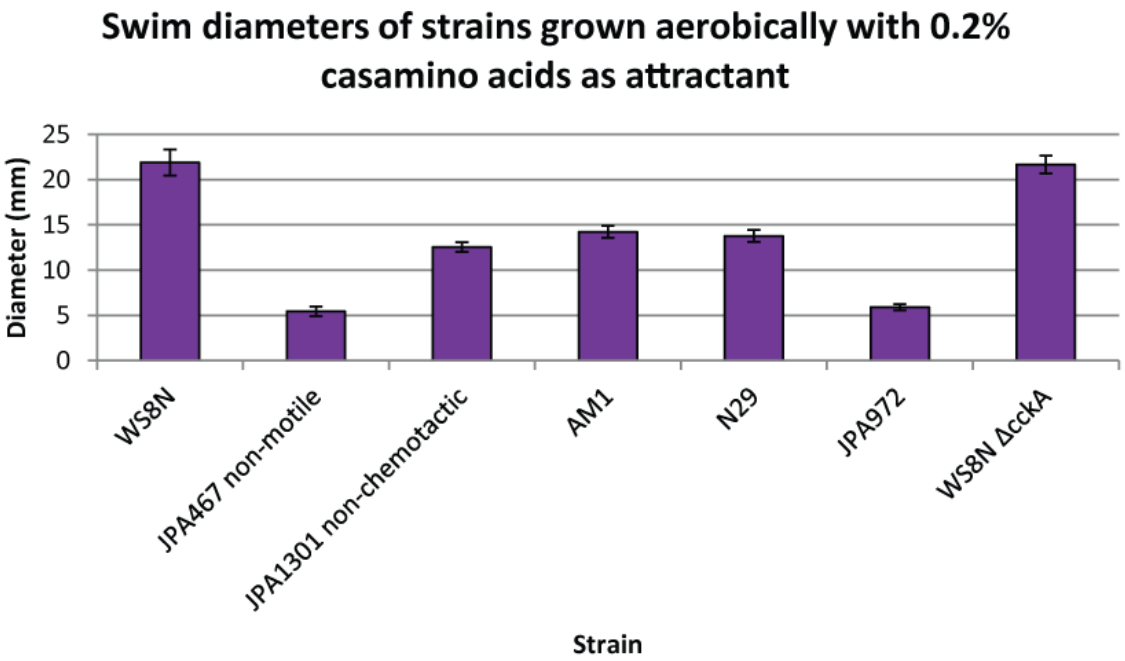

B

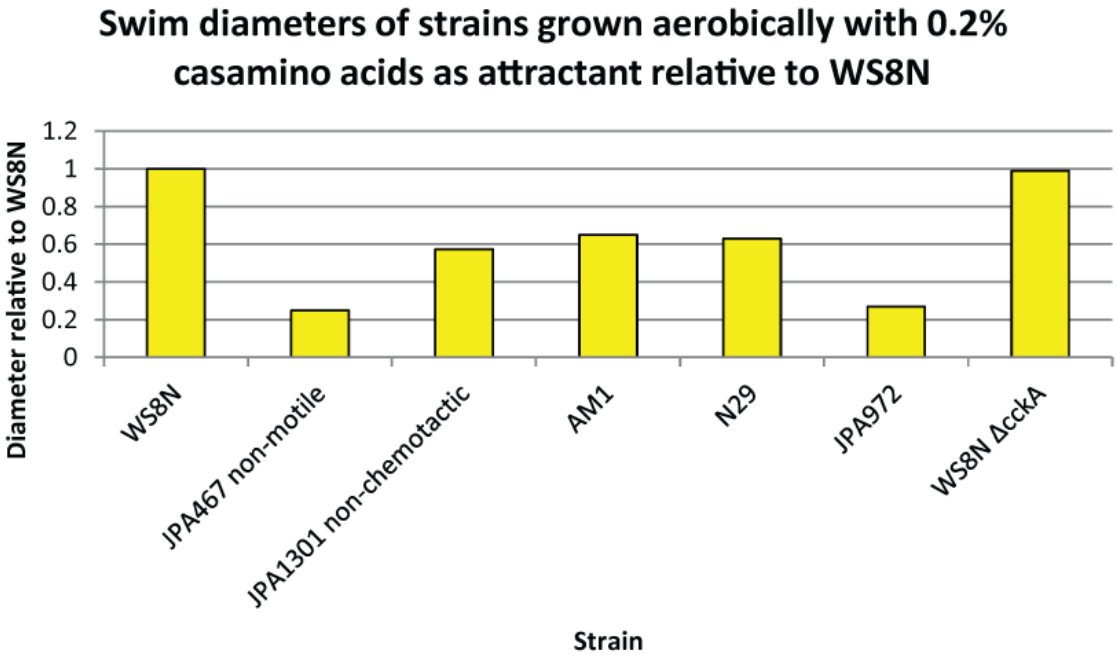

Figure 4.6: **A**: Mean swim diameters of strains using 0.2% casamino acids as attractant. Strains inoculated onto 0.25% agar in M22 medium and incubated in aerobic conditions . Mean values calculated from 3 technical repeats of 3 biological replicates. Error bars represent 1 standard deviation from the mean. **B**: Mean diameters relative to WS8N under aerobic conditions.

A

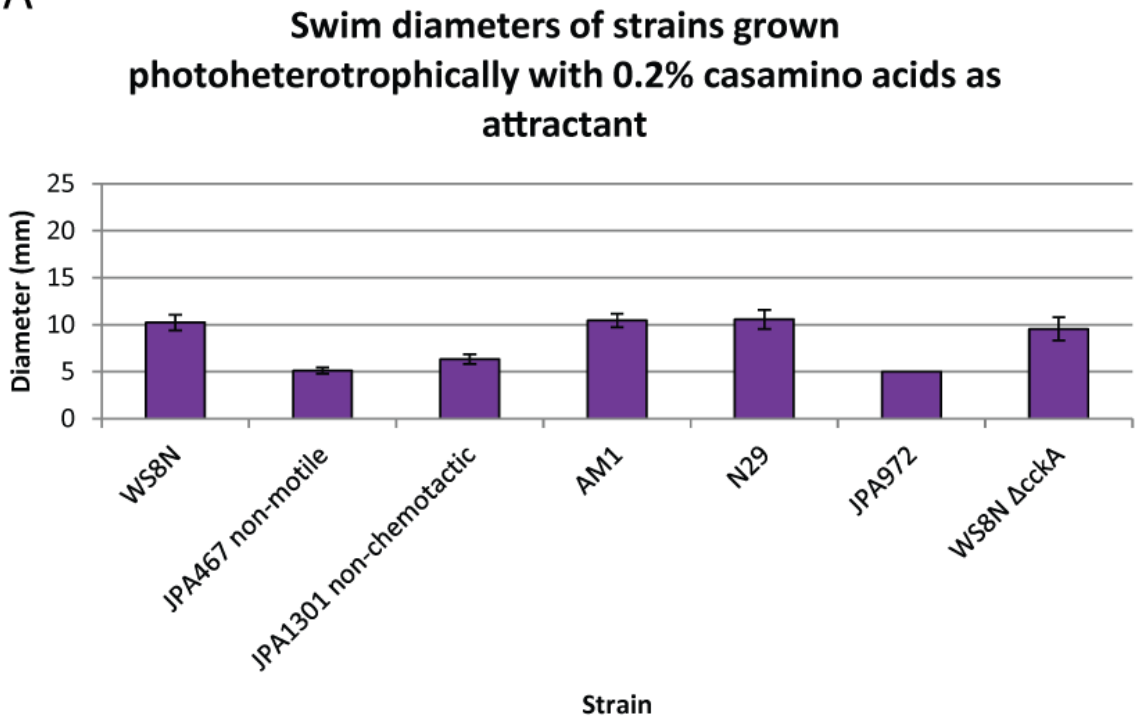

B

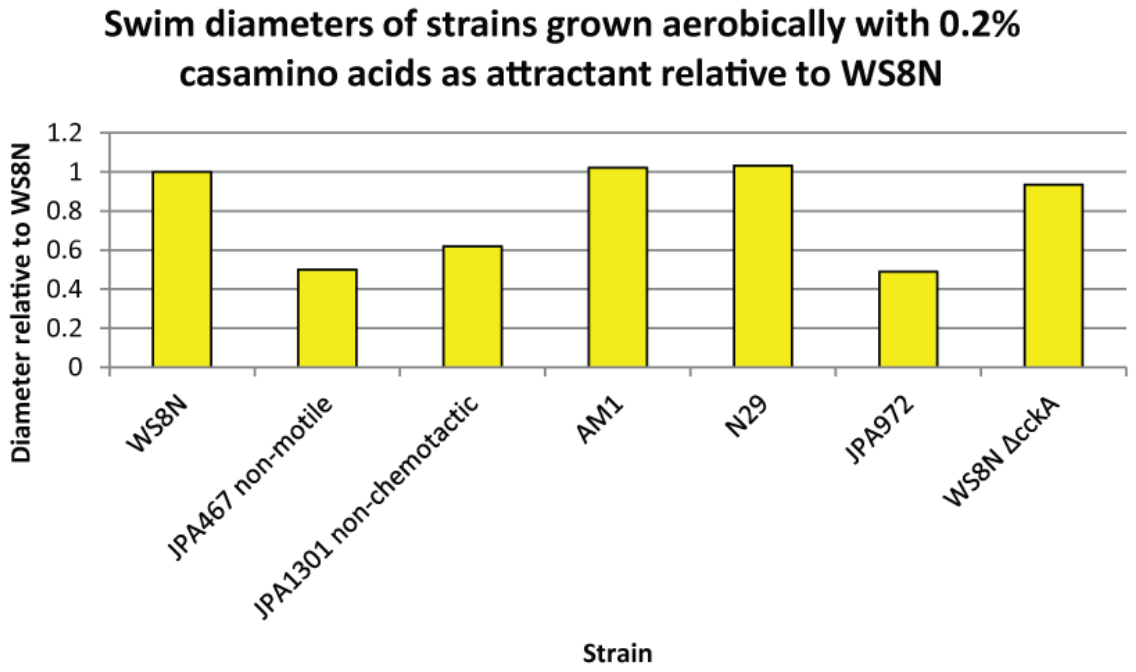

Figure 4.7: **A**: Mean swim diameters of strains using 0.2% casamino acids as attractant. Strains inoculated onto 0.25% agar in M22 medium and incubated in photoheterotrophic conditions . Mean values calculated from 3 technical repeats of 3 biological replicates. Error bars represent 1 standard deviation from the mean. **B**: Mean diameters relative to WS8N under photoheterotrophic conditions.

The swim plate data in Fig. 4.6 and Fig. 4.7 confirms the conclusion in Vega-Baray et al. (2015) that deletion of CckA does not affect Fla1 expression. To express Fla2 and potentially *che*Op$_1$, *cckA* mutants were expressed in the JPA2744 (WS8N Δ*cckA*) strain.

4.3.2 Introducing mutant *cckA* into JPA2744

To replace *cckA* in WS8N, it was necessary to introduce the mutant *cckA* alleles from AM1 and N29 into JPA2744. It was decided to clone the mutants, as well as a WT *cckA* sequence, into the expression plasmid pIND4, which uses IPTG as an inducer. This allows some level of induction control as opposed to introducing *cckA* mutants to the genome where their expression would be under the control of the *cckA* promoter.

Plasmid Design

Primers were engineered to amplify *cckA* from the *R. sphaeroides* genome: ST_pind4_*cckA*_F and ST_pind4_*cckA*_R . These were designed to include a *Psc*I and a *Hind*III restriction site at the 5' and 3' ends of the *cckA* sequence, respectively. PCR was undertaken using these primers and either WS8N, AM1 or N29 genomic DNA as template.

The PCR products were separated using agarose gel electrophoresis and the 2328 bp bands purified. The products were digested using *Hind*III and *Psc*I and ligated into expression vector pIND4 that had been digested with *Nco*I and *Hind*III. The resulting plasmids were introduced into *E. coli* XL1 Blue cells. Cultures of these strains were miniprepped to collect a 50 μl sample of plasmid DNA which was sequenced with ST_*cckA*_seq primers to confirm their sequence. 3 plasmids were identified that contain the sequences for WS8N, AM1 and N29 *cckA* : pIND4_*cckA*_WT ,

pIND4_*cckA*_L391F and pIND4_*cckA*_G588C .

These three plasmids, along with an empty pIND4 control, were conjugated through *E. coli* S17-1 λ*pir* into JPA2744 (WS8N Δ*cckA*) to form JPA2732 (JPA2744 pIND4), JPA2733 (JPA2744 pIND4_cckA_WT), JPA2734 (JPA2744 pIND4_cckA_L391F) and JPA2735 (JPA2744 pIND4_cckA_G588C).

4.3.3 CckA activity in JPA2744

Flagellar expression of the resulting strains was measured using western blotting, as this was proved to be the most categorical assay to prove either Fla1 or Fla2 expression. JPA2732, JPA2733, JPA2734 and JPA2735 were grown in the presence of 20 μm IPTG, a reasonable concentration to expect induction of expression from pIND4 (Ind et al., 2009). Cells were sheared as per the protocol in Section 6.3 and the sheared solution loaded onto SDS-PAGE gels which were either dyed with coomassie stain or underwent Western blotting with FlaA- or FliC- specific antibodies, Fig. 4.8.

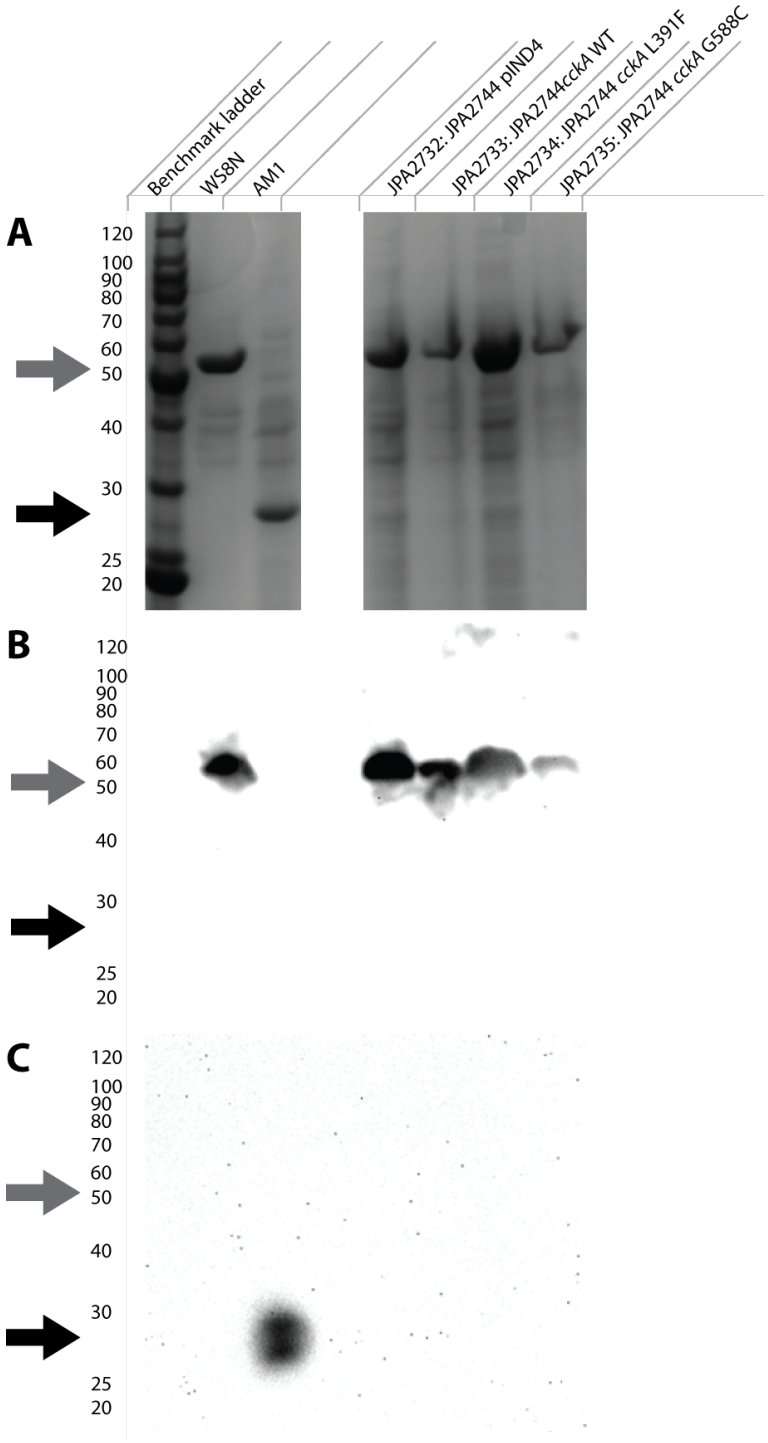

Figure 4.8: **A**: Coomassie stained SDS-PAGE gel containing Benchmark ladder and sheared flagella from WS8N and AM1 controls and from JPA2744-derived strains expressing *cckA* mutants from pIND4 plasmids. **B**: Western blot of the above gel with anti-FliC (Fla1) antibody. **C**: Western blot of the above gel with anti-FlaA (Fla2) antibody. Contrast of western blots adjusted for clarity

As before, we expected to see the presence of proteins corresponding to the size of FliC or FlaA onn the agarose gel, indicating expression of Fla1 or Fla2, respectively. This was confirmed with Western blotting with anti-flagellin antibodies. As expected, based on Section 4.3.1 and data presented in Vega-Baray et al. (2015), JPA2732 (JPA2744 pIND4) has a band corresponding to Fla1$^+$ FliC (Fig. 4.8 **B**) corresponding to the WS8N control, indicating that deleting *cckA* does not alter flagellar expression. JPA2733 (JPA2744 pIND4_cckA_WT) was expected to return WS8N CckA activity, albeit at an altered expression level and we would expect to see Fla1$^+$ FliC being expressed. This strain was Fla1$^+$ as expected.

The presence of L391F and G588C mutations in CckA in AM1 and N29, respectively, led to the expectation that both of these mutants would induce Fla2 expression when introduced into the *cckA* deletion strain JPA2744. However, JPA2734 (JPA2744 pIND4_cckA_L391F) and JPA2735 (JPA2744 pIND4_cckA_G588C) do not produce FlaA bands as expected. Instead they also cause Fla1$^+$ FliC expression. It had been expected for CckA L391F and G588C to directly initiate Fla2 expression (Vega-Baray et al., 2015; Woods, 2007).

As introducing the mutant alleles on expression plasmids in a Δ*cckA* strain had failed to activate Fla2 expression, it was decided to introduce the plasmids into wild-type WS8N to detect whether Fla2 could be expressed in a Fla1$^+$ background.

4.3.4 CckA activity in WS8N

To determine whether background expression levels of *cckA* are necessary to express Fla2 in addition to the mutant alleles, the *cckA*-containing pIND4 plasmids were introduced into WS8N. These strains were sheared and the solutions separated using SDS-PAGE with western blotting used to confirm Fla1 or Fla2 expression (Fig. 4.9).

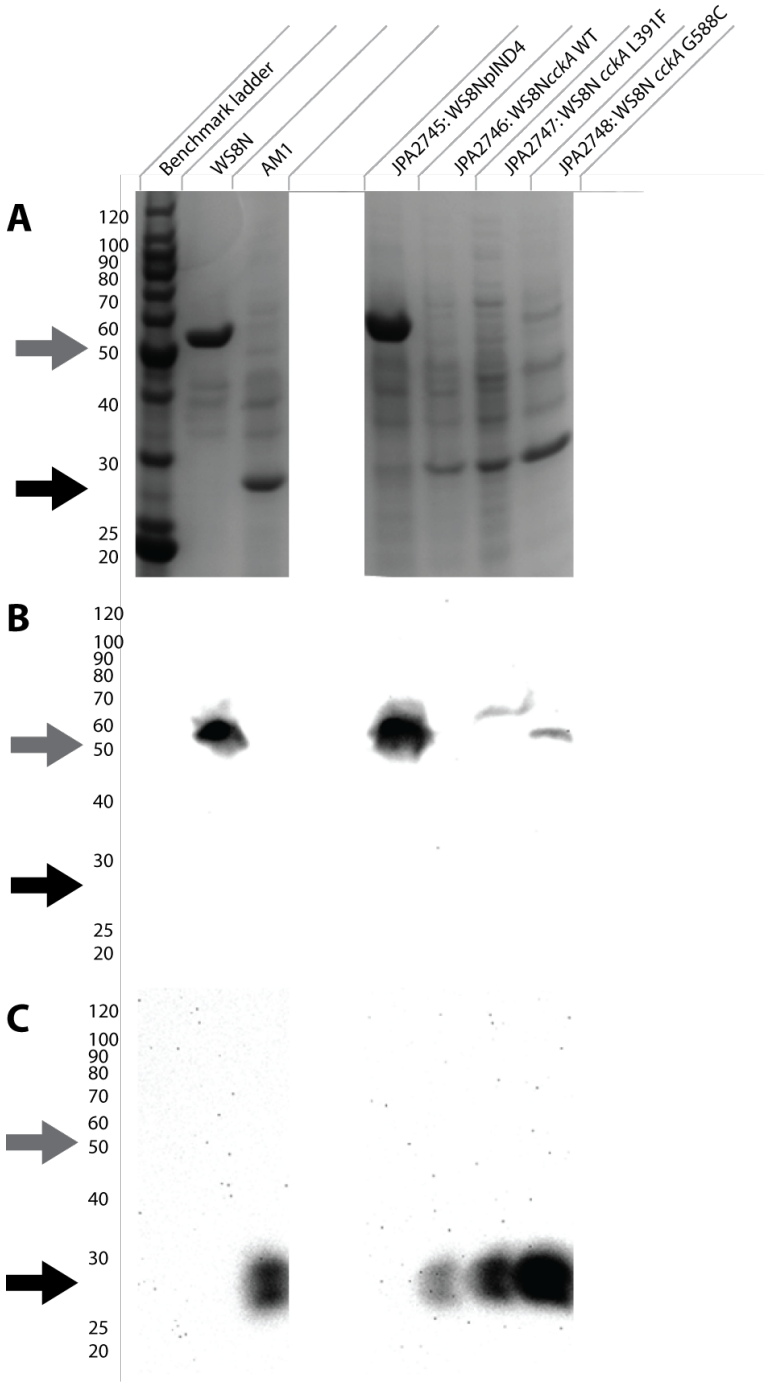

Figure 4.9: **A**: Coomassie stained SDS-PAGE gel containing Benchmark ladder and sheared flagella from WS8N and AM1 controls and from WS8N-derived strains expressing *cckA* mutants from pIND4 plasmids. **B**: Western blot of the above gel with anti-FliC (Fla1) antibody. **C**: Western blot of the above gel with anti-FlaA (Fla2) antibody. Contrast of western blots adjusted for clarity

As expected to be the case with an empty plasmid, JPA2745 (WS8N pIND4) expresses Fla1$^+$ FliC. Interestingly, JPA2746 (WS8N pIND4_cckA_WT), JPA2747 (WS8N pIND4_cckA_L391F) and JPA2748 (WS8N pIND4_cckA_G588C) are all able to switch expression from Fla1 to Fla2, evidenced by the removal of proteins that associate with FliC (Fig. 4.9 **B**) and the presence of proteins identifying with FlaA (Fig. 4.9 **C**).

This is a surprising discovery as it has been previously thought that Fla1 must be inhibited for Fla2 to express. This appears not to be the case as CckA mutants or overexpressed CckA WT (from the genome and the plasmid in JPA2746) can switch off Fla1 expression.This implies that overexpression of *cckA* may be enough to not only turn on Fla2 but also turn off Fla1, either directly or indirectly.

Vega-Baray et al. (2015) identified the heightened kinase ability of CckA L391F as a cause of Fla2 expression. It is probable that an increase in CckA concentration (caused by expression of WT *cckA* from the genome and from the plasmid pIND4_*cckA*_WT) has a similar effect; phosphotransfer from a heightened population of CckA donors to an unchanged population of CtrA proteins simulates increased phosphotransfer from kinase-dominant CckA to the CtrA population. The same result occurs from both mechanisms, that of an increase in the concentration of active, phosphorylated CtrA. In the case of CckA G588C an identical result may also be caused by a decrease in CckA phosphatase activity, which would favour the CckA forward reaction, (Section 4.2).

It can therefore be concluded that JPA2747 and JPA2748, WT and mutant CckA are working in concert and that instead of either CckA population dominating the other, there is instead heightened phosphotransfer to CtrA from a combination of both CckA populations. There also exists the possibility that heterodimers form between a WT cckA monomer and a mutant cckA monomer. However, if present, these heterodimers are not the sole causative agent of Fla2 expression. If so, there

would not be Fla2 expression in AM1, N29 or JPA2746 which all can only produce homodimers.

Additionally, in Fig. 4.9, JPA2747 and JPA2748 produce faint bands correcponding to the Fla1 flagellin FliC. These are confirmed with Western blotting with anti-FliC antibody (Fig. 4.9 **B**). Vega-Baray et al. (2015) confirmed that mutant strains could exhibit both Fla1 and Fla2 expression, but that each individual cell examined is either $Fla1^+$ or $Fla2^+$. Therefore it is possible that the bands seen are due to a small proportion of cells in the population that have retained Fla1 expression.

4.4 Chemotaxis operon expression

The previous section showed that with WT *cckA* expressed from the genome it is possible to express the Fla2 system by introducing either WT or mutant *cckA* on an expression plasmid. It is therefore possible that these same conditions can influence expression of chemotaxis operons, specifically by inhibiting the expression of *che*Op_2 and *che*Op_3 and by promoting *che*Op_1 expression to coincide with the expression of the Fla2 system. These same plasmids were introduced into Armitage laboratory *R. sphaeroides* WS8N-derived strains that had genomic fusions of fluorescent tags to component genes of the chemotaxis operons, using the methods described in Sections 4.3.2 and 6.9. When possible, strains were chosen that had a fluorescent marker tagged to a *cheW* gene which have been shown not to inhibit chemotaxis functionality (Wadhams et al., 2005).

4.4.1 Data collection and analysis

Resulting strains were grown in Sistrom's media to OD_{600} 0.2-0.4 as these conditions have been shown to induce Fla2 expression in WS8N background strains (Section 4.3.4). Cells were visualised at 150x magnification (Section 6.10). Strains were

inoculated with 20 μm IPTG to induce expression of the *cckA* alleles from the plasmids. A minimum of 5 fields of view were captured for 1 biological sample for each strain. Images were captured with the appropriate excitation and emission wavelengths for the fluorescent protein fusions and resulting images processed with the ImageJ software (Abràmoff et al., 2004). The background fluorescence was removed from each cell manually by calculating the mean fluorescence from a large section of the image that did not contain any cells and subtracting this value from the mean fluorescence value of each cell measured from that image.

The mean fluorescence intensity of a cell should accurately confer how much fluorescence is being produced by the cell, regardless of areas of localisation, and will not be affected by cell size or shape. Significance was calculated using the SPSS statistical analysis software. The data for each strain were calculated to be not normal using a Shapiro-Wilks test for normality and therefore, unless otherwise specified, a Mann-Whitney U-test with a p-value of 0.05 was used to calculate the similarity significance between data sets. A median and an interquartile range was derived from a minimum of 90 cells to appropriately illustrate the variation in fluorescence for each strain.

Representative images of the DIC channel, the fluorescence channel and a composite of the two have also been included for each strain. For each strain, the contrast of images was adjusted for clarity. Contrast differs between the fluorescent strains but remained consistent for each of the strain's 4 conjugants. The composite image uses red to reference the DIC image and green for the fluorescence. Box plots have been used to illustrate not only the median fluorescence for each strain but also the spread of the data. The total range is shown in brackets and the interquartile range, containing 50% of the data, is shown in a yellow rectangle.

4.4.2 *che*Op_2 expression

CheW2-YFP (JPA1462)

Fig. 4.10 shows the median fluorescence intensity and a box plot to illustrate the spread of data for JPA1462 (CheW2-YFP) with WT and *cckA* mutants introduced on an inducible plasmid, which allows estimation of CheW2 expression based on the intensity of the fluorescent marker tagged to it. It was predicted that flagellar expression would be linked to chemotactic operon expression, and that *che*Op_2 expression would decrease with all 3 experimental plasmids to match the decrease in Fla2 expression as detailed in Section 4.3.4.

The level of CheW2 in the cells is significantly heightened with all the experimental plasmids against the empty pIND4 control (unaltered expression of CheW2) which indicates that all copies of *cckA* can affect *che*Op_2 expression. The biggest increase in CheW2-YFP expression is caused by pIND4_*cckA*_G588C. This is another indication that *cckA* G588C and *cckA* L391F have different phenotypes as the expression of CheW2-YFP is significantly more enhanced with *cckA* G588C than *cckA* L391F. Interestingly, the expression of CheW2-YFP does not decrease in conjunction with Fla1 expression, as expected. This implies that *che*Op_2 is under the genetic control either directly or indirectly of CckA but that it is independent of Fla1 expression.

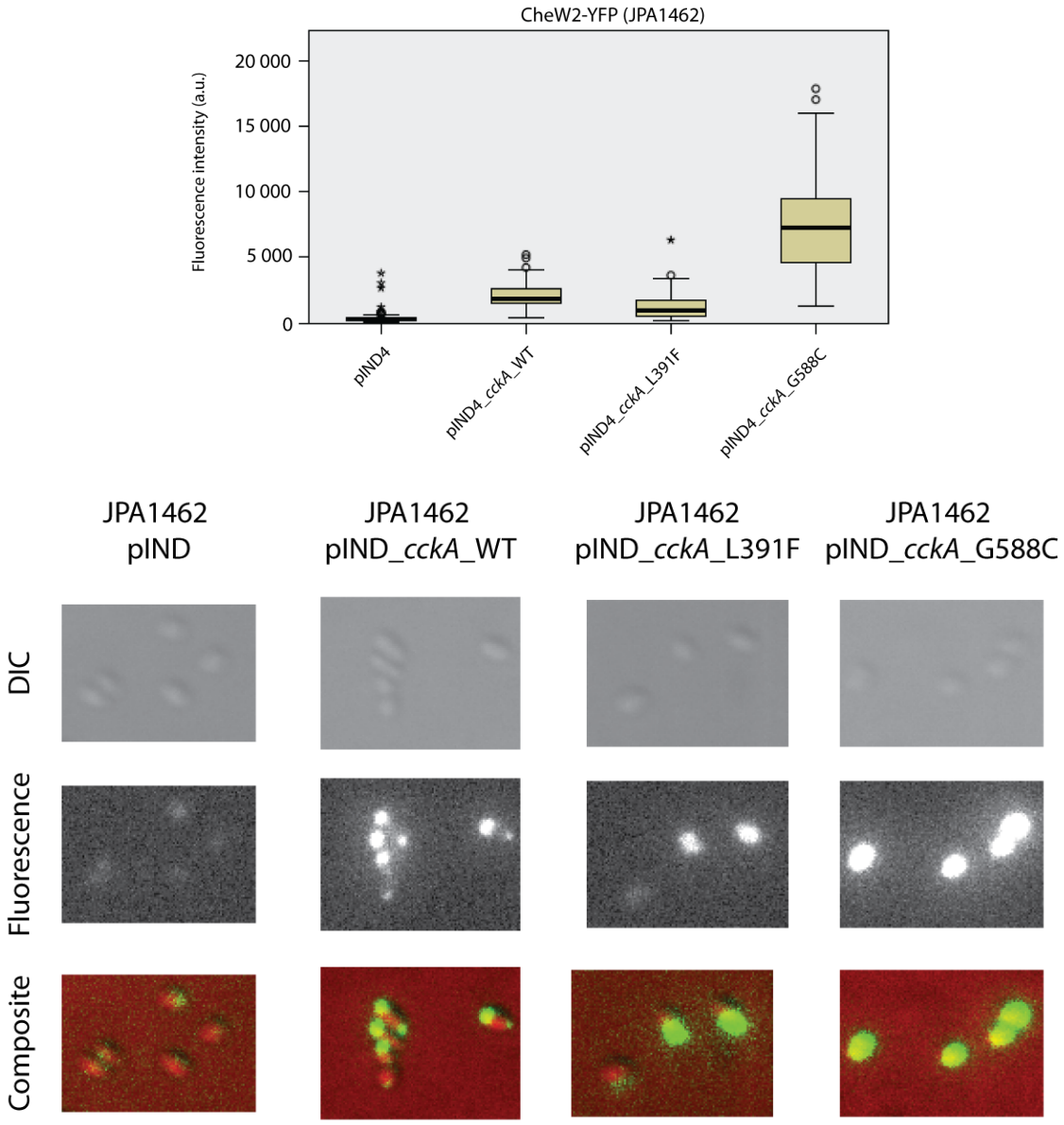

Figure 4.10: (Above) Median fluorescence intensity relative to background for JPA1462 (CheW2-YFP) containing empty pIND4 or pIND4 containing *cckA*mutants illustrated using boxplots to convey the variation of the data sets. Background fluorescence of each image removed from the mean fluorescence for each cell. Minimum 90 cells imaged to generate median values. Median represented by bold black line, interquartile range represented by yellow box. Range represented within brackets. Near and Extreme outliers represented by dots and stars, respectively. (Below) Representative images of the strains showing the DIC and fluorescent channel and a composite of the two, where the DIC image is coloured red and the fluorescent channel is coloured green.

It should also be noted that CckA G588C appears to cause delocalisation of the chemotaxis cluster. However, this is a product of the heightened contrast of the image, the parameters of which were defined by the representative images of JPA1462 pIND4 which had the lowest fluorescence. Adjusting the contrast of the images shows that fluorescence originates from the cell poles (Fig. 4.11).

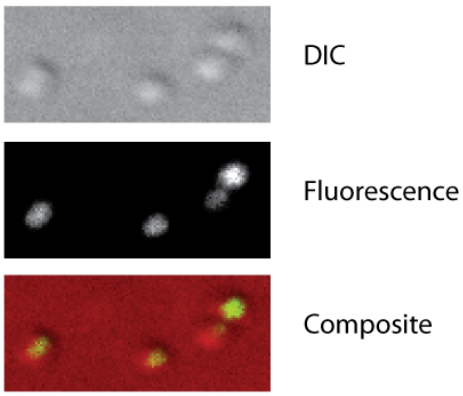

Figure 4.11: JPA1462 pIND2_*cckA*_G588C representative image with a low fluorescence contrast. Fluorescence originates from the cell pole. Image contains DIC and fluorescent channel and a composite of the two, where the DIC image is coloured red and the fluorescent channel is coloured green.

4.4.3 *che*Op_3 expression

CFP-CheW4

The median fluorescence intensity for JPA1456 (CFP-CheW4) with *cckA* mutants inserted on a plasmid is shown in Fig. 4.12. CFP fluorescence intensity is proportional to the expression level of *cheW4*, a component of *che*Op_3 . It is hypothesised that the expression of *che*Op_3 , typified by the expression of the gene *cheW4*, will be reduced by WT and mutant *cckA* to match the cognate flagellar system of *che*Op_3 Fla1.

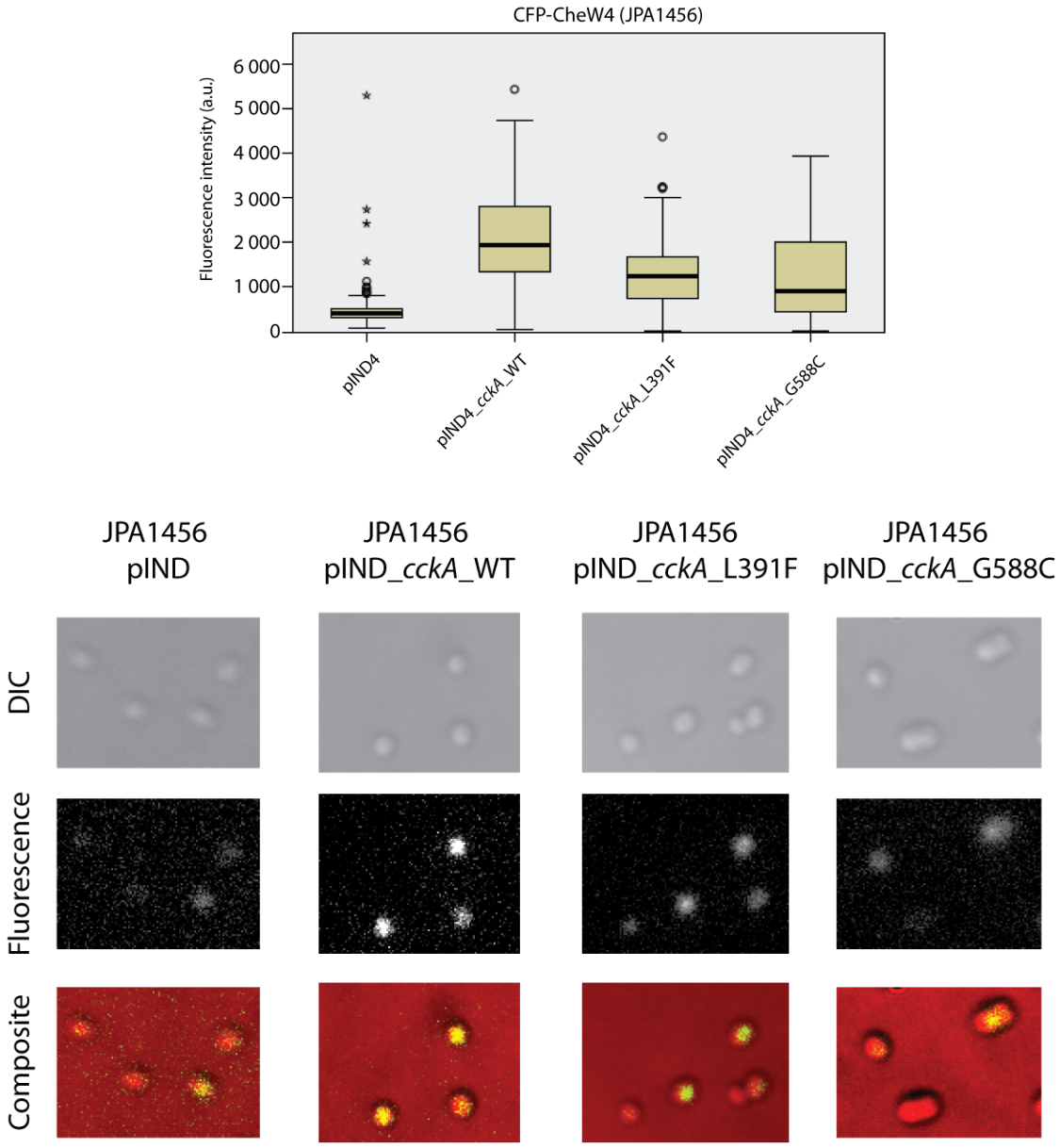

Figure 4.12: (Above) Median fluorescence intensity relative to background for JPA1456 (CFP-CheW4) containing empty pIND4 or pIND4 containing *cckA*mutants illustrated using boxplots to convey the variation of the data sets. Background fluorescence of each image removed from the mean fluorescence for each cell. Minimum 90 cells imaged to generate median values. Median represented by bold black line, interquartile range represented by yellow box. Range represented within brackets. Near and Extreme outliers represented by dots and stars, respectively. (Below) Representative images of the strains showing the DIC and fluorescent channel and a composite of the two, where the DIC image is coloured red and the fluorescent channel is coloured green.

JPA1456 with pIND4_*cckA*_WT has a significantly higher fluorescence intensity than JPA1456 with wild-type CFP-CheW4 expression levels. This indicates that overexpression of the wild-type *cckA* in WS8N is related to an increase in *che*Op_3 expression. Both mutant forms of *cckA* tested produce a statistically significant increase in the expression levels of *cheW4*, and these are statistically similar to each other. This does not match the prediction that the *che*Op_3 system will have a similar expression pattern to the Fla1 system.

4.4.4 *che*Op_1 expression

McpA-GFP

The Armitage laboratory strain library does not contain a fluorescent fusion to *cheW1* so alternative strains were used to map the expression of *che*Op_1. Fig. 4.13 illustrates the median fluorescence intensity for JPA507 (McpA-GFP) strains with the *cckA*-containing plasmids. It is hypothesised that the expression of *che*Op_1, which should be proportional to GFP fluorescence, will mirror the expression of the Fla2 system and increase in the presence of the WT and mutant *cckA*.

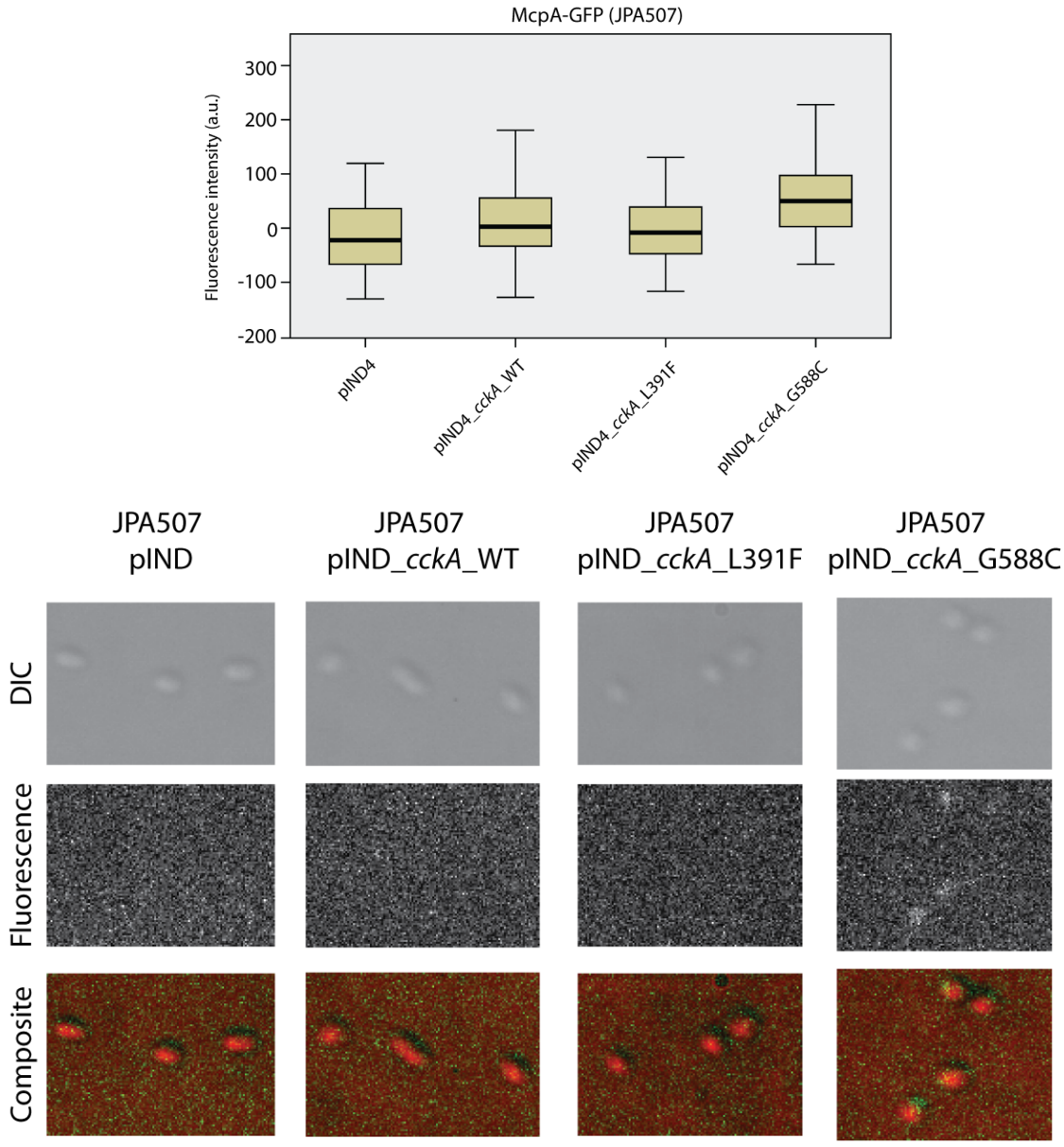

Figure 4.13: (Above) Median fluorescence intensity relative to background for JPA507 (McpA-GFP) containing empty pIND4 or pIND4 containing *cckA*mutants illustrated using boxplots to convey the variation of the data sets. Background fluorescence of each image removed from the mean fluorescence for each cell. Minimum 90 cells imaged to generate median values. Median represented by bold black line, interquartile range represented by yellow box. Range represented within brackets. Near and Extreme outliers represented by dots and stars, respectively. (Below) Representative images of the strains showing the DIC and fluorescent channel and a composite of the two, where the DIC image is coloured red and the fluorescent channel is coloured green.

Firstly, we note that there is negative fluorescence for some of the data points. This is due to the background fluorescence of the images being removed, leading to cells with little or no fluorescence having slight negative fluorescence in relation to the background, as is the case with JPA507 with empty pIND4 and with pIND4_*cckA*_L391F.

The low fluorescence in JPA507 pIND4 is expected as we have not previously witnessed expression of *che*Op_1 in a WS8N-derived strain.

All 3 experimental plasmids cause an increase in fluorescence compared to the JPA507 pIND4 control strain judged to be statistically significant. The ex-conjugant with the largest margin is pIND4_*cckA*_G588C. This mirrors the data presented in Fig. 4.10 which similarly shows this plasmid causing a large increase in expression, except in *che*Op_2. However, the increase in this figure shows that it is 2 orders of magnitude less than that above. This is attributed to the differing effects of GFP and YFP as markers. This also confirms a hypothesis that the L391F and G588C *cckA* mutants produce different phenotypes, despite both being $\mathrm{Fla2}^+$.

The prediction that under the conditions which cause expression of the Fla2 system, there is also expression of the *che*Op_1 system.

4.5 Chapter Summary

One of the aims of this project was to successfully initate the expression of *che*Op$_1$ which has hitherto remained unexpressed under laboratory conditions. It was proposed in Chapter 2 that *che*Op$_1$ might be expressed in Fla2$^+$ strains. The last chapter investigated an alternate hypothesis for the motility data presented and found that Fla2$^+$ cells were not faster than Fla1$^+$. Therefore, the possibility that *che*Op$_1$ was being expressed in a WS8N strain was explored.

Firstly, it was necessary to distinctly express Fla2 in WS8N. Full genome sequencing of Fla2$^+$ AM1 and N29 found mutations in the gene *cckA*. Deleting *cckA* in WS8N and expressing either *cckA* mutant from a plasmid is not sufficient to express Fla2, nor is it possible if FleQ, the Fla1 master regulator, is deleted.

However, expressing these mutants or WT *cckA* in a Fla1$^+$ WS8N strain was sufficient to switch off Fla1 expression and turn on Fla2 expression. This is attributed to the need for the bacterium to have WT *cckA* expression levels to reach a threshold level of *cckA* activity to initate Fla2 expression.

These plasmids do not have a single phenotype as shown by examining the *che*Op expression patterns with these mutants. *che*Op$_2$ and *che*Op$_3$, cognate chemotaxis operons for the Fla1 system, are more highly expressed with WT and mutant *cckA* expressed from a plasmid. These conditions also initiate expression of *che*Op$_1$, previously unexpressed under laboratory conditions. This allows for further exploration of the function of *che*Op$_1$.

Chapter 5

Discussion

The study of chemotaxis and motility has a far-reaching impact on various topics. For example, the colonisation of root nodules by *Rhizobium* or of the mammalian gut by *Helicobacter* and *Vibrio* species (Wadhams and Armitage, 2004; Porter et al., 2008).

Key to understanding how these systems work is studying the integration of chemotactic signals to co-ordinate a cellular response. This research attempts to investigate how and why *R. sphaeroides*, a model for chemotaxis, has two motility and chemotaxis systems and how they interact, if at all.

Many bacterial species have multiple chemotaxis and flagellar systems. In some cases, these different flagella systems are differentially expressed and may be optimised for motility on solid surfaces or for swimming through liquid media (Mcclain et al., 2002). *R. sphaeroides* is a model organism for motility and chemotaxis (Porter et al., 2008) although almost all research has focussed on the Fla1 flagellum and the chemotaxis system encoded by *che*Op_2/*che*Op_3. Here we set out to characterise the putative *che*Op_1-controlled Fla2 system of *R. sphaeroides*.

We have shown by Western blotting and mass spectrometry that the motile ΔFla1 suppressor strain AM1 expresses the Fla2 system. The Western blotting and mass

spectrometry also confirmed similar findings in Woods (2007) that N29 was Fla2$^+$. Free swimming analysis of these strains shows that their motility pattern significantly differs from that of Fla1$^+$ WS8N. Interestingly, an extremely high number of recorded tracks from AM1 and N29 showed corkscrew-like motility patterns. This suggests that the tuft of Fla2 filaments may not propel cells in as smooth a manner as seen in Fla1-driven motility but rather in a helical or corkscrew-like motion.

Corkscrew-like motility has been seen in helical-shaped bacteria, for example the spirochetes, and is suggested to benefit motility in viscous environments (Shaevitz et al., 2005; Li et al., 2000). The spirochete *Borrelia burgdorferi* swims with a higher velocity as the viscosity of the medium increases (Kimsey and Spielman, 1990). It is possible that this helical motility is better adapted for moving through polymeric solutions like through the cross-linked polysacharides of soft nutrient agar plates or through the exopolysaccharide matrix of a biofilm. We propose that that *R. sphaeroides* uses Fla2-driven corkscrew motility to navigate through viscous environments that can be found in the bacterium's natural habitat of a stagnant body of water. Perhaps after decades of growth in liquid media in a laboratory, WS8N has lost the ability to upregulate Fla2 expression, and that the mutations discussed in this work are returning function to this silenced system. It would be interesting to further characterise *R. sphaeroides* Fla2 motility in different environments.

Motility and chemotaxis have been shown to be important for the initial stages of biofilm formation in many motile bacterial species, including *R. sphaeroides* (Wilkinson et al., 2011). We therefore measured the efficiency of WS8N, AM1 and N29 at forming an initial attachment to a surface in a biofilm assay. Fla2$^+$ AM1 and N29 were highly deficient in their ability to attach to a surface compared to Fla1$^+$ WS8N. This implies that the corkscrew-like Fla2-mediated motility is less beneficial to cells in the initial stage of biofilm formation than Fla1 motility. We therefore suggest that the functions of the two flagella systems in *R. sphaeroides* may be for motil-

ity and biofilm-forming (Fla1) and for swimming through viscous or biofilm-like environments (Fla2).

Whole genome sequencing of WS8N, AM1 and N29 suggested that mutations in *cckA* may result in the expression of the Fla2 system in a Fla1$^-$ strain. *cckA* has been shown to regulate motility through its cognate response regulator CtrA in a range of species from the α-proteobacteria including *Caulobacter crescentus*, *Rhodobacter capsulatus* and *Sphingomonas meloni* (Mercer et al., 2012; Francez-Charlot et al., 2015; Panis et al., 2015).

The CckA-ChpT-CtrA pathway has been shown to be essential for the regulation of the cell cycle in *C. crescentus* (Greene et al., 2012). CtrA is known to inhibit DNA replication in motile swarmer cells and initiate stalk biogenesis as the cell transitions from a motile, swarmer cell to a non-motile, stalked cell. CtrA then controls the biosynthesis of the flagellum and the chemotaxis machinery in the budding swarmer cells (Laub et al., 2000) in a temporally-defined cyclical nature. However, in other members of the α-proteobacteria including *R. capsulatus*, CtrA is not essential for cell cycle control but is necessary for motility (Greene et al., 2012). In *S. meloni*, CtrA is necessary for both flagella-mediated motility and biofilm formation (Francez-Charlot et al., 2015). CtrA also controls expression of genes involved with exopolysaccharide synthesis and c-di-GMP signalling, a second messenger known to regulate the lifestyle switch from motile growth to biofilm-forming sessility. The flagellar system in *S. meloni* is highly similar to the Fla1 system in *R. sphaeroides* and we can assume that as CtrA controls both motility and biofilm formation in the former, the two functions may be linked by the Fla1 flagellar system in the latter (Francez-Charlot et al., 2015).

We investigated the link between CckA and motility in *R. sphaeroides* by introducing the CckA mutations (L391F and G588C) from AM1 and N29 on the inducible plasmid pIND4. Western blotting confirmed that expression of mutant *cckA* or wt

cckA was sufficient to induce a switch from Fla1 to Fla2 expression even with the presence of wt *cckA* on the genome. This implies that there may be an expression threshold for the Fla2-induction activity of *ctrA*. In WS8N with pIND4_*cckA*_WT the genomic and vector-derived WT CckA are proposed to lead to an increased population of CckA phosphoryl-donors. This leads to increased phosphotransfer to CtrA. The same result, an increase in concentration of phosphorylated CtrA, is caused by the increase in kinase activity of CckA L391F coupled to the phosphotransfer from genome-derived WT CckA in WS8N with the vector pIND4_*cckA*_L391F. Additionally, CckA G588C may have increased kinase or decreased phosphatase activity. Both outcomes would lead to an increase in phosphorylated CtrA in WS8N with pIND4_*cckA*_G588C. All 3 strains are proposed to result in an increase in active CtrA above a threshold which is proposed to initiate Fla2 expression and inhibit Fla1 expression.

A wide range of fluorescent protein fusions to chemotaxis genes exist in the Armitage laboratory strain library. The finding that expression of mutant *cckA* from pIND4 is sufficient to induce a switch in flagella systems even in a WS8N background allowed us to study the effects of these *cckA* mutations on *che*Op expression. We showed that expression of both *che*Op_2 and *che*Op_3 is elevated by mutant *cckA* and the expression of wt *cckA* from pIND4. Fluorescence of a component of *che*Op_1, which has never before been seen to be expressed in WS8N, was significantly higher with expression of the mutant *cckA* G588C. This indicates that *che*Op_1 may also be under the influence of CckA/CtrA.

These data suggest that although in WS8N the Fla1 system is switched off by expression of the *cckA* mutants to be replaced by Fla2, the expression of the chemotaxis operons is not similarly controlled. This may be due to the fact that two separately functioning flagellar systems would conflict with each other due to them both attempting to control motility, whereas multiple chemotaxis systems may not

interfere with each other if there is no cross-talk. Alternatively, they might work co-operatively if they can both signal to the same flagella system.

Just prior to completion of this thesis, Vega-Baray et al. (2015) published a paper on the role of *cckA* mutants on the expression of the Fla1 and Fla2 systems. Our data confirm their findings that CckA mutant can cause a switch from Fla1 to Fla2 expression under specific growth conditions. Vega-Baray et al. (2015) only found Fla2 expression in the presence of mutant *cckA*. However, we found that expression of wt *cckA* from an inducible plasmid was also able to induce Fla2 expression, which is supported by their finding that mutant CckA proteins have elevated expression leading to increased phosphotransfer to CtrA and that there might exist a threshold CtrA concentration for Fla2-inducing activity. Vega-Baray et al. (2015) also found that a high concentration of organic acids, including succinate, represses Fla2 expression. We support this finding as Fla2 was not found to express when strains were grown on succinate medium.

Our hypothesis that the Fla2 system is necessary for *R. sphaeroides* to swim under environments of high polymer concentration, for example in soft agar swim plates, is supported by Vega-Baray et al. (2015) who found that motility returned to a non-suppressor Fla1$^-$ mutant when incubated on soft nutrient agar but not in liquid media. Therefore, *R. sphaeroides* might express the Fla2 system naturally without the influence of mutant *cckA* and it would be interesting to know if this motility is seen with Fla1$^+$ WS8N incubated in high-viscous media.

This work extends our understanding of Fla2-mediated motility to show that this motility drives corkscrew-like motion which, unlike Fla1 motility, is not able to bring about efficient surface attachment. We also show that despite being able to switch expression of flagella systems, the CckA mutants are not capable of switching the expression of chemotaxis operons. There is some evidence that the mutants, and CckA G588C in particular, are able to upregulate chemotaxis operons. This opens

up interesting questions about how *che*Op expression is regulated in *R. sphaeroides* and why this might be separate from flagellar expression.

Chapter 6

Materials and Methods

6.1 Growth conditions

6.1.1 Antibiotics

Final antibiotic concentration in media for both *E. coli* and *R. sphaeroides*:

Kanamycin- 25 μg/ml

Nalidixic acid- 20 μg/ml

6.1.2 *E. coli*

Grown at 37°C in shaking liquid cultures of LB broth (Section. 6.15) or plated onto LB 2% agar typically for 16 hours with appropriate antibiotics.

6.1.3 *R. sphaeroides*

Grown at 30°C in liquid cultures of SUX or Sistrom's medium (Section 6.15) without shaking in the presence of light (illuminated at 10 W m^{-2} with 60 W tungsten bulbs)

or plated onto LB 2% agar typically for 48 hours with appropriate antibiotics.

6.2 Flagellar staining

6 μl of *R. sphaeroides* photoheterotrophic cells grown to OD_{600} 0.2-0.4 were placed between a glass slide and coverslip after growth in Sistrom' media with appropriate antibiotics. 6 μl of filtered Ryu stain was allowed to diffuse between the slide and coverslip (Heimbrook et al., 1989). To prevent flow and to keep slides from drying, coverslips were fixed to the slide with commercial nail varnish.

Cells were imaged on a Nikon Eclipse TE2000-E microscope with Andor camera at 60x magnification. NIS-elements 3.2 was used to capture data and images processed and analysed as detailed in Section 3.1.2 using ImageJ 1.46r (Abràmoff et al., 2004).

6.3 Flagellar shearing

300 ml of *R. sphaeroides* mid-log photoheterotrophic cells grown to to OD_{600} 0.2-0.4 was centrifuged at 2162 g for 15 mins. The pellet was resuspended in 7 ml PBS buffer. Motility was tested for as outlined in Section 6.7 to ensure centrifugation had not sheared cells prematurely. The solution was passed through two syringes with 26-gauge needles connected by polyethylene tubing between 40 and 60 times to achieve flagellar shearing. The solution was centifuged at 2060 g for 15 mins to remove cellular matter. The supernatant was concentrated in an Amicon Ultra 15 ml 10 kDa cut-off concentrating collumn and centrifuged at 2060 g for multiple 5 minute intervals until a final volume of 0.5 ml was reached.

6.4 SDS-PAGE

Sheared flagella solutions were subjected to SDS-PAGE onto a 4-20% precast Expedeon RunBlue^{TM} gel at 40 W, 220 mA and 175 V in RAPID buffer. Benchmark protein ladder (Invitrogen) was used for standard molecular weights and Prestained benchmark ladder was used if gels were being subjected to western blotting. Gels were visualised using InstantBlue coomassie stain (Expedeon).

6.5 Western Blotting

6.5.1 Antibodies

anti-FliC

The FliC-specific antibody was generated by members of the Armitage Laboratory using sheared *R. sphaeroides* flagella which were purified by ultracentrifugation. An external company generated polyclonal antibodies from the purified protein by immunising rabbit hosts with the protein and cultivating the host bleeds.

anti-FlaA

The FlaA-specific antibodies were generated by choosing a peptide sequence that was specific to FlaA but to no other *R. sphaeroides* WS8N protein. The peptide chosen was 18 amino acids in length with the sequence (from the amino terminal to the carboxyl terminal):

LLKTDINGSGGTAYDVL

Crucially, this sequence was not found in FliC. The peptide was synthesised and antibodies created by Generon. Rabbit hosts were immunised with the peptide and

antibodies cultivated and purified from the final bleed after 69 days.

6.5.2 Western blotting procedure

Gels were blotted onto a PVDF membrane using cold Blotting buffer at 500 mA, 175V and 40 W. The primary antibody used were anti-FliC or anti-FlaA raised in rabbits and the secondary antibody was goat-raised anti-rabbit HRP (Dakocytomation). Binding of the secondary antibody was visualised using Immobilon^{TM} Western chemiluminescent HRP (horseradish peroxidase) substrate.

6.6 Mass Spectrometry

6.6.1 MS sample preparation

WS8N and AM1 were sheared of flagella as described above (Section 6.3) and the flagellar proteins separated by SDS-PAGE. The bands corresponding to the putative filament proteins FlaA and FliC were excised from an SDS gel with a clean scalpel. Samples were prepared for Mass Spectrometery by the Central Proteomics Facility (Dunn School, University of Oxford). Samples were washed in 25 mM ammonium bicarbonate with 50% acetonitrile and reduced 10 mM DTT and 55 mM iodoacetamide. Samples were then digested with 0.5 mg trypsin overnight at 37 °C and extracted with 0.1% formic acid in 50% acetonitrile.

6.6.2 MS data analysis

Mass Spectrometry was performed by the Central Proteomics Facility. Samples were analysed using a Q Exactive mass spectrometer (Thermo Scientific) coupled to an Ultimate 3000RSLCnano system (Dionex). Separation of peptides was performed by

reverse-phase chromatography using a 25 cm long by 75 mm inner diameter picotip analytical column (New Objective) packed in-house and at a flow rate of 300 nl/min using a 120 min gradient.

The mass spectrometer was operated in a "Top 10" data-dependent acquisition mode. Charge state +1 ions were rejected from selection and fragmentation. Data were converted to a .mzXML format using MSconvert from Proteowizard and analysed using the Central Proteomics Facilities Pipeline (CPFP) (Trudgian et al., 2010). Search parameters were two missed cleavage sites by trypsin, cysteine carbamidomethylation fixed modification, methionine oxidation and N-terminal protein acetylation variable modifications. Peptide results were filtered to 1% false discovery rate by MaxQuant and Proteome Discoverer. Mass tolerances for MS and MS/MS peak identifications were 20 ppm and 0.1 Da, respectively. IProphet was used to derive the sequence probability. The Modification Localisation Score (ModLS) algorithm assesses the confidence by which phosphorylation sites can be assigned on a peptide (Beausoleil et al., 2006). For each variable modification in the custom WS8N UniProt-derived database, all amino acid specificities in the database were considered during localisation. Protein identifications against this custom database were uploaded to ProteinCenter (Proxeon for interpretation (Paster et al., 2013; Hutchinson et al., 2012).

6.7 Motility assay

Motility was measured using mid-log/early stationary cells (0.2-0.4 OD_{600}) placed in a 0.2 x 2 mm capillary slide and visualised using a Nikon phase-contrast microscope with a Ph2 Plan 20/0.50 DL lens. Strains were labelled motile if cells were seen swimming.

6.8 Swim plates

5 μl of photoheterotrophic, stationary phase cells (0.8-1.2 at OD_{700}) were inoculated onto 0.25 % Bacto^{TM} agar (Becton, Dickinson and Company) plates made from M22 media in the presence of appropriate antibiotics and 100 μM attractant. Diameters of cultures measured after 2 days aerobic incubation or 3 days photoheterotrophic incubation. Statistical significance was measured using Mann-Whitney U-test.

6.9 Molecular biology techniques

6.9.1 Plasmid Extraction

Plasmids were extracted from cells using a Qiagen miniprep kit according to manufacturers instructions.

6.9.2 PCR

PCR was conducted using the following protocol:

	Stage	Temperature (°C)	Duration
	Initial denaturation	98	5 min
	Denaturation	98	36 sec
30 Cycles	Annealing	Variable	36 sec
	Elongation	72	Varied with target gene length
	Final elongation	72	5 min

PCR assay followed from Phusion (New England Biolabs) polymerase kits.

Colony PCR

For colony PCR, a template was derived by resuspending a colony from a LBA plate in 100 μl Milli-Q water and boiling for 5 minutes.

6.9.3 DNA purification

DNA was purified using a Qiagen Gel Extraction kit, carried out according to manufacturers instructions.

6.9.4 Agarose Gel Electrophoresis

DNA products were separated on a 1.2 % agarose gel at 100V for a 100 ml gel and 200 V for a 200ml gel. Gels were composed of 1/2 x TBE buffer and run in 1/2 x TBE buffer.

6.9.5 Restriction digests

Restriction digests were performed at 37 °C for one hour at 50 μl total volume: 1 μl each restriction endonuclease 5 μl 10x Buffer 3/Buffer 4 dependant on conditions set out by NEB double digest finder 40 μl PCR product or 1 μg plasmid DNA

6.9.6 Alkaline Phosphatase

Digested plasmids were treated with Antarctic Phosphatase (New England Biolabs) according to manufacturers instructions.

6.9.7 Ligations

Ligations were performed with T4 DNA ligase (New England Biolabs) according to manufacturers instructions.

6.9.8 Cloning conditions

Competent cell production

Cells were made chemically competent as detailed in Sambrook and Russell (1989).

E. coli

Plasmids were transformed into competent XL1 BLue or S17-1λ*pir* *E. coli* cells by heat shock at 42 °C for 45 sec. Cells were placed on ice for a further 45 seconds and then grown with LB media for 1 hour at 37 °C before plating onto LBA.

R. sphaeroides

S17-1λpir*E. coli* cells with plasmid were grown to early log phase, centrifuged and resuspended in 1 ml LB without antibiotic. 10 μl was mixed with 100 μl stationary phase *R. sphaeroides* that had been similarly resuspended. The mixture was placed on a sterile nitrocellulose filter on LBagar for 16 hours. The filter was placed in 1 ml LB and vortexed. 100 μl aliquots were plated onto LB agar with Nalidixic acid and Kanamycin to select for conjugates.

Recombination procedure

Successful pK18*mobsacB* conjugates that complete the first round of recombination (Fig. 6.1) were selected for with Kan. Cultures were inoculated into liquid cultures

of Sux without Kan for 2 days aerobic incubation to allow for the second round of recombination to occur. These cultures were serially diluted to 1 in 100 000 and plated onto 10% sucrose, 2% agar plates and incubated at 30 °C for up to 5 days. Sucrose selects for colonies that have lost the pK18*mobsacB* plasmid after the second round of recombination (Fig. 6.1) as *sacB* on the plasmid encodes a sucrase that catalyses the reaction of sucrose into a toxin, thus the plasmid inhibits growth on sucrose. Colonies were replica plated onto LBA Nal and LBA Nal Kan plates for additional selection as successful recombinants should be Nal^R not Kan^R. Colony PCR of the target region and sequencing was used to confirm recombination.

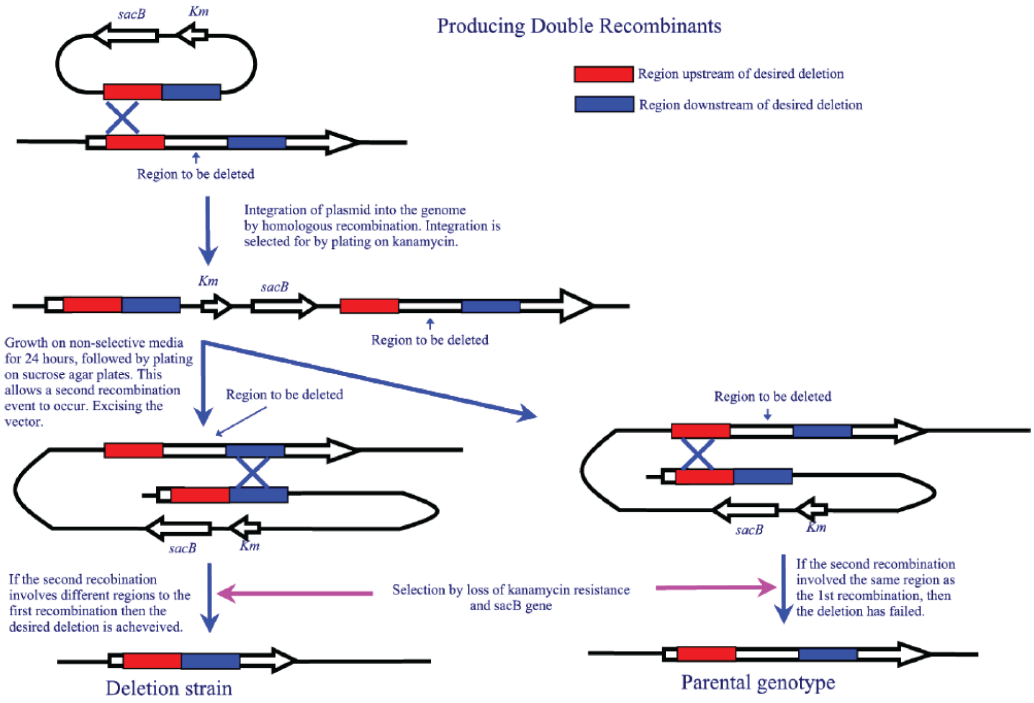

Figure 6.1: Recombination procedure resulting in either a successful deletion of a gene on the genome or of a revertant to the parental genotype. Adapted from Roberts (2007)

6.9.9 Sequencing

DNA was sequenced by Source BioScience and matched to known sequences using BLAST at the NCBI database (URL: http://blast.ncbi.nlm.nih.gov/Blast.cgi).

6.9.10 Genomic sequencing

Genomic DNA was submitted to the University of Exeter sequencing service who sequenced it using an Illumini HiSeq 2000. 100bp paired end libraries were prepared using the Nextera XT kit. Approximately X50-fold coverage was obtained. The reads were aligned to the WS8N reference genome and SNPs identified using BWA.

6.10 Fluorescence microscopy

Cells were grown to 0.2-0.4 OD_{600} with appropriate antibiotic and 20 μM IPTG. 1.2% agarose in H_2O was pipetted onto glass micrscope slides with a coverslip placed on top. When dry the coverslip was removed to leave a film of agarose. 5 μl of culture was placed on this film covered by an additional coverslip.

Slides were imaged as stated above (Section 6.2) with 60 ms exposure for the DIC channel, a multiplier of 13 and a conversion gain of 5.1 x. The following fluorescence channels appropriate to the strain being imaged:

- YFP - Exposure - 500 ms, Multiplier - 300, Conversion gain - 5.1 x, Ex λ- 520, Em λ- 575
- CFP - Exposure - 300 ms, Multiplier - 300, Conversion gain - 5.1 x, Ex λ- 436, Em λ- 485
- GFP - Exposure - 300 ms, Multiplier - 300, Conversion gain - 5.1 x, Ex λ- 470, Em λ- 525

Images were analysed in ImageJ (Abràmoff et al., 2004) and statistical significance judged using a Mann-Whitney U-test in the SPSS software.

6.11 Biofilm assay

Cultures were grown to OD_{700} 0.4-0.6 and diluted in either SUX or Sistrom's medium so that each sample was at OD_{700} 0.5 exactly, to ensure that the number of cells in each well are as close to each other as possible. 100 μl of culture was added to the wells of a non-tissue culture treated 96-well plate (BD Falcon). Plates were left for 1 hour in a light cabinet at 30 °C with white light at 10 Wm^{-2} with parafilm sealing the lid to the plate to reduce aerobicity. Wells were washed with Milli-Q water to remove unattached cells and 125 μl of 0.1 M crystal violet was added to each well for 10 minutes for staining. Wells were washed again with water to remove excess stain and air dried for 10 minutes. 200 μl of 10% v/v acetic acid was added to the wells for 10 minutes to destain the attached cells and 125 μl of this solution was removed from each well and added to a fresh clear bottomes 96 well plate (Costar). OD was measured at 595 nm in a Tecan M200 inifinite platereader.

6.12 Alignments and protein structure

Sequences were aligned with the alignment program Muscle v3.8 (Edgar, 2004). Structures were downloaded from the PDB website and adapted to show residue locations with Pymol Molecular Graphics System, v1.3, Schodinger, LLC.

6.13 Statistical analysis

Statistical analysis was performed using SPSS Statistics software (IBM). Data were judged not-normal using a Shapiro-Wilk test and in these cases a non-parametric test was needed to judge significance. Mann-Whitney U-tests were used with a p-value of 0.05 as it is appropriate for independent non-parametric samples.

6.14 Strains, primers and plasmids used in this study

6.14.1 Primers used in this work

Name	Sequence	Function
ST_pind4_cckA_F	GAGAATACATGTCAGTGCACAGGC	insert cckA into pIND
ST_pind4_cckA_R	CTTCTGAAGCTTATCAGTGCACCTGCTC	insert cckA into pIND
ST_cckA_upstream_F	GCATAATCTAGAAGGTGCGGCGGCTCG	amplify upstream region of *cckA*
ST_cckA_upstream_R	CGGAGTGCATGCTGACTGCCTGTGCACTGACATC	amplify upstream region of *cckA*
ST_cckA_downstream_F	GAATATGCATGCCAGGAGCAGGTGCACTGAC	amplify downstream region of *cckA*
ST_cckA_downstream_R	GAGTTTAAGCTTCACGGCAGGAGAGCCTTTC	amplify downstream region of *cckA*
ST_*cckA*_seqA_F	GATCCTCGCGCAGATTAAAC	Confirm sequence of cloned *cckA*
ST_*cckA*_seqB_F	ATGCTGGTCGCGAACAAG	Confirm sequence of cloned *cckA*
ST_*cckA*_seqC_F	CGGATTTCTCCGATCTGTTC	Confirm sequence of cloned *cckA*
ST_*cckA*_seqD_F	CGTGCTGACCGAAGAGTTG	Confirm sequence of cloned *cckA*
ST_*cckA*_seqE_F	GTGTTCGTGACCGATGTG	Confirm sequence of cloned *cckA*
ST_*cckA*_seqF_F	CGGCATGAGGTAGATTTCC	Confirm sequence of cloned *cckA*
ST_*cckA*_seqG_F	CGTCGCTGCCGAACTTCATC	Confirm sequence of cloned *cckA*

Table 6.1: Primers

6.14.2 Plasmids used in this work

Name	Description	Reference
pIND4	Cloning Vector. Kan^R	Ind et al. (2009)
pIND4_cckA_WT	pIND4 inserted with *cckA* WT variant	This Study
pIND4_cckA_L391F	pIND4 inserted with *cckA* L391F variant	This Study
pIND4_cckA_G588C	pIND4 inserted with *cckA* G588C variant	This Study
pK18*mobsac*B	Kan^R recombination plasmid	Schafer et al. (1994)
pK18_Δ*cckA*	Deletion plasmid for *cckA*	This Study

Table 6.2: Plasmids

6.14.3 Strains used in this work

Strain	Description	Reference
E. coli		
S17-1λpir	Optimised for inter-specific genetic transfer. recA pro hsdR RP4-2Tc::Mu-Km::Tn7	(Penfold and Pemberton, 1992)
Xl1 Blue	General cloning and expression strain. Laclq TcR	Stratagene
R. sphaeroides		
WS8N	Nalidixic acid resistant derivative of motile WS8	(Sockett and Armitage, 1991)
WS8N pIND4_cckA_WT	WS8N with WT *cckA* on pIND4	This Study
WS8N pIND4_cckA_L391F	WS8N with *cckA* L391F on pIND4	This Study
WS8N pIND4_cckA_G588C	WS8N with WT *cckA* G588C on pIND4	This Study
JPA467	WS8N with non-motile sigma 28 deletion	Martin et al. (2006)
JPA467 pIND4	JPA467 with empty pIND4 for use on swim plates	This study
JPA1301	WS8N with non-chemotactic *che*Op$_3$ deletion	Porter et al. (2002)
JPA1301 pIND4	JPA1301 with empty pIND4 for use on swim plates	This study
JPA1353	WS8N *che*Op$_1$, *che*Op$_2$, cheopiiinospace, *cheY4* and *cheY5* deletions	Steve Porter
AM1	*fleQ* omega suppressor strain of WS8N displaying expression of second flagella system	(Poggio et al., 2007)
N29	his- *flic* suppressor strain of WS8N displaying expression of second flagella system	Liz Sockett, personal communication
JPA972	WS8N with Δ*fleQ*	Elaine Byles and Steve Porter
JPA2744	WS8N with Δ*cckA*	This Study
JPA2732	JPA2744 with pIND4	This Study
JPA2733	JPA2744 with pIND4_*cckA*_WT	This Study
JPA2734	JPA2744 with pIND4_*cckA*_L391F	This Study
JPA2735	JPA2744 with pIND4_*cckA*_G588C	This Study
JPA507	WS8N with McpA-GFP	George Wadhams and Angela Martin
JPA2728	JPA507 with pIND4	This Study
JPA2729	JPA507 with pIND4_*cckA*_WT	This Study
JPA2730	JPA507 with pIND4_*cckA*_L391F	This Study
JPA2731	JPA507 with pIND4_*cckA*_G588C	This Study
JPA1456	WS8N with CFP-CheW4	George Wadhams
JPA2716	JPA1456 with pIND4	This Study
JPA2717	JPA1456 with pIND4_*cckA*_WT	This Study
JPA2718	JPA1456 with pIND4_*cckA*_L391F	This Study
JPA2719	JPA1456 with pIND4_*cckA*_G588C	This Study
JPA1462	WS8N with CheW2-YFP	Wadhams et al. (2003)
JPA2720	JPA1462 with pIND4	This Study
JPA2721	JPA1462 with pIND4_*cckA*_WT	This Study
JPA2722	JPA1462 with pIND4_*cckA*_L391F	This Study
JPA2723	JPA1462 with pIND4_*cckA*_G588C	This Study

Table 6.3: Strains

6.15 Buffers and media

All media and buffers autoclaved before use.

LB media (adjusted to pH7 with potassium hydroxide and monopotassium phosphate)

5 g/L yeast extract

5 g/L NaCl

10 g/L bactotryptone

M22 media (adjusted to pH7 with potassium hydroxide and monopotassium phosphate)

20 ml/1L 1M Phosphate buffer pH7

20 ml/1L concentrated base containing:

- 5.94 g/L Nitrilotriacetic acid
- 25 ml/L Metals 44 solution containing:
  - 2.5 g/L Ethylenediaminetetraacetic acid (EDTA)
  - 11 g/L $ZnSO_4$ $7H_2O$
  - 5 g/L $FeSO_4$ $7H_2O$
  - 1.5 ml/L 3M sulphuric acid (98%)
  - 2 g/L $MnSO_4$ $4H_2O$
  - 0.39 g/L $CuSO_4$ $5H_2O$
  - 0.12 g/L H_3BO_3 (boric acid)

0.2 g/L CoCL2 $6H_2O$ (cobaltous chloride)

14.5 g/L $MgSO_4.7H_2O$

2.5 g/L $CaCl_2.6H_2O$

0.05 g/L $FeSO_4.7H_2O$

0.0046 g/L Ammonium Molybdate($.4H_2O$)

2 ml/1L growth factors containing:

0.02 g/L Biotin

0.5 g/L $NaHCO_3$

1 g/L Nicotinic acid

0.5 g/L Thiamine HCl

0.5 g/L $(NH_4)2SO_4$

0.5g/L NaCl

Succinate (SUX) media (adjusted to pH7 with potassium hydroxide and monopotassium phosphate)

M22 with added:

2 g/L Sodium succinate

1 g/L Casamino acids

Sistrom's media (adjusted to pH7 with potassium hydroxide and monopotassium phosphate)

M22 with added:

1 g/L Monosodium glutamate

0.4 g/L Aspartate

TBE buffer (adjusted to pH8.3 with sodium hydroxide)

108 g/L Tris base

55 g/L Boric acid

7.4 g/L anhydrous EDTA

PBS buffer

10 phosphate buffered saline (Dulbecco A) tablets per 1 L Milli-Q water, resulting in:

137 mM Sodium chloride

3 mM Potassium chloride

8 mM Disodium hydrogen phosphate

1.5 mM Potassium dihydrogen phosphate

10 mM PIPES buffer (adjusted to pH7.2 with hydrochloric acid)

3.02 g/L PIPES in Milli-Q water

RAPID buffer

6.28 g/L MOPS (free acid)

7.26 g/L Tris (base)

1 g/L SDS

0.65 g/L Sodium Bisulfite

Made up to 1 L with Milli-Q water

Blotting buffer (adjusted to pH 8.3with hydrochloric acid and sodium hydroxide)

3 g/L Tris (base)

14.4 g/L Glycine

200 ml/L Methanol

10 ml/L 10% SDS

Add Milli-Q water to 1 L

6.15.1 Plating bacteria

All species and strains were plated onto LBA (LB media with 200 g/L agar).

Bibliography

Abràmoff, M. D., Magalhães, P. J., Ram, S. J., 2004. Image Processing with ImageJ. Biophotonics International **11**, 36–42.

Armitage, J. P., Macnab, R. M., 1987. Unidirectional, intermittent rotation of the flagellum of *Rhodobacter sphaeroides*. Journal of Bacteriology **169**, 514–8.

Armitage, J. P., Schmitt, R., 1997. Bacterial chemotaxis: *Rhodobacter sphaeroides* and *Sinorhizobium meliloti*-variations on a theme? Microbiology **143**, 3671–3682.

Atsumi, T., Maekawa, Y., Yamada, T., Kawagishi, I., Imae, Y., Homma, M., 1996. Effect of viscosity on swimming by the lateral and polar flagella of *Vibrio alginolyticus*. Journal of Bacteriology **178**, 5024–5026.

Barnett, M., Hung, D., 2001. A homolog of the CtrA cell cycle regulator is present and essential in *Sinorhizobium meliloti*. Journal of Bacteriology **183**, 3204–3210.

Beausoleil, S. a., Villén, J., Gerber, S. a., Rush, J., Gygi, S. P., 2006. A probability-based approach for high-throughput protein phosphorylation analysis and site localization. Nature Biotechnology **24**, 1285–92.

Bellefontaine, A.-F., Pierreux, C. E., Mertens, P., Vandenhaute, J., Letesson, J.-J., De Bolle, X., 2002. Plasticity of a transcriptional regulation network among alpha-proteobacteria is supported by the identification of CtrA targets in *Brucella abortus*. Molecular Microbiology **43**, 945–60.

Berg, H. C., 2003. The rotary motor of bacterial flagella. Annual Review of Biochemistry **72**, 19–54.

Berg, H. C., Brown, D. A., 1972. Chemotaxis in *Escherichia coli* analysed by three-dimensional tracking. Nature **239**, 500–4.

Blair, D. F., 1995. How bacteria sense and swim. Annual Review of Microbiology **49**, 489–522.

Brown, M. T., 2009. Control of the unidirectional motor in *Rhodobacter sphaeroides*. Ph.D. thesis, University of Oxford.

Charon, N. W., Goldstein, S. F., 2002. Genetics of motility and chemotaxis of a fascinating group of bacteria: the spirochetes. Annual Review of Genetics **36**, 47–73.

Chen, Y. E., Tsokos, C. G., Biondi, E. G., Perchuk, B. S., Laub, M. T., 2009. Dynamics of two phosphorelays controlling cell cycle progression in *Caulobacter crescentus*. Journal of Bacteriology **191** (24), 7417–7429.

Chilcott, G. S., Hughes, K. T., 2000. Coupling of flagellar gene expression to flagellar assembly in *Salmonella enterica* serovar *typhimurium* and *Escherichia coli*. Microbiology and Molecular Biology Reviews **64**, 694–708.

Cornelis, G. R., 2006. The type III secretion injectisome. Nature Reviews. Microbiology **4**, 811–25.

Dang, H., Lovell, C. R., 2002. Numerical dominance and phylotype diversity of marine *Rhodobacter* species during early colonization of submerged surfaces in coastal marine waters as determined by 16S ribosomal DNA sequence analysis and fluorescence *in situ* hybridization. Applied and Environmental Microbiology **68**, 496–504.

De Beyer, J, A., 2013. Roles of the two chemotaxis clusters in *Rhodobacter sphaeroides*. Ph.D. thesis, University of Oxford.

Duffy, K. J., Ford, R. M., 1997. Turn angle and run time distributions characterize swimming behavior for *Pseudomonas putida*. Journal of Bacteriology **179**, 1428–1430.

Dyer, C. M., Vartanian, A. S., Zhou, H., Dahlquist, F. W., 2009. A molecular mechanism of bacterial flagellar motor switching. Journal of Molecular Biology **388**, 71–84.

Edgar, R. C., 2004. MUSCLE: multiple sequence alignment with high accuracy and high throughput. Nucleic Acids Research **32**, 1792–7.

Eraso, J. M., Roh, J. H., Zeng, X., Callister, S. J., Lipton, M. S., Kaplan, S., 2008. Role of the global transcriptional regulator PrrA in *Rhodobacter sphaeroides* 2.4.1: combined transcriptome and proteome analysis. Journal of Bacteriology **190**, 4831–48.

Francez-Charlot, A., Kaczmarczyk, A., Vorholt, J. A., 2015. The branched CcsA/CckA-ChpT-CtrA phosphorelay of *Sphingomonas melonis* controls motility and biofilm formation. Molecular Microbiology **97**, 47–63.

Gao, R., Stock, A. M., 2009. Biological insights from structures of two-component proteins. Annual Review of Microbiology **63**, 133–154.

Greene, S. E., Brilli, M., Biondi, E. G., Komeili, A., 2012. Analysis of the CtrA pathway in *Magnetospirillum* reveals an ancestral role in motility in alphaproteobacteria. Journal of Bacteriology **194**, 2973–86.

Gupta, R. S., Mok, A., 2007. Phylogenomics and signature proteins for the alphaproteobacteria and its main groups. BMC Microbiology **7**, 106.

Harshey, R. M., 1994. Dimorphic transition in *Escherichia coli* and *Salmonella*

typhimurium: Surface-induced differentiation into hyperflagellate swarmer cells. Proceedings of the National Academy of Sciences of the United States of America **91**, 8631–8635.

Heimbrook, M. E., Wang, W. L., Campbell, G., 1989. Staining bacterial flagella easily. Journal of Clinical Microbiology **27**, 2612–5.

Hengge, R., 2009. Principles of c-di-GMP signalling in bacteria. Nature Reviews. Microbiology **7**, 263–73.

Hoch, J. A., 2000. Two-component and phosphorelay signal transduction. Current Opinion in Microbiology **3**, 165–170.

Hutchinson, E. C., Denham, E. M., Thomas, B., Trudgian, D. C., Hester, S. S., Ridlova, G., York, A., Turrell, L., Fodor, E., 2012. Mapping the phosphoproteome of influenza A and B viruses by mass spectrometry. PLoS Pathogens **8**, e1002993.

Ikeda, T., Homma, M., Lino, T., Asakura, S., Kamiya, R., 1987. Localisation and stoichiometry of hook-associated proteins within *Salmonella typhimurium* flagella. Journal of Bacteriology **169**, 1168–1173.

Imae, Y., Atsumi, T., 1989. Na^+-driven bacterial flagellar motors. Journal of Bioenergetics and Biomembranes **21**, 705–716.

Ind, A. C., Porter, S. L., Brown, M. T., Byles, E. D., de Beyer, J. a., Godfrey, S. a., Armitage, J. P., 2009. Inducible-expression plasmid for *Rhodobacter sphaeroides* and *Paracoccus denitrificans*. Applied and Environmental Microbiology **75**, 6613–5.

Jacobs, C., Domian, I. J., Maddock, J. R., Shapiro, L., 1999. Cell cycle-dependent polar localization of an essential bacterial histidine kinase that controls DNA replication and cell division. Cell **97**, 111–20.

Jones, S. E., Ferguson, N. L., Alley, M. R. K., 2001. New members of the *ctrA* regulon

: the major chemotaxis operon in *Caulobacter* is CtrA dependent. Microbiology **147**, 949–958.

Kehry, M. R., Doak, T. G., Dahlquist, F. W., 1985. Sensory adaptation in bacterial chemotaxis : regulation of demethylation. Journal of Bacteriology **163**, 983–990.

Kimsey, R. B., Spielman, A., 1990. Motility of lyme disease spirochetes in fluids as viscous as the extracellular matrix. The Journal of Infectious Diseases **162**, 1205–1208.

Kuchma, S. L., Delalez, N. J., Filkins, L. M., Snavely, E. a., Armitage, J. P., O'Toole, G. a., 2014. c-di-GMP-Mediated repression of swarming motility by *Pseudomonas aeruginosa* PA14 requires the MotAB stator. Journal of Bacteriology **197**, 420–430.

Lang, A. S., Beatty, J. T., 2002. A bacterial signal transduction system controls genetic exchange and motility. Journal of Bacteriology **184**, 913–918.

Larsen, S. H., Reader, R. W., Kort, E. N., Tso, W.-W., Adler, J., 1974. Change in direction of flagellar rotation is the basis of the chemotactic response in *Escherichia coli*. Nature **249**, 74–77.

Laub, M. T., Goulian, M., 2007. Specificity in two-component signal transduction pathways. Annual Review of Genetics **41**, 121–145.

Laub, M. T., McAdams, H. H., Feldblyum, T., Fraser, C. M., Shapiro, L., 2000. Global analysis of the genetic network controlling a bacterial cell cycle. Science **290**, 2144–8.

Li, C., Motaleb, A., Sal, M., 2000. Spirochete periplasmic flagella and motility. Journal of Molecular Microbiology and Biotechnology **2**, 345–354.

Macnab, R. M., 2003. How bacteria assemble flagella. Annual Review of Microbiology **57**, 77–100.

Martin, A. C., Gould, M., Byles, E., Roberts, M. a. J., Armitage, J. P., 2006. Two chemosensory operons of *Rhodobacter sphaeroides* are regulated independently by sigma 28 and sigma 54. Journal of Bacteriology **188**, 7932–40.

Martínez-del Campo, A., Ballado, T., Camarena, L., Dreyfus, G., 2011. In *Rhodobacter sphaeroides*, chemotactic operon 1 regulates rotation of the flagellar system 2. Journal of Bacteriology **193**, 6781–6.

McCarter, L. L., 2004. Dual flagellar systems enable motility under different circumstances. Journal of Molecular Microbiology and Biotechnology **7**, 18–29.

McCarter, L. L., 2006. Regulation of flagella. Current Opinion in Microbiology **9**, 180–6.

Mcclain, J., Rollo, D. R., Rushing, B. G., Bauer, C. E., 2002. *Rhodospirillum centenum* utilizes separate motor and switch components To control lateral and polar flagellum rotation. Journal of Bacteriology **184**, 2429–2438.

Mercer, R. G., Callister, S. J., Lipton, M. S., Pasa-Tolic, L., Strnad, H., Paces, V., Beatty, J. T., Lang, A. S., 2010. Loss of the response regulator CtrA causes pleiotropic effects on gene expression but does not affect growth phase regulation in *Rhodobacter capsulatus*. Journal of Bacteriology **192**, 2701–10.

Mercer, R. G., Quinlan, M., Rose, A. R., Noll, S., Beatty, J. T., Lang, A. S., 2012. Regulatory systems controlling motility and gene transfer agent production and release in *Rhodobacter capsulatus*. FEMS Microbiology Letters **331**, 53–62.

Miller, T. R., Belas, R., 2006. Motility is involved in *Silicibacter* sp. TM1040 interaction with dinoflagellates. Environmental Microbiology **8**, 1648–59.

Minamino, T., Imada, K., Namba, K., 2008. Molecular motors of the bacterial flagella. Current Opinion in Structural Biology **18**, 693–701.

Moens, S., Michiels, K., Keijers, V., Leuven, F. V. A. N., 1995. Cloning, sequencing,

and phenotypic analysis of *laf*1, encoding the flagellin of the lateral flagella of *Azospirillum brasilense* Sp7. Journal of Bacteriology **177**, 5419–5426.

Panis, G., Murray, S. R., Viollier, P. H., 2015. Versatility of global transcriptional regulators in alpha-proteobacteria: from essential cell cycle control to ancillary functions. FEMS Microbiology Reviews **39**, 120–33.

Paster, W., Brockmeyer, C., Fu, G., Simister, P. C., de Wet, B., Martinez-Riaño, A., Hoerter, J. A. H., Feller, S. M., Wülfing, C., Gascoigne, N. R. J., Acuto, O., 2013. GRB2-mediated recruitment of THEMIS to LAT is essential for thymocyte development. Journal of Immunology **190**, 3749–56.

Penfold, R. J., Pemberton, J. M., 1992. An improved suicide vector for construction of chromosomal insertion mutations in bacteria. Gene **118**, 145–146.

Perraud, A. L., Weiss, V., Gross, R., 1999. Signalling pathways in two-component phosphorelay systems. Trends in Microbiology **7**, 115–20.

Poggio, S., Abreu-Goodger, C., Fabela, S., Osorio, A., Dreyfus, G., Vinuesa, P., Camarena, L., 2007. A complete set of flagellar genes acquired by horizontal transfer coexists with the endogenous flagellar system in *Rhodobacter sphaeroides*. Journal of Bacteriology **189**, 3208–16.

Poggio, S., Osorio, A., Dreyfus, G., Camarena, L., 2005. The flagellar hierarchy of *Rhodobacter sphaeroides* is controlled by the concerted action of two enhancer-binding proteins. Molecular Microbiology **58**, 969–83.

Poole, P. S., Smith, M. J., Armitage, J. P., 1993. Chemotactic signalling in *Rhodobacter sphaeroides* requires metabolism of attractants. Journal of Bacteriology **175**, 1–5.

Porter, S. L., Wadhams, G. H., Armitage, J. P., 2008. *Rhodobacter sphaeroides*: complexity in chemotactic signalling. Trends in Microbiology **16**, 251–260.

Porter, S. L., Wadhams, G. H., Armitage, J. P., 2011. Signal processing in complex chemotaxis pathways. Nature Reviews. Microbiology **9**, 153–65.

Porter, S. L., Wadhams, G. H., Martin, A. C., Byles, E. D., Lancaster, D. E., Armitage, J. P., 2006. The CheYs of *Rhodobacter sphaeroides*. The Journal of Biological Chemistry **281**, 32694–704.

Porter, S. L., Warren, A. V., Martin, A. C., Armitage, J. P., 2002. The third chemotaxis locus of *Rhodobacter sphaeroides* is essential for chemotaxis. Molecular Microbiology **46**, 1081–94.

Pratt, L. A., Kolter, R., 1998. Genetic analysis of *Escherichia coli* biofilm formation: roles of flagella, motility, chemotaxis and type I pili. Molecular Microbiology **30**, 285–293.

Quon, K. C., Yang, B., Domian, I. J., Shapiro, L., Marczynski, G. T., 1998. Negative control of bacterial DNA replication by a cell cycle regulatory protein that binds at the chromosome origin. Proceedings of the National Academy of Sciences of the United States of America **95**, 120–125.

Roberts, M. A. J., 2007. The cytoplasmic chemotaxis protein cluster of *Rhodobacter sphaeroides*. Ph.D. thesis, University of Oxford.

Rosser, G., Fletcher, A. G., Wilkinson, D. A., de Beyer, J. A., Yates, C. A., Armitage, J. P., Maini, P. K., Baker, R. E., 2013. Novel methods for analysing bacterial tracks reveal persistence in *Rhodobacter sphaeroides*. PLoS Computational Biology **9**, e1003276.

Ryu, E., 1937. A simple method of staining bacterial flagella. Kitasato Arch. Exp. Med **14**, 218–219.

Sambrook, J., Russell, D. W., 1989. Molecular Cloning. Cold Spring Harbour Laboratory Press, New York.

Schafer, A., Tauch, A., Jager, W., Kalinowski, J., Thierbach, G., Puhler, A., 1994. Small mobilizable multi-purpose cloning vectors derived from the *Escherichia col*i plasmids pK18 and pK19: selection of defined deletions in the chromosome of *Corynebacterium glutumicum*. Gene **145**, 69–73.

Shaevitz, J. W., Lee, J. Y., Fletcher, D. a., 2005. *Spiroplasma* swim by a processive change in body helicity. Cell **122**, 941–5.

Shi, W., Zusman, D., 1993. The two motility systems of *Myxococcus xanthus* show different selective advantages on various surfaces. Proceedings of the National Academy of Sciences of the United States of America **90**, 3378–3382.

Shrout, J. D., Chopp, D. L., Just, C. L., Hentzer, M., Givskov, M., Parsek, M. R., 2006. The impact of quorum sensing and swarming motility on *Pseudomonas aeruginosa* biofilm formation is nutritionally conditional. Molecular Microbiology **62**, 1264–77.

Slovak, P. M., Wadhams, G. H., Armitage, J. P., 2005. Localization of MreB in *Rhodobacter sphaeroides* under conditions causing changes in cell shape and membrane structure. Journal of Bacteriology **187**, 54–64.

Sockett, R. E., Armitage, J. P., 1991. Isolation, characterization, and complementation of a paralyzed flagellar mutant of *Rhodobacter sphaeroides* WS8. Journal of Bacteriology **173**, 2786–90.

Solovyev, V., Salamov, A., 2011. Automatic Annotation of Microbial Genomes and Metagenomic Sequences. In: Li, R. W. (Ed.), Metagenomics and its applications in agriculture, biomedicine and environmental studies. Nova Science Publishers, pp. 61–78.

Soutourina, O. a., Bertin, P. N., 2003. Regulation cascade of flagellar expression in Gram-negative bacteria. FEMS Microbiology Reviews **27**, 505–523.

Stock, A. M., Robinson, V. L., Goudreau, P. N., 2000. Two-component signal transduction. Annual Review of Biochemistry **69**, 183–215.

Suaste-Olmos, F., Domenzain, C., Mireles-Rodríguez, J. C., Poggio, S., Osorio, A., Dreyfus, G., Camarena, L., 2010. The flagellar protein FliL is essential for swimming in *Rhodobacter sphaeroides*. Journal of Bacteriology **192**, 6230–9.

Trudgian, D. C., Thomas, B., McGowan, S. J., Kessler, B. M., Salek, M., Acuto, O., 2010. CPFP: a central proteomics facilities pipeline. Bioinformatics **26**, 1131–2.

Turner, L., Ryu, W. S., Berg, H. C., 2000. Real-time imaging of fluorescent flagellar filaments. Journal of Bacteriology **182**, 2793–2801.

Ulrich, L. E., Zhulin, I. B., 2009. The MiST2 database: A comprehensive genomics resource on microbial signal transduction. Nucleic Acids Research **38**, 1–7.

Vega-Baray, B., Domenzain, C., Rivera, A., Alfaro-López, R., Gómez-César, E., Poggio, S., Dreyfus, G., Camarena, L., 2015. The flagellar set Fla2 in *Rhodobacter sphaeroides* is controlled by the CckA pathway and is repressed by organic acids and the expression of Fla1. Journal of Bacteriology **197**, 833–847.

Wadhams, G. H., Armitage, J. P., 2004. Making sense of it all: bacterial chemotaxis. Nature Reviews Molecular Cell Biology **5**, 1024–37.

Wadhams, G. H., Martin, A. C., Warren, A. V., Armitage, J. P., 2005. Requirements for chemotaxis protein localization in *Rhodobacter sphaeroides*. Molecular Microbiology **58**, 895–902.

Wadhams, G. H., Warren, a. V., Martin, a. C., Armitage, J. P., 2003. Targeting of two signal transduction pathways to different regions of the bacterial cell. Molecular Microbiology **50**, 763–770.

Wang, C., Sang, J., Wang, J., Su, M., Downey, J. S., Wu, Q., Wang, S., Cai, Y., Xu, X., Wu, J., Senadheera, D. B., Cvitkovitch, D. G., Chen, L., Goodman, S. D.,

Han, A., 2013. Mechanistic insights revealed by the crystal structure of a histidine kinase with signal transducer and sensor domains. PLoS Biology **11**, e1001493.

Wilkinson, D. a., Chacko, S. J., Vénien-Bryan, C., Wadhams, G. H., Armitage, J. P., 2011. Regulation of flagellum number by FliA and FlgM and role in biofilm formation by *Rhodobacter sphaeroides*. Journal of Bacteriology **193**, 4010–4.

Wood, T. M., Yates, C. A., Wilkinson, D. A., Rosser, G., 2012. Simplified multitarget tracking using the PHD filter for microscopic video data. IEEE Transactions on Circuits and Systems for Video Technology **22**, 702–713.

Woods, D., 2007. Functionalised flagellar nanotubes. Ph.D. thesis, University of Nottingham.